

Department of Civil and Structural Engineering

# Computerised prediction of the deterioration of concrete building facades caused by moisture and changes in temperature

---

Fahim Al-Neshawy



**A!**

DOCTORAL  
DISSERTATIONS



# Computerised prediction of the deterioration of concrete building facades caused by moisture and changes in temperature

**Fahim Al-Neshawy**

Dissertation for the degree of Doctor of Science in Technology to be presented with due permission of the School of Engineering, Aalto University for public examination and debate in Auditorium R3 (Rakentajanaukio 4A) at the Aalto University (Espoo, Finland) on the 7th of June 2013, at 12 noon.

**Aalto University**  
**School of Engineering**  
**Department of Civil and Structural Engineering**

**Supervising professor**

Professor Jari Puttonen

**Thesis advisor**

Professor (fixed term) Esko Sistonen

**Preliminary examiners**

Professor Anders Ansell, KTH Royal Institute of Technology, Sweden

Professor Emeritus Lennart Elfgren, Luleå University of Technology,  
Sweden

**Opponent**

Professor Vagelis G. Papadakis, University of Ioannina, Greece

Aalto University publication series

**DOCTORAL DISSERTATIONS** 96/2013

© Fahim Al-Neshawy

ISBN 978-952-60-5202-1 (printed)

ISBN 978-952-60-5203-8 (pdf)

ISSN-L 1799-4934

ISSN 1799-4934 (printed)

ISSN 1799-4942 (pdf)

<http://urn.fi/URN:ISBN:978-952-60-5203-8>

Unigrafia Oy

Helsinki 2013

Finland





**Author**

Fahim Al-Neshawy

**Name of the doctoral dissertation**

Computerised prediction of the deterioration of concrete building facades caused by moisture and changes in temperature

**Publisher** School of Engineering

**Unit** Department of Civil and Structural Engineering

**Series** Aalto University publication series DOCTORAL DISSERTATIONS 96/2013

**Field of research** Structural Engineering and Building Physics

**Manuscript submitted** 15 February 2013

**Date of the defence** 7 June 2013

**Permission to publish granted (date)** 7 May 2013

**Language** English

**Monograph**

**Article dissertation (summary + original articles)**

**Abstract**

Environmental conditions, mainly temperature and relative humidity, are the major factors in the physical, chemical, and biological deterioration of concrete building facades. The purpose of this thesis is to investigate the effect of the environmental conditions on the deterioration of concrete building facades, develop a system for monitoring these conditions, and predict the deterioration and remaining service life of these facades on the basis of the monitoring data.

The thesis consists of a literature review, laboratory and field investigation, the development of a hygrothermal monitoring and deterioration predicting system, and its application to concrete building facades. The literature review covered the concrete deterioration caused by moisture and changes in temperature. Special attention was given to the corrosion of steel reinforcement as a result of carbonation, damage caused by repeated freezing and thawing, and mould growth. The laboratory investigation and field monitoring of relative humidity and temperature were carried out to assess the impact of environmental factors on the performance of the structure under concern. The laboratory and field measurement data were used to validate the concrete deterioration prediction models.

The results confirm that the hygrothermal field monitoring is significant for: (i) collecting real relative humidity and temperature data within the concrete facades and the surrounding environmental conditions; (ii) integrating the effects of the measured data into different indicators for calculating the potential for deterioration, and (iii) working as an early warning alarm to ensure appropriate renovation and maintenance measures by comparing the predicted deterioration levels with different threshold values of deterioration indicators. Based on the monitoring data, the environmental factors that affect the deterioration of concrete building facades are characterized.

The result of the research will improve the building construction industry by providing methodologies and systems for monitoring and predicting the performance of structures. A scientific relevance of this research will be the improved understanding between the results received in laboratory studies and observations of deterioration in practice. The implementation of the RHT-MAPS monitoring system developed can be carried out cost-effectively in comparison to the construction and maintenance expenses of concrete facades. The maintenance costs can also be optimized by the monitoring results.

**Keywords** concrete building facades, deterioration, relative humidity, temperature, monitoring, ICT

**ISBN (printed)** 978-952-60-5202-1

**ISBN (pdf)** 978-952-60-5203-8

**ISSN-L** 1799-4934

**ISSN (printed)** 1799-4934

**ISSN (pdf)** 1799-4942

**Location of publisher** Espoo

**Location of printing** Helsinki

**Year** 2013

**Pages** 222

**urn** <http://urn.fi/URN:ISBN:978-952-60-5203-8>



# Acknowledgements

This thesis would not have been possible without the support of several thoughtful and generous individuals.

Foremost among those I would like to thank my supervisor, Professor Jari Puttonen, for his guidance and support throughout this thesis. I would also like to thank Professor Vesa Penttala for his support during the early stages of this work.

I wish to express my thanks to Professor Lennart Elfgren and Professor Anders Ansell for their valuable criticism and for comments on this thesis.

I would like to acknowledge the members of the research team, Professor Esko Sistonen, Jukka Piironen, M.Sc. and Olli-Pekka Kari, M.Sc., Susanna Peltola, M.Sc., for their valuable contributions to this research. Many thanks also go to Sami Mahgary, M.Sc., for revising the language of this thesis.

The main financing for the work was provided by the National Technology Agency of Finland (TEKES) and the Academy of Finland. I would also like to thank all the companies and institutions that have been involved for their support and cooperation. I gratefully acknowledge the generous support of the Graduate School in Construction IT, especially Professors Tor-Ulf Weck, Bo-Crister Björk, and Brian Atkin. Special thanks go to my colleagues in the graduate school, Wafa Al-Sakini, Ph.D. and Ersen Firat, M.Sc., for their support.

I am deeply grateful to the Confederation of Finnish Construction Industries (Rakennusteollisuus RT ry) Fund, the Technology Development Foundation, (TES - Tekniikan edistämistätiö), and the

Kerttu and Jukka Vuorinen Fund for the grants that supported the writing of my thesis.

Finally, I would like to express my sincere appreciation and gratitude to all my friends, wherever they are, particularly my dear friends Professor Saleh Ibrahim, Christopher Ariyo, Lic.Sc. Mika Tulimaa, Lic.Sc., Mr. Abdel Hady Habeib and Mr. Mohammed Elfatih Elsayed for their encouragement and support. Special thanks to Mr. Raimo Peuranen for teaching me how to survive in Finland and for encouraging and inspiring me to reach my dream.

Finally, my most important acknowledgments go to my family, who have been the biggest motivating force in my life. I am grateful to my wife Madeha, my daughter Noora, and my son Akram for their encouragement, advice, and the many sacrifices they have made over a number of years. This dissertation is dedicated to them.

Above all, I thank Allah the Almighty for making this thesis a reality.

Espoo 06.05.2013.

---

Fahim Al-Neshawy

# Contents

ACKNOWLEDGEMENTS.....	I
CONTENTS.....	III
LIST OF ABBREVIATIONS AND SYMBOLS.....	VII
1 INTRODUCTION.....	1
1.1 Background.....	1
1.2 Objectives.....	2
1.3 Scope and limitations of the research.....	3
1.4 Research methodology.....	4
1.5 Organisation of the thesis.....	5
1.6 Contribution of the thesis.....	7
2 LITERATURE REVIEW.....	9
2.1 Types of concrete building facades.....	9
2.2 Thermal and moisture-related definitions.....	13
2.2.1 Surface humidity.....	13
2.2.2 Saturated water vapour pressure.....	13
2.2.3 Actual water vapour pressure.....	14
2.2.4 Water vapour content.....	14
2.2.5 Time of wetness.....	15
2.3 Hygrothermal response indices.....	15
2.3.1 Moisture index.....	15
2.3.2 Relative humidity and temperature index.....	18
2.3.3 Freezing and thawing index.....	20
2.4 Heat and moisture transfer in concrete building facades..	20
2.4.1 Heat transfer mechanisms.....	21
2.4.2 Moisture transfer mechanisms.....	24
2.5 Exposure classes for concrete building facades.....	27

2.5.1	Environmental exposure classes .....	28
2.5.2	Exposure class-specific requirements for concrete building facades .....	29
2.6	Environmental deterioration of concrete structures.....	30
2.6.1	Carbonation of concrete .....	32
2.6.2	Corrosion of steel in concrete as a result of carbonation .....	35
2.6.3	Damage caused by repeated freezing and thawing	40
2.6.4	Mould growth on concrete building facades .....	47
2.6.5	Alkali-Silica Reaction .....	48
3	MONITORING AND PREDICTION SYSTEM (RHT-MAPS).....	51
3.1	Review of monitoring and prediction related research.....	51
3.2	RHT-MAPS architecture and components.....	53
3.2.1	Sensory system.....	54
3.2.2	Data acquisition system .....	59
3.2.3	Data-processing and deterioration predicting module.....	64
3.3	RHT-MAPS testing.....	67
3.4	RHT-MAPS expenses .....	69
3.5	RHT-MAPS evaluation .....	69
3.6	Summary.....	72
4	LABORATORY INVESTIGATIONS .....	75
4.1	Material selection .....	76
4.1.1	Cement.....	76
4.1.2	Aggregates .....	77
4.1.3	Water .....	77
4.1.4	Air-entraining agent .....	77
4.2	Mix design and sampling.....	78
4.2.1	Accelerated and natural carbonation .....	78
4.2.2	Thermal expansion of concrete .....	80
4.2.3	Freezing and thawing resistance of concrete.....	81
4.3	Experimental test equipment and procedures.....	82
4.3.1	Accelerated and natural carbonation .....	82
4.3.2	Thermal expansion of concrete .....	84
4.3.3	Slab test: freezing-thawing resistance of concrete.	86
4.4	Results and data analysis.....	87

4.4.1	Carbonation depth of concrete.....	87
4.4.2	Thermal expansion of concrete.....	89
4.4.3	Frost damage to concrete.....	95
4.5	Summary.....	97
5	<b>FIELD MONITORING OF RELATIVE HUMIDITY AND TEMPERATURE .....</b>	<b>99</b>
5.1	Installation of the RHT-MAPS sensor network.....	100
5.1.1	Concrete building facade RF1-EPS .....	100
5.1.2	Concrete building facade RF2-MWOOL .....	102
5.2	Reliability and accuracy of the measurements .....	104
5.3	The climate exposure parameters.....	105
5.3.1	Relative humidity and temperature.....	106
5.3.2	Moisture index.....	109
5.3.3	Freezing and thawing.....	111
5.4	Response of concrete building facades to the outdoor conditions .....	113
5.4.1	Hygrothermal conditions at different locations in the facade wall .....	114
5.4.2	Time-dependent moisture and thermal indices ...	116
5.4.3	Freezing and thawing cycles.....	118
5.5	Summary.....	119
6	<b>DETERIORATION AND SERVICE LIFE PREDICTION.....</b>	<b>123</b>
6.1	Overview of the durability and service life of concrete structures .....	123
6.2	Heat and moisture transport modelling.....	125
6.3	Carbonation-induced corrosion.....	128
6.3.1	Carbonation model.....	128
6.3.2	Validation of the carbonation model .....	131
6.3.3	Service life of carbonated concrete .....	134
6.4	Frost damage to concrete .....	139
6.4.1	The frost damage model .....	139
6.4.2	Predicting the frost damage to concrete.....	142
6.4.3	Remaining service life as a result of frost damage	143
6.5	Estimation of mould growth .....	145
6.5.1	Mould growth potential model.....	145
6.5.2	Estimating the risk of mould growth.....	146

6.6	Summary.....	150
7	CONCLUSIONS AND DISCUSSIONS .....	153
7.1	Concluding the research objectives.....	153
7.2	Evaluating the research work.....	153
7.3	Scientific and industrial contribution.....	157
7.4	Limitations.....	157
7.5	Future research.....	158
	REFERENCES.....	159
	APPENDICES.....	A-1
	Appendix A. RHT-MAPS sensor network component.....	A-1
	Appendix B. RHT-MAPS sensor network configuration .....	B-1
	Appendix C. RHT-MAPS monitoring software user’s guide ..	C-1
	Appendix D. Laboratory testing of concrete .....	D-1
	Appendix E. Data of Tanesi and Meininger, 2006.....	E-1



# List of abbreviations and symbols

## List of abbreviations

AVG	Average
CAT5	Category 5 unshielded twisted pair cable
COMSY	Condition Oriented ageing and plant life Monitoring System
CV	Coefficient of variation
DI	Drying index
FTI	Freezing and Thawing Index
HMP44	Humidity and Temperature Probe
IP/UDP	Internet Protocol/User Datagram Protocol
LICo4	Network Controller card
LN1003	Network hybrid data node
MEWS	Moisture Management for Exterior Walls. MEWS is a joint research project between IRC-NRC Canada and several external partners.
MI	Moisture index
PT100	Common type of RTD (Resistance Temperature Detector)
RDM	Relative Dynamic Modulus
RHTI	Relative humidity and temperature index within the part of the structure under consideration
RHT-MAPS	Relative humidity and temperature monitoring and concrete facade deterioration prediction system
SHT15	Digital humidity and temperature sensor
WI	Wetting index

## List of symbols

$\varepsilon$	Emissivity of the object ( $\varepsilon = 1.0$ , for black)	
$\sigma$	Stefan-Boltzmann constant $\sigma = 5.6703 \cdot 10^{-8}$	[W/m <sup>2</sup> K <sup>4</sup> ]
$\phi$	Diameter of the reinforcement	[mm].
$\rho_a$	Mass density of aggregates	[kg/m <sup>3</sup> ]
$\rho_c$	Mass density of cement	[kg/m <sup>3</sup> ]
$\Delta L$	Length change during temperature change	[ $\mu$ m]
$\Delta T$	Measured temperature change	[°C]
$\rho_w$	Density of water	[kg/m <sup>3</sup> ]
$A$	Heat flow area	[m <sup>2</sup> ]
$a/c$	Aggregate-to-cement ratio	[-]
$C$	Concentration of the diffusing agent	[mol/m <sup>3</sup> ]
$C_{CO_2}$	Carbon dioxide content by volume	[%]
$dc$	Cover thickness	[mm]
$D_{eff}$	Diffusion coefficient of carbon dioxide	[m <sup>2</sup> /s]
$D_l$	Allowed frost damage level	[%]
$D_s$	Water vapour saturation deficit	[g/m <sup>3</sup> ]
$H$	Enthalpy	[J/m <sup>3</sup> ]
$h_c$	Convective heat transfer coefficient	[W/m <sup>2</sup> K]
$h_v$	Latent heat of phase change	[J/kg]
$k$	Thermal conductivity of the material	[W/mK]
$k_{CO_2}$	Coefficient of carbon dioxide content in air	[-]
$k_{con}$	Quality of concrete related coefficient	[-]
$k_{cur}$	Concrete curing factor	[-]
$k_{RH}$	Relative humidity related coefficient	[-]
$k_T$	Temperature related coefficient	[-]
$L_o$	Length of specimen at room temperature	[m]
$m_v$	Mass of vapour in a volume of air g	
$M_w$	Molecular weight of water ( $M_w = 18.01528$ )	[g/mol]
$N_a$	Annual number of freezing and thawing cycles	[cycle/a]
$N_{FT}$	Number of freezing and thawing cycles	[cycle]
$N_{tot}$	Total number of freezing and thawing cycles to reach a certain level of frost damage	[cycle]
$Pa$	Actual vapour pressure	[Pa]
$Ps$	Saturated vapour pressure	[Pa]
$P_{s\ ice}$	Saturated vapour pressure over ice	[Pa]

$P_{s \text{ water}}$	Saturated vapour pressure over water	[Pa]
$q$	Heat transfer rate	[W]
$Q$	Activation energy of the carbonation process	[kJ/mol]
$R$	Gas constant ( $R = 8.3145$ )	[J/mol·K]
$RH$	Relative humidity	[%]
$RH_{\text{crit}}$	User-defined critical threshold value of relative humidity level above which moisture damage is more likely to occur	[%]
$RH_{p,i}$	Potential relative humidity for moisture damage at time (i)	[%]
$R_i$	Hourly precipitation	[(mm/m <sup>2</sup> )/h]
$T$	Temperature	[°C]
$t$	Time	[s]
$T_{\text{crit}}$	User-defined critical threshold value of temperature level above which moisture damage is more likely to occur	[°C]
$t_d$	Time required to reach the frost level of damage	[a]
$TOW$	Time of wetness within the part of the structure under consideration	[h/a]
$t_p$	Propagation time	[a]
$T_{p,i}$	Potential temperature for moisture damage at time (i)	[°C]
$v_a$	Actual water vapour content	[g/m <sup>3</sup> ]
$V_{\text{corr}}$	Corrosion rate	[µm/a]
$v_s$	Saturated water vapour content	[g/m <sup>3</sup> ]
$w/c$	Water-to-cement ratio	[-]
$w_a$	Air content of the fresh concrete	[%]
$w_{\text{act}}$	Humidity ratio under ambient conditions	[-]
$w_{\text{sat}}$	Humidity ratio at saturation	[-]
$X_{\text{ca}}$	Average carbonation depth	[mm]
$\alpha_L$	Coefficient of thermal expansion	[(µm/m)/°C]



# 1 Introduction

## 1.1 Background

The deterioration of concrete building facades is a common phenomenon in Finnish buildings built in the 1960s and 1970s. The facades of the buildings at that time were most often reinforced concrete sandwich elements. The most common mechanisms for the deterioration of concrete building facades are cracking caused by restrained volume changes in the concrete and the corrosion of the embedded reinforcing steel. Two of the most important factors that contribute to the deterioration of buildings are moisture and temperature. Moisture is the major factor in physical deterioration processes related to restrained moisture movements, freezing chemical deterioration caused by harsh climates, and biological deterioration. Changes in moisture and temperature lead to the swelling and shrinking of building materials. Furthermore, the freezing and thawing of the water in the pores and cracks leads to an increase in the volume of moisture. In addition, this moisture leads to an increase in the heat flowing through structures and thus increases the total consumption of heating energy for the whole building.

Repairing concrete building facades has been practised on a large scale for a few decades in Finland. According to the Official Statistics of Finland (2013), in the year 2010 the financial costs for the annual renovation of the external structures of buildings were 227.4 million euros, compared to 85.7 million euros for basic repairs. The financial value of the repair works to the facades is significant, which emphasises the need to understand the basic phenomena of the deterioration and repair of concrete building facades.

This PhD research and its related activities are part of three projects funded by TEKES - the Finnish Funding Agency for Technology and Innovation. These projects were:

- i) Effect of maintenance measures on service life of concrete building facades. One of the objectives of the research was to test new possibilities offered by ICT (Information and Communication Technology) for use in the real estate and construction sector. For that purpose a new thermal and moisture monitoring network system for monitoring the relative humidity and temperature of two facades that were repaired using different methods was developed, tested, and installed;
- ii) The reliability of integrated moisture sensors in building applications. In this research project the reliability of the relative humidity and temperature sensors used in the monitoring network system was tested;
- iii) Effect of interacting deterioration parameters on the service life of concrete structures in cold environments. In this research project the deterioration of concrete caused by moisture and changes in temperature was tested and its prediction models were validated.

## 1.2 Objectives

The aim of this research is to develop a network system for monitoring the environmental factors which affect concrete building facades, and help to predict the deterioration and remaining service life of such facades. The system should allow for easy on-site installation and be cost-effective. The network system applications should also operate as an early warning system to ensure the appropriate renovation and maintenance of concrete building facades. The following specific objectives were defined:

- to identify the damage mechanisms related to moisture and changes in temperature and generate the damage functions caused by moisture and changes in temperature;
- to monitor, assess, and document the moisture- and heat-related performance of concrete building facades;

- to assess the impact of environmental factors on the durability and performance of concrete building facades;
- to increase the understanding of the behaviour of concrete building facades under repeated moisture and thermal cycles and thus to enable their service lives to be predicted theoretically;
- to let the system act as an early warning system to ensure appropriate renovation and maintenance.

### **1.3 Scope and limitations of the research**

Because of the extended nature of the thesis, certain limitations had to be imposed to make the research work manageable. These can be summarised as follows.

The target facade materials were restricted to the concrete used in facade structures according to the EN 206-1 (2000). Air-entrained C30/37 and C35/45 concretes were selected for the experimental tests and non-air-entrained C20/25, C30/37 and C35/45 concretes were used as the reference concrete types.

Two repaired concrete facade sites were identified as relevant to the study. The first facade was repaired by adding external mineral wool insulation and a rendering system consisting of 6 mm of rendering coat and glass fibre mesh. The second facade was repaired by adding an external expanded polystyrene (EPS) insulation and rendering system that consisted of 6 mm of rendering coat and glass fibre mesh.

Field monitoring was carried out to monitor the temperature and relative humidity of the repaired facades. The precipitation data were collected from the weather forecast for the city of Espoo for the purpose of calculation.

The damage to the concrete caused by caused by moisture and changes in temperature that was used for prediction was limited to the carbonation of concrete (chemical deterioration), corrosion induced by carbonation (chemical deterioration), frost damage (physical deterioration), and mould growth (biological deterioration).

## 1.4 Research methodology

This thesis is based on original research on (i) ICT technology, (ii) building physics and (iii) building materials research fields. The ICT technology research was to apply new possibilities offered by the ICT for the construction sector such as sensing, monitoring and data acquisition technologies. The building physics research aimed to analyse the hygrothermal performance of concrete building facades components in their environment. The building materials research concentrated on investigating the deterioration of reinforced concrete structures due to the impact of the ambient environmental factors like moisture and thermal gradients.

The main subjects dealt with in this thesis are, as shown in Figure 1.1, the effect of the moisture and temperature on the deterioration of concrete building facades, the relevant environmental data acquisition techniques, and the prediction of the deterioration processes of concrete building facades.

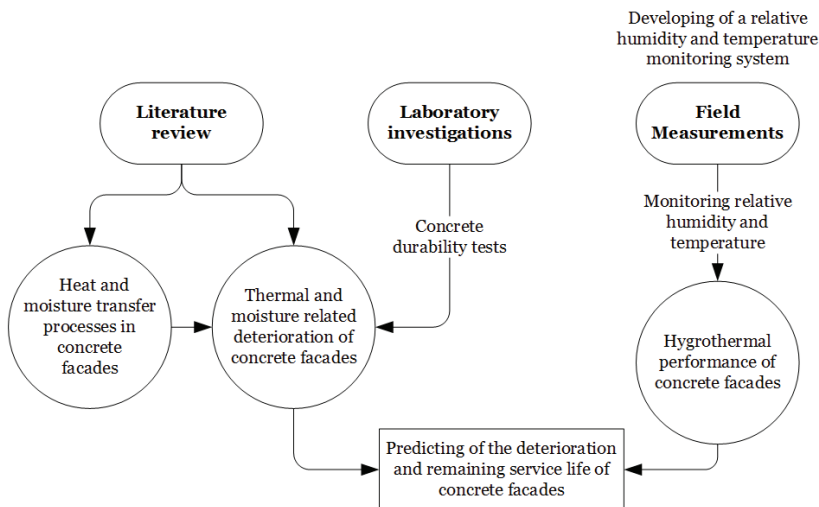


Figure 1.1: Thesis work methodology data collection and data interpretation.

As shown in Figure 1.1, the thesis is divided into the following special topics:

- literature studies and analyses of the scientific basis of the effect of the temperature and moisture on the deterioration of concrete building facades



- studies on the theoretical considerations of the deterioration of concrete building facades resulting from moisture and changes in temperature
- experimental research on the deterioration of concrete building facades resulting from moisture and changes in temperature
- the development and use of a network system and computer program for collecting relative humidity and temperature data from concrete facade structures and their ambient environment
- predicting the environmental response-based deterioration of concrete building facades
- developing computerised monitoring and prediction of the remaining service life of concrete building facades

All the measurements were planned and carried out by the author.

## **1.5 Organisation of the thesis**

The research work introduced in this thesis is divided into four main sections:

- a literature review,
- the design and implementation of the monitoring system,
- the experimental investigation and field monitoring of the thermal and moisture behaviour of repaired concrete building facades, and
- the deterioration and prediction of the remaining service life of the repaired concrete building facades.

The general organisation of the thesis is shown in Figure 1.2.

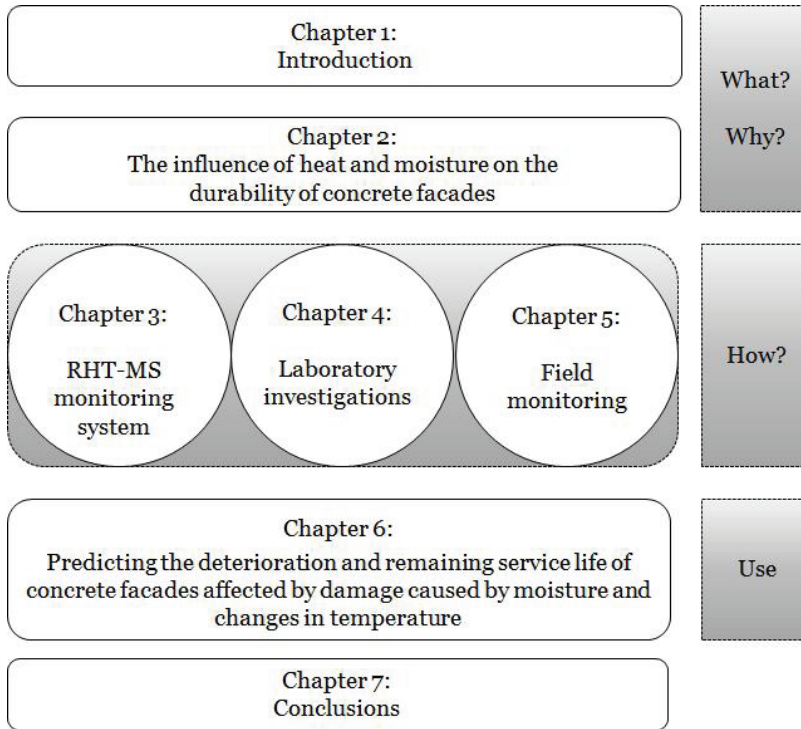


Figure 1.2: Flow chart of the organisation of the thesis.

The contents of the chapters are summarised below:

- Chapter 1: Introduces the thesis and its methodology.
- Chapter 2: A literature review explains the basic terms and formulae for heat and moisture transfer in concrete building facades. The durability problems of concrete that are related to environmental causes such as the reinforcement corrosion caused by carbonation, the damage resulting from frost action, and the damage caused by the alkali-silica reaction are also discussed. The potential for the growth of mould in insulation materials is also reviewed.
- Chapter 3: Describes the design and implementation of the RHT-MAPS system sensor network and its data acquisition and analysing software.
- Chapter 4: Describes the laboratory investigations of the thermal and moisture-related durability characteristics of concrete. The results of the

laboratory tests are used for validating the deterioration prediction models.

- Chapter 5: Describes the installation of the RHT-MAPS that was developed in the field, the analysis of the relative humidity and temperature data that were monitored, and the hygrothermal performance of the concrete building facades that were monitored. The monitored relative humidity and temperature data are used for predicting the deterioration of the concrete building facades.
- Chapter 6: Describes a comparison between laboratory experimental and monitoring results with predicted values of the deterioration of concrete building facades, according to which the prediction model is made. The moisture and thermal-based remaining service life model is presented.
- Chapter 7: The conclusions and major findings of the research are summarised.

## 1.6 Contribution of the thesis

Parts of the work described herein have been published by the author and others in the following publications that supplement this thesis:

1. Fahim Al-Neshawy; Jukka Piironen; Susanna Peltola; Esko Sistonen; Jari Puttonen (2011). Network system for assessing the moisture and thermal behaviour of repaired concrete building facades. *Journal of Information Technology in Construction* 2011 ITcon Vol. 16, pages 601-616 <http://www.itcon.org/2011/34>
2. Penttala Vesa; Al-Neshawy Fahim (2002). Stress and strain state of concrete during freezing and thawing cycles. *Cement and Concrete Research* 2002. Volume 32 Issue 9, pages 1407-1420.

3. Al-Neshawy F.; Sistonen E.; Piironen J.; Huovinen S. (2006). Monitoring the Hygrothermal Performance of Repaired Concrete Facades. Proceedings of the European Symposium on Service Life and Serviceability of Concrete Structures (ESCS-2006). Helsinki, 12-14 June 2006. Concrete Association of Finland. pages 333-339.
  
4. Al-Neshawy F.; Sistonen E.; Piironen J.; Huovinen S. (2007). New Method for Monitoring the Hygrothermal Condition of Repaired Facades. Proceedings of the Fifth International Conference on Concrete under Severe Conditions: Environment and Loading (CONSEC'07). Tours, France, 4-6 June 2007. pages 1807-1812.

## 2 Literature review

This chapter explores the literature that is relevant to understanding the hygrothermal behaviour of concrete building facades and predicting their deterioration and remaining service life. The first part of this literature review will describe the types of concrete building facades and their wall assembly. The second part of the review is a summary of the thermal and moisture-related definitions. The third part describes the heat and moisture transfer processes on concrete building facades, followed by a summary of the damage to concrete building facades caused by the thermal and moisture conditions. This is not meant to be a complete review of the literature, but to familiarise the reader with the effects of the thermal and moisture conditions on the deterioration of concrete building facades.

### 2.1 Types of concrete building facades

Lemieux and Totten (2010) described the overall function of the envelope of a building as providing a barrier between indoor and outdoor environments, so that the indoor environment can be adjusted and maintained within acceptable limits. In general, the facade of a building has to provide: (i) structural resistance to wind and gravity loads; (ii) environmental protection from the elements, including moisture and temperature, and (iii) architectural appearance and aesthetics.

Concrete was first used as a significant building material in the late 19<sup>th</sup> century with the invention of Portland cement. Originally, it was seen as a substitute for natural stone and was used extensively in precast reconstructed stone blocks. Later, as the building industry

became more mechanised, larger precast units were developed which could be lifted by crane.

Historically, according to Jukkola (1997), Huovinen et al. (1998), and Hannula et al. (2007), concrete building facades are classified as follows:

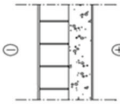
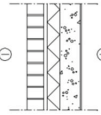
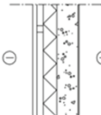
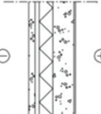
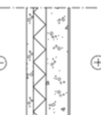
- 1920-1940 era
  - Start of using concrete as building material in supporting structures.
  - Mostly building facades with red bricks, air bricks, or rendering systems.
- 1940-1960 era
  - Introduction of industrial prefabricated concrete elements with thermal insulation.
  - Concrete building facades with coarse or splash rendering systems.
  - Start of the use of concrete building facades with a sandwich element.
- 1960-1980 era
  - Start of the use of concrete element systems (columns – slab systems).
  - Concrete building facades with exposed aggregate concrete surfaces.
  - Concrete building facades with cladding materials such as brick and clinker slabs.
- 1980-present
  - Different types of prefabricated sandwich elements with ventilation gaps.
  - Concrete building facades with cladding such as metal sheets, boards, bricks, or concrete panels.



Figure 2.1: Examples of concrete building facades in Finland between 1940 and the present (Hannula et al. 2007)

Facade construction has been classified according to the framework construction and the surface materials used as the outer layer in wall structures. The type of the facade also depends on the construction of the walls. Some typical concrete building facades and wall constructions that are used in Finland are shown in Table 2.1.

Table 2.1: Typical types of concrete building facades (Huovinen et al. 1998)

Wall type	Framework construction	Surface materials	Cross-section
Concrete wall with rendered lightweight concrete block cladding	Massive concrete cast-in-situ	Lime cement rendering	
Concrete wall with cladding of brick, board or metal sheeting	Cast-in-situ massive concrete	Brick	
	Cast-in-situ massive concrete	Fibre cement boards or profiled metal sheet cladding	
Concrete wall with cladding of concrete panels	Cast-in-situ massive concrete	Prefabricated concrete panels	
Concrete wall of prefabricated sandwich panels	Prefabricated concrete units	Prefabricated sandwich panels	

Sandwich wall systems of precast concrete are frequently used in many countries for residential houses, as well as commercial buildings. The sandwich wall consists of two concrete panels separated by a layer of thermal insulation, with the thickness being selected as required according to the location and climate. A load-bearing part is normally an internal panel with a thickness in the range of 120 mm-150 mm, depending on the design situation. In a Nordic climate, an insulation thickness in the range of 100 mm-200 mm is typical. The exterior concrete panel has a thickness of 75 mm-80 mm. The external concrete panel is connected to the load-bearing

panel by specially designed connectors made of high-quality stainless steel to ensure a long life span for the building facade. The facade element joints are sealed with an elastic joint compound, which protects the element from moisture and allows thermal expansion of the elements. The element surface may be painted, unpainted, faced with natural stone or exposed-aggregate concrete, or tiled (Neuvonen 2009). Ventilated sandwich facades are open joint cladding systems where the external panel acts as a rain screen. The air gap of 20-40 mm between the insulating and the external panel is used to make possible the vertical ventilation of the insulation material layer of the facade. Examples of sandwich panel facades fabricated in Finland are shown in Figure 2.2 and Figure 2.3.

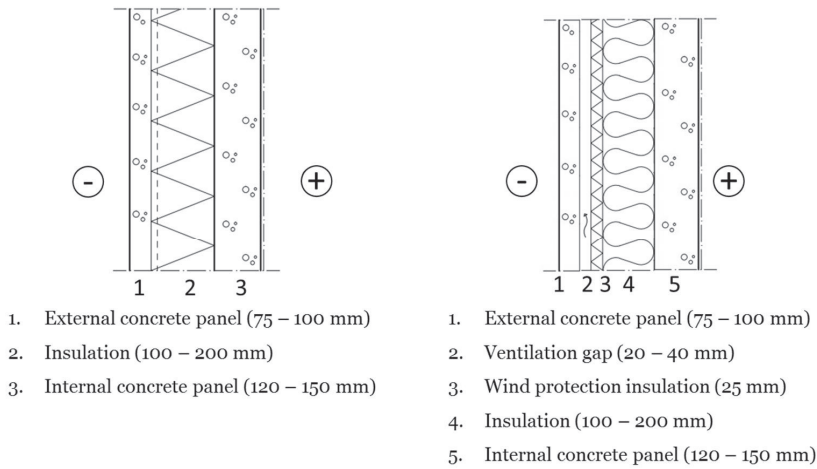


Figure 2.2: Cross-section of ventilated and non-ventilated sandwich panel facades.

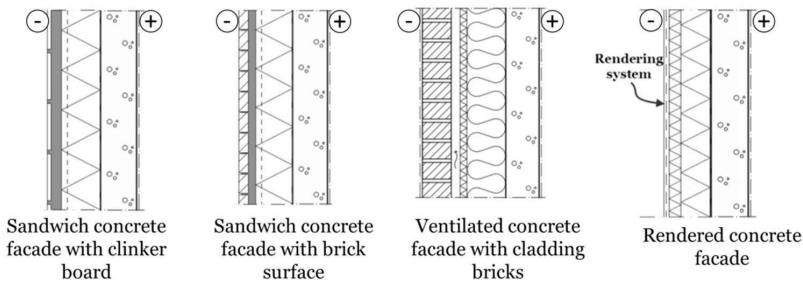


Figure 2.3: Examples of concrete building facades fabricated in Finland.



## 2.2 Thermal and moisture-related definitions

### 2.2.1 Surface humidity

Relative humidity is a measure of the amount of water vapour in the air at a specific temperature compared to the maximum amount of water vapour that the same amount of air can hold at that temperature and is given as a percentage value (%RH). Relative humidity depends on the temperature of the air, as warm air can hold more moisture than cold air. As the temperature decreases, the amount of moisture in the air does not change but the relative humidity goes up since the maximum amount of moisture that cooling air can hold is smaller. A relative humidity of 100%RH indicates that the air is holding all the water it can at the current temperature and any additional moisture at that point will result in condensation.

### 2.2.2 Saturated water vapour pressure

In a closed container partly filled with water there will be some water vapour in the space above the water. The vapour pressure of the water that can be held by the atmosphere is called the saturation pressure, which can be assumed to be dependent only on temperature. The saturated water vapour pressure is calculated according to the German standard DIN 4108-5 “Heat insulation in buildings; Calculation methods” as shown in Equation (2.1).

$$P_s = a * \left( b + \frac{T}{100} \right)^n \quad (2.1)$$

where

$P_s$  is the saturated vapour pressure [Pa],

$T$  is the temperature [°C] and

$a$ ,  $b$ , &  $n$  are constants

$a = 288.68$  Pa,  $b = 1.098$ , and  $n = 8.02$  for  $0 \leq T \leq 30^\circ\text{C}$

$a = 4.689$  Pa,  $b = 1.486$  and  $n = 12.3$  for  $-20 \leq T < 0^\circ\text{C}$

The saturation water vapour pressure over water can also be determined by Equation (2.2) and the saturation water vapour pressure over water below  $0^\circ\text{C}$  is determined by Equation (2.3) (Buck 1981).

$$P_{s,water} = 611.21 * EXP\left(\frac{17.502 * T}{240.97 + T}\right) \quad (2.2)$$

$$P_{s,ice} = 611.25 * EXP\left(\frac{22.452 * T}{272.55 + T}\right) \quad (2.3)$$

where:

- $P_{s,water}$  is the saturated vapour pressure over water [Pa],
- $P_{s,ice}$  is the saturated vapour pressure over ice [Pa], and
- $T$  is the temperature [°C].

### 2.2.3 Actual water vapour pressure

The actual water vapour pressure is the vapour pressure exerted by the water in the air. When the air is not saturated, the actual vapour pressure will be lower than the saturation vapour pressure. The relative humidity expresses the degree of saturation of the air as a ratio of the actual to the saturation water vapour pressure at the same temperature. The actual water vapour pressure is calculated by Equation (2.4).

$$P_a = P_s * \frac{RH}{100} \quad (2.4)$$

where

- $P_a$  is the actual vapour pressure [Pa],
- $P_s$  is the saturated vapour pressure [Pa], and
- $RH$  is the relative humidity [%].

### 2.2.4 Water vapour content

The amount of water vapour that can be held by the atmosphere depends on the saturated water vapour pressure, as shown in Equation (2.5), according to the German standard DIN 4108-5 “Heat insulation in buildings; Calculation methods”.

$$v_s = P_s * \left(\frac{M_w}{R * (273 + T)}\right) \quad (2.5)$$

where:

- $v_s$  is the saturated water vapour content [g/m<sup>3</sup>],
- $P_s$  is the saturated vapour pressure [Pa], and
- $R$  is the gas constant  $R = 8.3145$  [J/mol.K].
- $T$  is the temperature [°C], and
- $M_w$  is the molecular weight of water  $M_w = 18.02$  [g/mol].

### 2.2.5 Time of wetness

The time of wetness or TOW is defined as the fraction of the year when the relative humidity is above 80% and the temperatures are not below 0°C (ISO 9223 standard). The time of wetness is calculated using Equation (2.6). The TOW refers to the period of time during which the atmospheric conditions are favourable for the formation of a surface layer of moisture on a metal. This moisture film is extremely important for the chemical mechanisms of the corrosion process (Norberg 2002).

$$TOW = \sum_{i=1}^{t_{tot}} f_{Ti} * f_{RH_i} \quad (2.6)$$

where:

$TOW$  is the time of wetness [h/a],

$t_{tot}$  is the total duration of a year, i.e. 8760 or 8784 [h],

$f_{T,i}$  is the temperature factor at time (i),

$$f_{T,i} = \begin{cases} 1 & \text{if } T > 0 \text{ } ^\circ\text{C} \\ 0 & \text{if } T \leq 0 \text{ } ^\circ\text{C} \end{cases}$$

$f_{RH,i}$  is the relative humidity factor at time (i),

$$f_{RH,i} = \begin{cases} 1 & \text{if } RH > 80\% \\ 0 & \text{if } RH \leq 80\% \end{cases}$$

Because both the temperature and relative humidity can vary significantly during a day, a large database of temperature and relative humidity should be accumulated before calculating the time of wetness (TOW).

## 2.3 Hygrothermal response indices

### 2.3.1 Moisture index

The moisture index describes the environmental moisture and thermal load. The moisture index is a function of two components: the potential for wetting (wetting index) and the potential for drying (drying index). The wetting index is based on the amount of rainfall (kg/m<sup>2</sup>), while the drying index is based on the annual potential for evaporation. The moisture index is independent of the construction of the wall and design strategies that might be used to manage moisture loading. The MEWS (Moisture Management for Exterior

Walls) moisture index approach described in Cornick et al. (2002) was used to define moisture reference years.

The monthly moisture index (MI) approach has been used in this thesis to describe the monthly moisture and thermal loads during the year. The monthly moisture index is calculated on the basis of the monthly wetting index (WI) and the monthly drying index (DI).

The monthly wetting index is defined by the monthly amount of rainfall (mm) on the ground. In Finland, daily rainfall is defined as the 24-hour accumulated amount of rain recorded between 6:00 AM on a given day and 6:00 AM on the following day. Monthly rainfall is obtained by summing the individual daily rainfalls. The average rainfall for a specific month is the average of 30 monthly values for the period 1981-2010. (Pirinen et al. 2012)

Measuring the drying potential relates to evaporation, which is the difference between the humidity ratio at saturation and the humidity ratio of the ambient air. This is a measure of the capacity of the air to absorb water vapour, calculated from the dry bulb temperature and relative humidity. The monthly drying index is the total of the differences between the humidity ratio at saturation and the humidity ratio under ambient conditions during one month. The humidity ratios can be calculated using Equations (2.7) and (2.8).

$$w_{sat} = \left( \frac{m_w}{m_a} \right)_{sat} = \frac{M_w}{M_a} * \left( \frac{v_{sat}}{P - v_{sat}} \right) = 0.625 * \left( \frac{v_{sat}}{P - v_{sat}} \right) \quad (2.7)$$

$$w_{act} = \left( \frac{m_w}{m_a} \right)_{act} = \frac{M_w}{M_a} * \left( \frac{v_{act}}{P - v_{act}} \right) = 0.625 * \left( \frac{v_{act}}{P - v_{act}} \right) \quad (2.8)$$

where:

- $w_{sat}$  is the saturation humidity ratio [-],
- $w_{act}$  is the humidity ratio under ambient conditions [-],
- $m_w$  is the mass of water vapour in the mixture [kg],
- $m_a$  is the unit mass of dry air [kg],
- $M_w$  is the molecular weight of water,  $M_w = 18.02$  [g/mol],
- $M_a$  is the molecular weight of air,  $M_a = 28.84$  [g/mol].
- $v_{sat}$  is the saturation vapour pressure in [kPa],
- $v_{act}$  is the actual vapour pressure [kPa], and
- $P$  is the total mixture pressure,  $P = 101.1$  [kPa].

The monthly drying index for a location can be calculated from Equation (2.9).

$$DI = \sum_{i=1}^{t_{mo}} (w_{sat,i} - w_{act,i}) \quad (2.9)$$

where:

- $DI$  is the drying index [-],
- $t_{mo}$  is the total duration of a month, i.e., 840-930 [h],
- $w_{sat}$  is the humidity ratio at saturation at time (i) [-], and
- $w_{act}$  is the humidity ratio under ambient conditions at time (i) [-].

Cornick and Dalglish (2003) recommended the normalisation of the moisture index in order to have comparative measures. They also suggested eliminating or ignoring units, particularly as they are different for the wetting index and the drying index. The drying and wetting indices are normalised according to the location and time under consideration. The normalisation scheme is given in Equation (2.10).

$$I_{norm} = \left( \frac{I - I_{norm}}{I_{max} - I_{min}} \right) \quad (2.10)$$

where:

- $I_{norm}$  is the normalised monthly wetting or drying index,
- $I$  is the monthly wetting or drying index,
- $I_{min}$  is the minimum value of the monthly wetting or drying index during the measurement period, and
- $I_{max}$  is the maximum value of the monthly wetting or drying index during the measurement period.

Cornick and Dalglish (2003) defined the moisture index (MI) as shown in Equation (2.11).

$$MI = \sqrt{(WI_{norm}^2 + (1 - DI_{norm})^2)} \quad (2.11)$$

where:

- $WI_{norm}$  is the normalised monthly wetting index [-] and
- $DI_{norm}$  is the normalised monthly drying index [-].

A simple classification of the moisture index was constructed by splitting the range of the normalised moisture index into a number of divisions. Each division represents a limit for moisture-related

problems. The classification of the moisture index which was represented in Cornik et al. (2002) is given in Table 2.2.

Table 2.2: Classification of normalised moisture index with respect to moisture problems.

<b>Normalized moisture index</b>	<b>Potential for moisture problems</b>
$MI \geq 1.00$	Severe
$1.00 > MI \geq 0.90$	High
$0.90 > MI \geq 0.80$	Moderate
$0.80 > MI \geq 0.70$	Limited
$MI < 0.70$	Low

### 2.3.2 Relative humidity and temperature index

The relative humidity and temperature index (RHTI) is a long-term hygrothermal response indicator derived from the relative humidity and temperature conditions inside the building envelope cross-section over a period of time for any specific area of the cross-section. The RHTI index is an indicator used to quantify and compare the hygrothermal response of the wall assembly. This index captures the duration of moisture and thermal conditions coexisting above threshold relative humidity and temperature levels.

Mukhopadhyaya et al. (2005) calculated the RHTI index by multiplying the potential temperature and the potential relative humidity for moisture damage as shown in Equation (2.12).

$$RHTI = \sum_{i=1}^{t_{tot}} (T_{p,i} * RH_{p,i}) \quad (2.12)$$

where:

$t_{tot}$  is the total duration of a year, i.e. 8760 or 8784 [h],

$T_{p,i}$  is the potential temperature for moisture damage at time (i) [°C],

$$T_{p,i} = \begin{cases} T - T_{crit} & \text{if } T > T_{crit} \\ 0 & \text{if } T \leq T_{crit} \end{cases}$$

$RH_{p,i}$  is the potential relative humidity for moisture damage at time (i) [%],

$$RH_{p,i} = \begin{cases} RH - RH_{crit} & \text{if } RH > RH_{crit} \\ 0 & \text{if } RH \leq RH_{crit} \end{cases}$$

$T_{crit}$  and  $RH_{crit}$  are the critical threshold values of the temperature and relative humidity level above which damage is more likely to occur, as shown in Table 2.3.

Table 2.3: The critical threshold values for temperature and relative humidity based on different potentials for damage.

Damage potential	$T_{crit}$	$RH_{crit}$	Reference
Biological growth	0 to +50°C	$RH \geq 75\%$	Viitanen, 2007
Metal corrosion	$T \geq 0^\circ\text{C}$	$RH \geq 80\%$	Bertolini, 2004
Concrete carbonation	$T \geq 0^\circ\text{C}$	$65 \leq RH \leq 75\%$	Tuutti, 1982
Frost damage	$T \leq 0^\circ\text{C}$	$RH \geq 95\%$	Mukhopadhyaya, 2005

Mukhopadhyaya et al. (2003) concluded that the RHTI index is used to assess the hygrothermal response at any location on the wall assembly and that the higher RHTI index values indicate an increased severity of the hygrothermal response. The long-term RHTI index of a wall response can be assessed in relation to the moisture index (climate severity) of various geographic locations.

The RHTI index has its limitations and is intended to be used with other analytical outputs. For example, different walls with similar cumulative RHTI values may have different hygrothermal responses. Similarly, different climates can produce similar cumulative RHTI values.

### 2.3.3 Freezing and thawing index

The freezing and thawing index (FTI) is defined as the number of freezing or thawing oscillations when temperatures oscillate around 0°C for those structures that are almost at the moisture saturation level  $RH_{crit}$  (Mukhopadhyaya et al. 2005). The freezing thawing index is defined in Equation (2.13).

$$FTI = \sum_{i=1}^{t_{tot}} C_i \quad (2.13)$$

where:

- $t_{tot}$  is the total duration of a year, i.e. 8760 or 8784 [h],
- $C_i$  is a freezing or thawing counter when temperatures oscillate around 0°C at time (i),
- $C_i = \begin{cases} 1 & \text{if } T_h * T_{h-1} \leq 0 \text{ and } RH \geq RH_{crit} \\ 0 & \text{if } T_h * T_{h-1} > 0 \text{ or } RH < RH_{crit} \end{cases}$
- $T_h$  is the temperature within the part of the structure under consideration at a particular time step (h) [°C],
- $RH$  is the relative humidity within the part of the structure under consideration at a particular time step (h) [%], and
- $RH_{crit}$  is the critical threshold value of the relative humidity level above which moisture damage is more likely to occur, as shown in Table 2.3 [%].

The FTI index is used to estimate the potential of frost damage as a result of repeating freezing and thawing cycles. Higher values of the FTI index indicate a greater potential for frost damage.

## 2.4 Heat and moisture transfer in concrete building facades

The failures of many concrete building facades are probably caused to a greater or lesser extent by hygrothermal stresses caused by thermal and moisture loads. Some studies of facade performance have considered the impacts of these two loads separately. However, heat and moisture transfer are two connected processes and they have a great interactive impact on the performance of the facade. The primary heat and moisture transport processes in concrete building facades are shown in Figure 2.4. Heat can be transported by conductivity, convection, and radiation. Moisture is transferred as



vapour by diffusion and convection within some porous materials and transferred as liquid water by capillarity suction and gravity flow through porous materials, cracks, and openings.

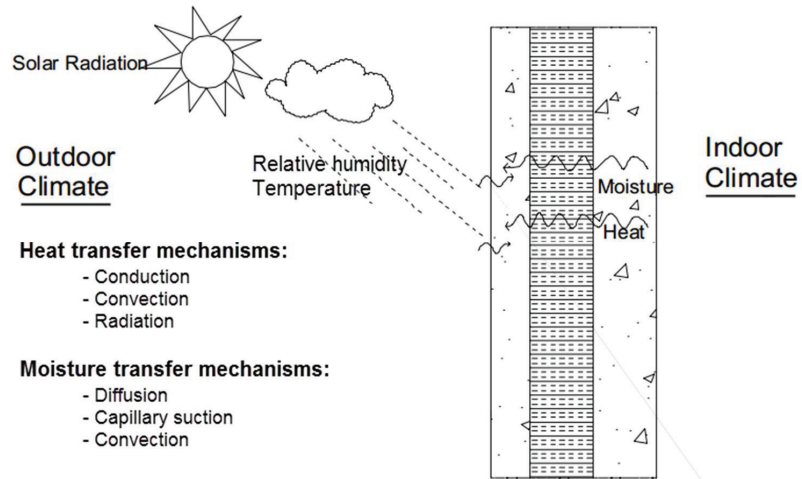


Figure 2.4: Heat and moisture transfer mechanisms for concrete building facades.

### 2.4.1 Heat transfer mechanisms

The heat balance for a building facade is a combination of (i) conductive heat transfer from the inside to the outside caused by temperature difference over the wall and (ii) radiation heat loss from the outer surface, together with convective heat transfer when outdoor air passes through a ventilated cavity (Gudum 2003).

#### Heat transfer by conduction

Conduction is viewed as the transfer of thermal energy from the more energetic to the less energetic particles of a wall as a result of interactions between the particles. A temperature gradient within a homogeneous material results in an energy transfer rate within the medium, which can be calculated by Fourier's law:

$$q = -k * A * \left( \frac{\Delta T}{\Delta x} \right) \quad (2.14)$$

where:

- $q$  is the heat transfer rate [W],
- $k$  is the thermal conductivity of the material [W/mK],

$A$  is the heat flow area [ $\text{m}^2$ ], and  
 $\Delta T/\Delta x$  is the temperature gradient in the direction normal to the area  $A$  [ $\text{K}/\text{m}$ ].

The thermal properties of a material are highly dependent on its structure and density. What is referred to as the thermal conductivity of a porous material is often a combination of conduction, radiation exchange, convection, and conduction in water in the pore structure. (Johannesson 2006)

For a homogenous wall with a temperature gradient in the direction normal to the surface, the consequence is that if no heat is being stored at any point in the wall, the temperature gradient has to be constant. This also implies that the temperature is linearly distributed between the surfaces (as shown in Figure 2.5).

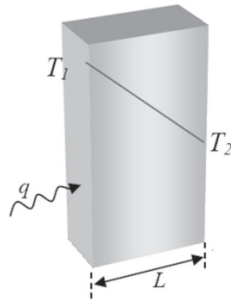


Figure 2.5: Temperature distributions for steady-state conduction

The density of heat flow rate can be expressed as:

$$q = -k * A * \left( \frac{T_1 - T_2}{L} \right) = \frac{T_1 - T_2}{R} \quad (2.15)$$

where:

$q$  is the heat transfer rate [ $\text{W}$ ],  
 $k$  is the thermal conductivity of the material [ $\text{W}/\text{mK}$ ],  
 $A$  is the heat flow area [ $\text{m}^2$ ],  
 $L$  is the wall thickness [ $\text{m}$ ],  
 $R$  is the thermal resistance of the wall  $R=L/(k*A)$  [ $\text{K}/\text{W}$ ], and  
 $T_1-T_2$  is the temperature difference in the material layers [ $\text{K}$ ].

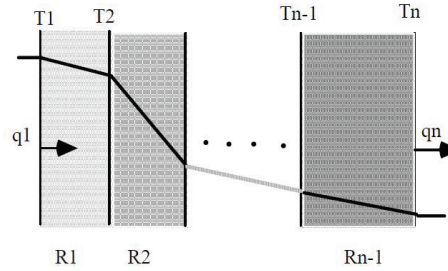


Figure 2.6: Steady-state heat flow and temperature distribution in a multilayer wall with no internal heat sources.

From the steady-state condition, it follows that the heat flow is constant through the construction. The density of heat flow rate in a multilayer wall shown in Figure 2.6 with no internal heat sources can be expressed as:

$$q = \frac{T_1 - T_2}{R_1} = \frac{T_2 - T_3}{R_2} = \dots = \frac{T_{n-1} - T_n}{R_{n-1}} \quad (2.16)$$

where:

- $q$  is the heat transfer rate [W],
- $R_n$  is the thermal resistance of the wall [K/W], and
- $T_{n-1} - T_n$  is the temperature difference in the material layers [K].

### Heat transfer by convection

Convection is the transfer of thermal energy between a solid and a moving fluid. Convection is governed by two processes: the movement of energy as a result of molecular vibrations and the bulk fluid motion. The movements can be caused by differences in air densities because of temperature variations (natural convection) or by the wind or ventilation systems (forced convection). If the upstream temperature of the fluid is ( $T_\infty$ ) and the surface temperature of the solid is ( $T_s$ ), the heat transfer per unit of time is given by Newton's Law of Cooling; see Equation (2.17).

$$q = h_c * A * (T_s - T_\infty) \quad (2.17)$$

where:

- $q$  is the heat transfer rate [W],
- $A$  is the heat transfer area of the surface [m<sup>2</sup>],
- $h_c$  is the convective heat transfer coefficient of the process [W/m<sup>2</sup>K], and

$T_s - T_\infty$  is the temperature difference between the surface and the bulk fluid [K]

The convective heat transfer coefficient,  $h_c$ , is dependent on the type of medium (gas or liquid), the flow properties, such as velocity and viscosity, and temperature-dependent properties. The free convective heat transfer coefficient for air is within the ranges of 5-25 (W/m<sup>2</sup>K) and 20-100 (W/m<sup>2</sup>K) for water. (Johansson 2006)

### Heat transfer by radiation

Radiation heat transfer occurs by electromagnetic waves through a gas (or vacuum) and requires a line of sight between the source and the contact surface. Since all objects above absolute zero radiate heat, the net transfer of heat condition must be considered. Radiation is a relatively common mechanism for some methods of heating and cooling (radiant heating or cooling, for example) and is a concept that must be understood to employ shading devices for passive heating and cooling of exterior wall systems and assemblies.

The radiation energy per unit time from a solid body is proportional to the fourth power of the absolute temperature and can be expressed with the Stefan-Boltzmann Law, as shown in Equation (2.18).

$$q = \varepsilon * \sigma * A * T^4 \quad (2.18)$$

where

$q$  is the heat transfer rate [W],  
 $\varepsilon$  is the emissivity of the object ( $\varepsilon = 1$  for black bodies),  
 $\sigma$  is the Stefan-Boltzmann constant  $\sigma = 5.6703 \cdot 10^{-8}$  (W/m<sup>2</sup>K<sup>4</sup>),  
 $A$  is the area of the emitting body [m<sup>2</sup>], and  
 $T$  is the absolute temperature (K).

#### 2.4.2 Moisture transfer mechanisms

Moisture found in concrete building facades could originate from three major sources. The first source is the construction moisture, such as moisture trapped within materials such as fresh concrete and wet-applied insulations. The construction moisture can only be important during the first two to three years of a new building's life. The second source is the interior moisture that results from indoor activities. The third source is the exterior moisture that could be

transported through the layers of the facade. Straube (2002) categorised the primary sources of moisture in buildings as:

- liquid water from precipitation (rain and melting snow) or plumbing leaks
- water vapour from the exterior and from internal activities and processes within the building
- liquid water and water vapour from the soil adjoining the building
- moisture built-in with the construction materials.

In porous building materials, moisture can exist in gaseous (water vapour), liquid, and solid (ice) states. Moisture transports only in gas and liquid states under the influence of a driving force such as airflow, gravity, or suction caused by differences in air pressure. Moisture transport in porous materials is due to diffusion, convection, and capillary action. Diffusion is the movement of water vapour resulting from a difference in vapour pressure. Convective transport of moisture refers to moisture carried by airflows through spaces and materials. Capillarity is the movement of liquid water in porous materials resulting from surface tension forces. Capillarity, or capillary suction, can also occur in the small space created between two materials. Capillary suction into the facades of buildings occurs primarily with moisture from exterior sources such as rainwater and groundwater, whereas the movement of moisture into the facades of buildings by diffusion or air movement can occur with moisture from interior or exterior sources. (Straube 2006)

### **Moisture transfer by diffusion**

The diffusive water vapour flow transfers of moisture in its gaseous state take place through the various layers of an exterior wall system or assembly. The rate and predominant direction of diffusive vapour flow are directly related to and influenced by interior and exterior ambient air temperatures and relative humidity, as well as differences between interior and exterior vapour pressures and the individual vapour permeability of each layer in an exterior wall system or assembly. (Lemieux and Totten. 2010)

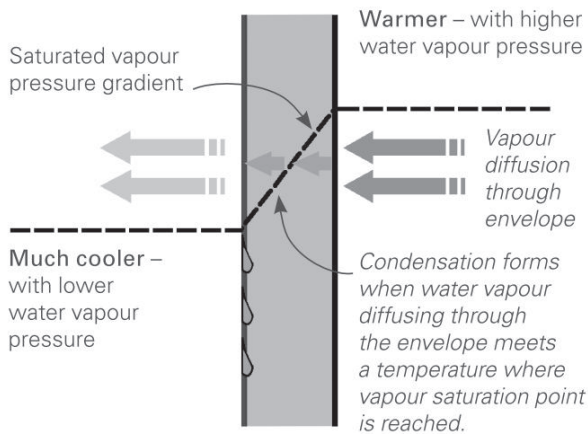


Figure 2.7: Moisture transfer by diffusion through building facades (Kay 2006).

The air on either side of an external wall will probably be at different temperatures and relative humidities, resulting in different water vapour pressures between the inside and outside air. Vapour pressures increase as relative humidity and temperatures rise. The greater the vapour pressure differential through the building envelope, the greater the tendency for water vapour to migrate from the high-pressure side to the low-pressure side. Vapour diffusion generally occurs from warm to cold surroundings.

At the molecular level the thickness and movement of water molecules adsorbed onto the external and internal surfaces (e.g. the internal pore walls) and within the envelope pores increase as relative humidity increases, resulting in the movement of moisture from regions with higher concentrations of adsorbed water to regions with lower concentrations. Surface diffusion occurs from moist to dry regions. (Haughton et al. 2003)

### Moisture transfer by convection

Convective transfer is subdivided into free (or natural) and forced convection. Natural convection originates from a pressure difference between an inflow area and an outflow area, which is based on differences in hygrothermal density. In the case of forced convection next to differences in density, the influence of forced ventilation, e.g. the wind, cannot be neglected. Exfiltration, the transport from the

inside to the outside, occurs if the pressure level is higher on the interior side of the exterior wall. Wind suction may increase the transfer rate. The opposite effect is called infiltration. In both cases, moisture and particles such as germs and dust may be introduced into the structure. Natural convection occurs mainly in regions that are enclosed on all-sides. Forced convection is only possible through leakages, which form a connection between the different pressures. The wind, as basic actuation potential, is able to influence the flow-through of leakages in the exterior walls of buildings significantly. (Schmidit and Kornadt 2012)

Moisture advection is horizontal transport of moisture. The advective moisture flow is defined as the bulk movement of moisture in its vapour state across an exterior wall system or assembly. For example, in humid climates saturated air that enters an enclosure and comes into contact with elements below the dew point (due to the element being at a cooler temperature) can result in condensation within the enclosure and may lead to long-term moisture problems. (Lemieux and Totten 2010)

### **Moisture transfer by capillary suction**

Capillary action is the flow of liquid moisture through small interconnected pores or spaces as a result of surface tension. This is a very powerful mechanism and depends on the pore size and available moisture. If the pore size is small, the capillary transfer becomes powerful but the flow is slow. Capillary rise plays an important role in construction materials in contact with the soil. Capillary transport in building materials such as concretes and mortars depends on different factors such as the water-to-cement ratio, sand size distribution, curing, the degree of saturation, and environmental conditions. (Paul 2009)

## **2.5 Exposure classes for concrete building facades**

The exposure classes depend on the provisions that are valid in the place where the concrete is in use. This exposure classification does not exclude consideration of special conditions existing in the place where the concrete is in use or the application of protective measures such as the use of stainless steel or other corrosion-resistant metal

and the use of protective coatings for the concrete or the reinforcement. The concrete may be subject to more than one of the actions described. The environmental conditions of concrete building facades may thus need to be expressed as a combination of exposure classes. (Hallberg 2005)

### 2.5.1 Environmental exposure classes

The environmental exposure classes for concrete building facades are classified as shown in Table 2.4.

Table 2.4: Exposure classes for the concrete building facades according to the EN 206-1, (2000).

	<b>Class</b>	<b>Description of the environment</b>	<b>Informative examples where exposure classes may occur</b>
No risk of corrosion or attack	<b>X0</b>	Inside buildings with very low air humidity	Concrete inside buildings with low air humidity
	<b>XC1</b>	Dry or permanently wet	(i) Concrete inside buildings with low air humidity (ii) Concrete permanently submerged in water
Corrosion induced by carbonation	<b>XC3</b>	Moderate humidity	(i) Concrete inside buildings with moderate or high air humidity (ii) External concrete sheltered from rain
	<b>XC4</b>	Cyclic wet and dry	Concrete surfaces subject to water contact
Freeze/thaw attack without de-icing agents	<b>XF1</b>	Moderate water saturation, without de-icing agent	Vertical concrete surfaces exposed to rain and freezing
	<b>XF3</b>	High water saturation, without de-icing agent	Horizontal concrete surfaces exposed to rain and freezing



Exposure classes for the concrete facade structures according to BY 50 (2005) for different environmental conditions are shown in Figure 2.8.

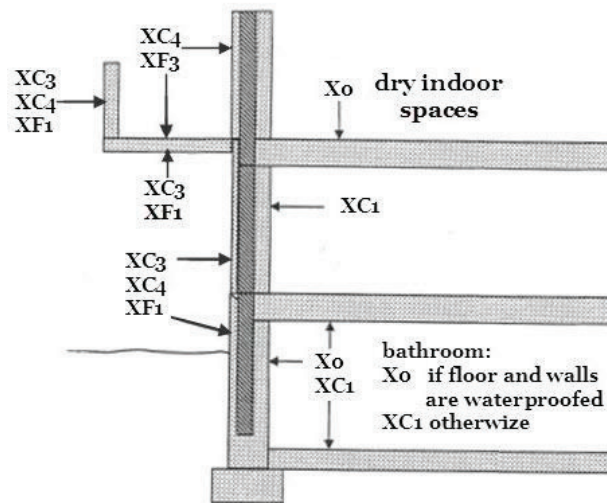


Figure 2.8: Classification of concrete facade structure into carbonation and frost exposure classes.

Hallberg (2005) proposed the connection of the values of the relative humidity to quantify the exposure classes describing the corrosion induced by carbonation as shown in Table 2.5.

Table 2.5: Quantitative description of the exposure classes resulting from corrosion induced by carbonation. (Hallberg 2005)

Class	Qualitative description	Quantitative description, RH [%]
XC1	Dry or constantly wet	< 60 or $\geq$ 100
XC2	Wet, rarely dry	> 95
XC3	Moderate humidity	60 – 85
XC4	Cyclic wet and dry	85 – 95

### 2.5.2 Exposure class-specific requirements for concrete building facades

Codes and specifications play an important role in ensuring the durability of concrete structures. The large majority of international

codes of structural concrete specify some limit values for the following five parameters:

- minimum cement (binder) content,
- maximum water-binder ratio,
- minimum compressive strength of concrete,
- minimum air content of concrete, and
- thickness of concrete cover of reinforcement.

The requirements for the composition of concrete and the concrete cover thickness of exposure classes where corrosion is induced by carbonation and induced by freezing and thawing attacks are shown in Table 2.6.

Table 2.6: Limiting values for concrete material used in concrete building facades.

Composition and properties	Corrosion induced by carbonation			Freezing and thawing	
	XC1	XC3	XC4	XF1	XF3
Max. W/C ratio	0.65	0.55	0.5	0.55	0.5
Min. strength class	C20/25	C30/37	C30/37	C30/37	C30/37
Min. cement content [kg/m <sup>3</sup> ]	260	280	300	300	320
Min. concrete cover [mm]	20	35	35	-	-
Min. air content (%)	-	-	-	4	4

## 2.6 Environmental deterioration of concrete structures

The environmental conditions, such as ambient temperature and relative humidity, have a significant influence on the deterioration of hardened concrete. Damage caused by moisture can be divided into three types of deterioration processes: biological, chemical, and physical deterioration. These deteriorations may lead to mechanical and structural degradation in the form of loss of stiffness, excessive deformation, cracking, delamination, spalling, and, in severe cases, to structural failure. (Carmeliet et al. 2009)

This thesis focuses on the deterioration mechanisms of concrete building facades caused by moisture and changes in temperature, which are highlighted in Figure 2.9. These highlighted deterioration

mechanisms are based on the non-marine environmental exposure classes which affect concrete building facades in Finland as shown in Figure 2.8. Concrete building facade deterioration may occur for two principal reasons: corrosion of the reinforcement as a result of carbonation and internal disintegration of the concrete. Reinforcement corrosion initiated by carbonation is usually related to moisture, and typically causes cracking and delamination of the concrete structure. The expansion of concrete creates tensile stresses that lead to internal cracking and therefore the disintegration of the concrete, which may also occur as a result of other phenomena such as frost attacks or alkali-aggregate reaction (Lahdensivu 2012).

The effect of the ingress of chloride on the corrosion of reinforcements is not discussed here because its impact in the non-marine environment is considered irrelevant. The alkali-silica reaction is not discussed either because the chemical reaction between Finnish aggregates and their surrounding environment is usually quite low. The alkali-silica reaction is dealt with only briefly in this chapter. Mould growth is included as in Finland microbial growth is frequently found in the insulation layers of sandwich concrete-type facades (Pessi et al. 1999).

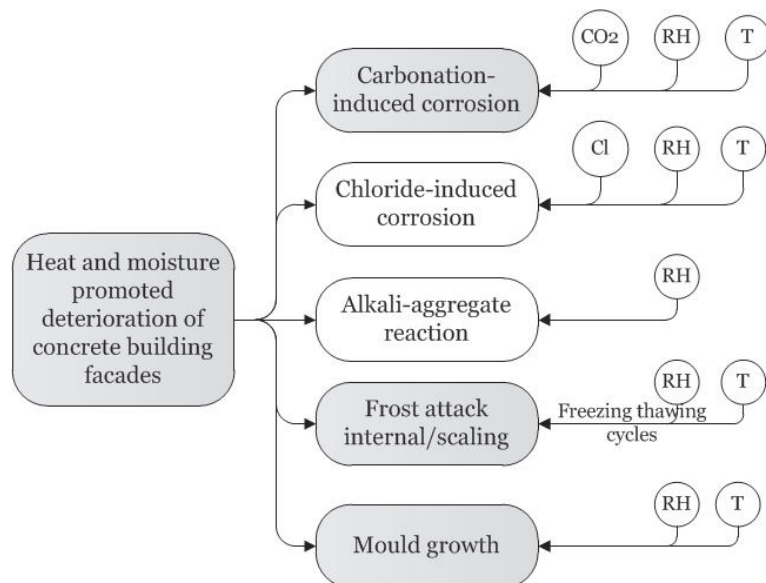


Figure 2.9: Overview of mechanisms leading to deterioration of concrete building facades and the environmental parameters that affect them.

Lambert (2002) described the deterioration mechanisms as chemical reactions in the concrete with the formation of products greater in volume than the reactants producing physical effects such as cracking and spalling. The deterioration occurs in three separate stages:

- i) **Stage 1: Initiation period** – Concentration of aggressive species is insufficient to initiate any chemical reactions or the chemical reaction occurs very slowly. No physical damage has occurred. The duration may vary from a few minutes to the design life of the structure;
- ii) **Stage 2: Propagation period** – Chemical reactions begin or continue; some physical damage may occur but is insufficient to cause distress. The acceleration of the deterioration process usually occurs during this stage as a result of the increased accessibility of aggressive ions or modification of the concrete environment;
- iii) **Stage 3: Deterioration** – Breakdown of the fabric of the structure. The combined effects of the physical and chemical processes cause the structure to cease to be serviceable (failure occurs) and major remedial work or, in extreme cases, demolition is required.

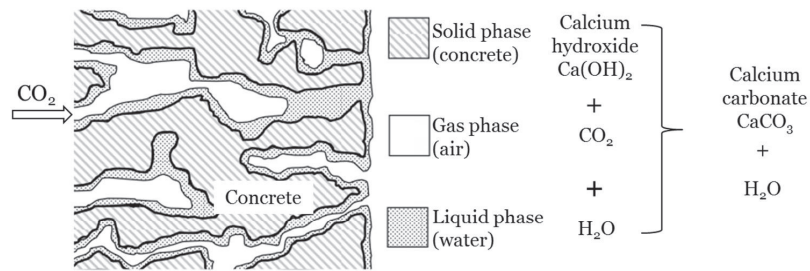
### **2.6.1 Carbonation of concrete**

A common reason for the degradation of reinforced concrete facades through corrosion of the steel reinforcement is the carbonation of concrete. Carbonation is the formation of calcium carbonate by a chemical reaction in the concrete. This phenomenon leads to depassivation of the reinforcement, which can start to corrode when oxygen and moisture are present.

#### **Carbonation process of concrete**

In concrete, carbonation occurs because the compounds containing calcium are attacked by the carbon dioxide in the air and converted to calcium carbonate. The creation of calcium carbonate, as shown in Figure 2.10, requires three equally important substances: carbon dioxide, calcium phases, and water. Carbon dioxide is present in the surrounding air, calcium phases, mainly calcium hydroxide  $\text{Ca}(\text{OH})_2$

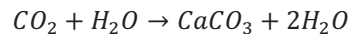
and calcium silicate hydrate -  $\text{CaO} \cdot \text{SiO}_2 \cdot \text{H}_2\text{O}$  - (CSH), are present in the cement paste, and water is present in the pores of the concrete.



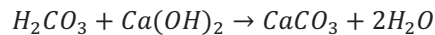
Step 1:	Step 2:	Step 3:
Diffusion inwards of $\text{CO}_2$	Reaction between $\text{CO}_2$ and water molecules	Reaction between resultant $\text{H}_2\text{CO}_3$ and the $\text{Ca(OH)}_2$ of concrete resulting in calcium carbonate $\text{CaCO}_3$ and water

Figure 2.10: Schematic diagram showing the carbonation process on concrete.

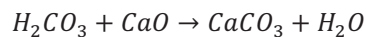
The first reaction is in the pores, where carbon dioxide and water react to form carbonic acid ( $\text{H}_2\text{CO}_3$ ):



The carbonic acid then reacts with the calcium phases:



Once the  $\text{Ca(OH)}_2$  has converted and is missing from the cement paste hydrated CSH will liberate  $\text{CaO}$ , which will then also carbonate:



When these reactions take place, the pH value will start falling. The normal pH value of concrete is above 13 and the pH value of fully carbonated concrete is below 9. Once the carbonation process reaches the reinforcement and the pH value drops beneath 13 the passive “film” on the re-bars will deteriorate and the initiation of propagation corrosion is possible.

### Factors affecting carbonation

Soroka (1994) explained that the rate of carbonation is determined by the rate of diffusion of carbon dioxide into the concrete. In turn, this diffusion depends on the porosity of the concrete and its moisture content. Hence, the rate of carbonation depends on the very

same factors. The rate of carbonation is mainly influenced by the permeability and alkali content of the concrete, as well as ambient atmospheric conditions such as the amount of carbon dioxide available and the relative humidity and temperature (Naik et al. 2010).

The carbonation process has an ongoing need for carbon dioxide from the atmosphere. For carbonation to spread fresh carbon dioxide from the surface needs to be supplied continuously and deeper and deeper into the concrete. Low porosity and permeability will reduce the speed of ingress of carbon dioxide, thereby delaying the ingress of the carbonation. The exposure conditions, particularly the relative humidity, have a significant effect on the depth and amount of CO<sub>2</sub> absorbed over time. In general, carbonation only occurs when the relative humidity is between 40 and 90%. If the humidity is less than 40%, then the CO<sub>2</sub> cannot dissolve in water to form the carbonic acid needed to react with the calcium compounds. If the humidity is higher than 90%, then the CO<sub>2</sub> cannot enter the saturated pores. Within the 40 to 90% range, shown in Figure 2.11, the humidity leads to a higher CO<sub>2</sub> absorption and thus a greater carbonation rate. (Bertolini et al. 2004)

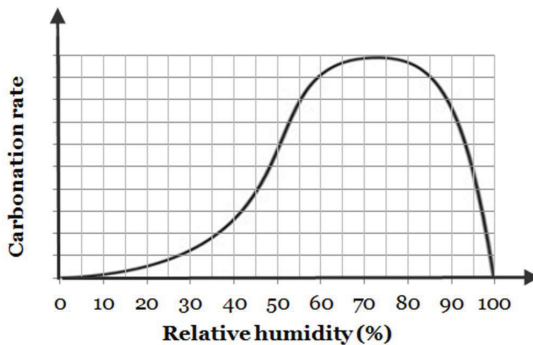


Figure 2.11: Schematic representation of the rate of carbonation as a function of the relative humidity. (Tuutti 1982)

Soroka (1994) emphasises that the effect of temperature on carbonation in the range 5–20°C is very small, while the carbonation increases with temperatures between 20 and 30°C.

The porosity of concrete is determined by the water-to-cement ratio and the degree of hydration. The degree of hydration is influenced by

the length of the curing time and the effectiveness of the curing. The carbonation rate will increase with an increase in the water-to-cement ratio and a decrease in the length of the curing time. However, curing periods longer than 7 days hardly affect the rate of carbonation significantly (Soroka 1994).

### 2.6.2 Corrosion of steel in concrete as a result of carbonation

The corrosion of steel in concrete is mostly associated with chloride ions. However, another cause of steel corrosion is the carbonation of the concrete cover that protects the reinforcement. Carbonation-induced corrosion tends to develop later and proceeds at slower rates than chloride-induced corrosion and leads to uniform steel corrosion that would accelerate the formation of cracks and reduce the structure's remaining service life. In non-marine environments, carbonation-induced corrosion would be the main corrosion mechanism in reinforced concrete. (Moreno et al. 2006)

In concrete, the presence of calcium hydroxide and relatively small amounts of alkali elements such as sodium and potassium gives concrete a high alkalinity with a pH of 13. The presence of carbonation reduces the alkalinity of the concrete to a pH value below 9 and the reinforcing steel starts to corrode. The corrosion of the concrete reinforcement as a function of the alkalinity of the concrete is shown in Figure 2.12.

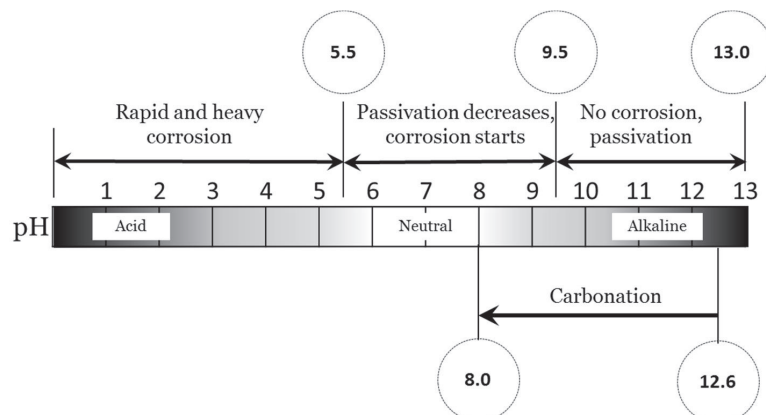
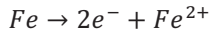


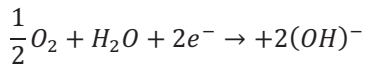
Figure 2.12: Corrosion of steel in concrete as a function of the alkalinity of the concrete.

## The corrosion process

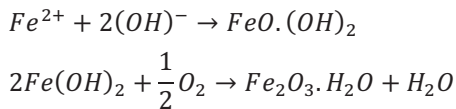
Corrosion is an electrochemical process involving the flow of charges (electrons and ions). At active sites on the bar called anodes, iron atoms lose electrons and move into the surrounding concrete as ferrous ions. This process is called a half-cell oxidation reaction or an anodic reaction and is represented as:



The electrons remain in the bar and flow to sites called cathodes, where they combine with water and oxygen in the concrete. The reaction at the cathode is called a reduction reaction. A common reduction reaction is:



To maintain electrical neutrality the ferrous ions migrate through the concrete pore water to these cathodic sites, where they combine to form iron hydroxides or rust:



This initial precipitated hydroxide tends to react further with oxygen to form higher oxides.

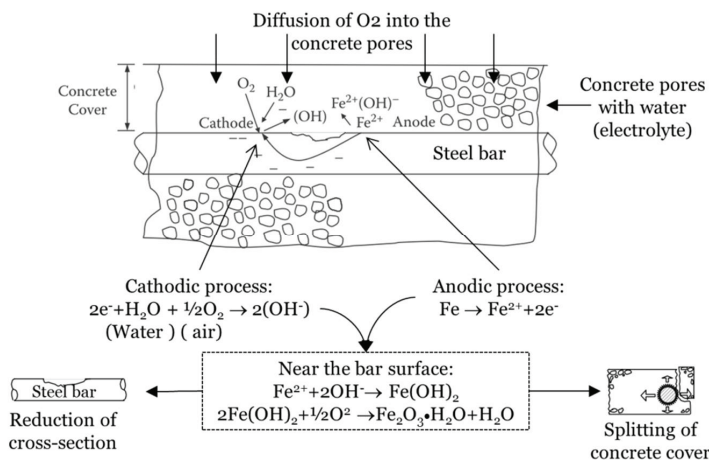


Figure 2.13: Mechanism and results of corrosion of steel in concrete (Papadakis 2005).



The effect of carbonation on concrete is to reduce the pH of the pore water in the cement matrix to a value of below 9. Once the carbonation front has reached the reinforcement, it destroys the thin protective and passive oxide film that formed on the steel surface during the cement hydration process. Corrosion can occur if oxygen and water are present. A schematic description of the carbonation of concrete and the resulting corrosion of the steel rebar is presented in Figure 2.14.

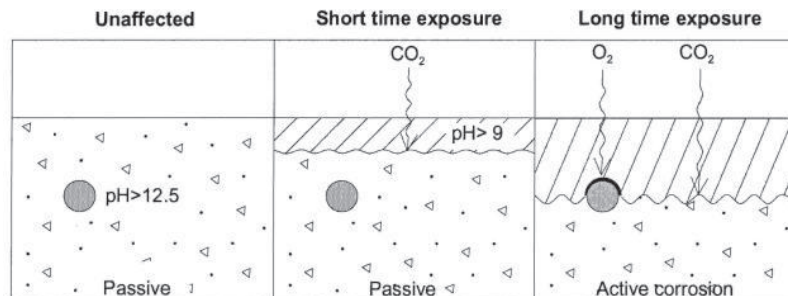


Figure 2.14: Schematic description of the mechanism of corrosion by carbonation.

Further, the concrete cover is cracked and these cracks provide additional paths for the ingress of carbon dioxide ( $\text{CO}_2$ ) to the steel surface, causing local depassivation. Thus, even though the carbonation front may not have reached the surface of the steel, corrosion can occur locally at cracks, causing spalling of the concrete cover. (Muller et al. 2009)

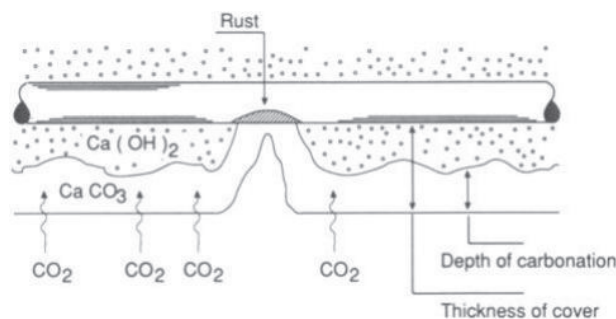


Figure 2.15: Schematic depiction of the mechanism of corrosion by carbonation at the cracked concrete cover (Soroka 1994)

The transformation of metallic iron to ferric oxide ( $\text{Fe}_2\text{O}_3$  - rust) is associated with an increase in volume. The increase in volume

associated with the transformation can cause cracking, spalling, and delamination of the concrete that can be visible in the form of rust spots, cracks in the concrete cover along the line of the bars, spalling, and delamination. The corrosion of the reinforcements causes a loss of steel cross-section and/or a loss of the bond between the steel and concrete, which could lead to a reduction in the structural strength and risks relating to its serviceability. Figure 2.16 summarises the effects of corrosion on reinforced concrete structures (Naus 2007).

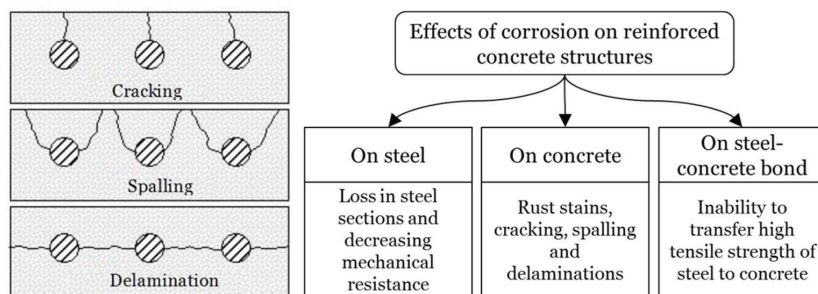


Figure 2.16: Effects of corrosion on reinforced concrete structures (Naus 2007).

### Factors influencing the corrosion rate

Once the corrosion resulting from the carbonation of the reinforcements is initiated, the factors influencing the corrosion rate include: (i) the availability of water and oxygen; (ii) the resistivity of the concrete; (iii) the temperature, and (iv) the relative humidity (both internal and external).

The availability of oxygen is a function of its rate of diffusion through the concrete, which is dependent on the saturation of the concrete. When concrete is totally submerged, the diffusion rate is slowed because the oxygen must diffuse through the pore water. When the concrete is dry, the oxygen can move freely through the pores. Alternating wet-dry cycles accelerate the corrosion process. Wet concrete has a lower resistivity than dry concrete because of the presence of water as an electrolyte. (Smith and Virmani 2000)

Broomfield and Millard (2002) pointed out that the electrical resistivity of concrete affects the rate of electric current (or migration of ions) driven by the potential differences between the cathodic and

anodic areas. This current is equal to the rate of corrosion. Hence, the corrosion current may be controlled by the resistivity. The factors influencing the ionic conductivity/resistivity of concrete include the internal relative humidity, the amount of free water, the amount of connected porosity in the cement paste, and the ionic strength of the pore water.

Temperature affects the corrosion rate, as well as all chemical reactions, directly. A general rule of thumb is that a 10°C increase in temperature roughly doubles the chemical reaction rate. The rate of corrosion significantly increases with an increase in temperature of the normal ambient temperature range but at high temperatures (probably around 40°C) the corrosion rate starts to decrease as a result of a lack of oxygen because the solubility of oxygen decreases with an increase in temperature. (Markeset 2009)

This effect of temperature on the corrosion rate is indicated in Figure 2.17, where the rate of corrosion is measured by the intensity of the corrosion current. Soroka (1994) explained that the effect of temperature on the rate of corrosion is negligible at the lower range of relative humidity and becomes significant at 85%RH and very significant at 95%RH.

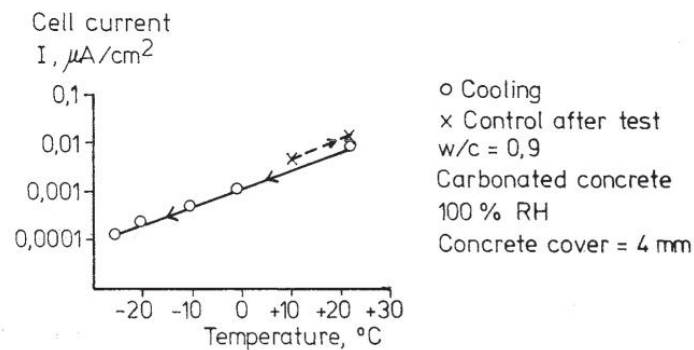


Figure 2.17: Effect of the temperature on corrosion rate at 100% relative humidity (Tuutti, 1982)

The effect of relative humidity on the rate of corrosion is presented in Figure 2.18. Bertolini et al. (2004) assumed that the corrosion propagates only while concrete is wet (relative humidity greater than 80%). Smith and Virmani (2000) also pointed out that an internal

relative humidity of 70 to 80% is essential to maintain corrosion activity and active corrosion does not occur below this level of relative humidity.

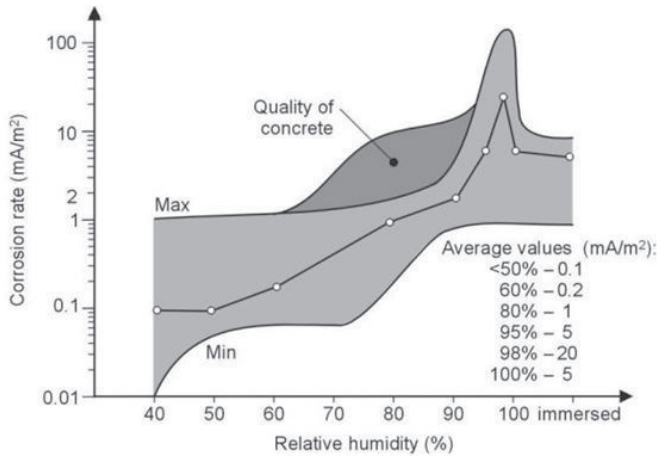


Figure 2.18: Corrosion rate in carbonated concrete as a function of relative humidity (Page, 1992)

A comparison between Figure 2.11 and Figure 2.18 shows that when the carbonation rate is at its highest the rate of corrosion is modest. Whether long dry and wet periods exist depends on the climate. In the “coastal” climate in Northern Europe dry periods are typically as short as a week. In Southern Europe, however, long dry seasons (summer) and long wet seasons (winter) occur. The latter climate is more probable to cause corrosion damage because of carbonation with regard to atmospheric structures. (Bertolini et al. 2004)

### 2.6.3 Damage caused by repeated freezing and thawing

In cold climates, physical damage to concrete structures resulting from frost action is a major concern requiring expensive repair and maintenance. This literature review includes the mechanism of damage to concrete caused by freezing and thawing and the main factors that influence the frost durability of concrete used in building facades.

The problem is common to all porous materials but the degree of damage depends on the pore system. Damage caused by freezing and thawing appears as degradation of the surface, including severe cracking and internal damage extending into the concrete. The basic

types of damage caused by freezing and thawing illustrated in Figure 2.19 are surface scaling, pop-outs, D-cracking, and internal damage. (Harrison et al. 2001)

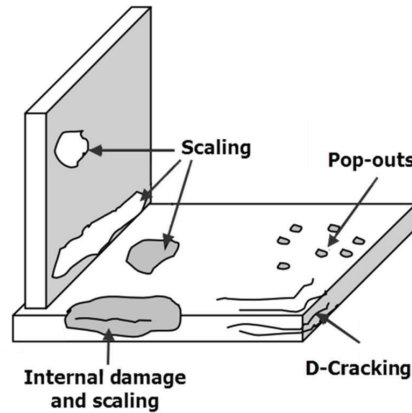


Figure 2.19: Examples of the types of damage caused by freezing and thawing.

The effect of de-icing agents on frost damage is not discussed, as the focus was on frost damage to concrete building facades.

### **Mechanism of freeze and thaw damage in concrete**

Many theoretical and experimental studies have been performed to characterise the frost resistance of concrete. Various theories have been developed to explain the deterioration of concrete as a result of freezing and thawing. The different freeze and thaw damage mechanisms can be divided into:

- i) hydraulic pressure theory: freezing of water and volume expansion of 9% in the pore space, which is the main risk in saturated concrete;
- ii) the ice lens growth theory: micro-ice lens formation in bigger pores as a result of the migration of water from fine to coarse pores;
- iii) osmotic pressure theory: water moves from the gel pores to the capillary pores according to the theory of osmosis;
- iv) thermodynamics and surface force considerations theory;
- v) the hindered movement mechanism (Litvan's theory).

**The hydraulic pressure theory** (also known as Powers' theory) is based on the fact that water expands 9% by volume during freezing. When water freezes in a porous medium the growth of ice crystals puts pressure on the pore walls. If this pressure exceeds the tensile strength of the pore walls, cracking will occur. The magnitude of the hydraulic pressure depends on the rate of freezing, the degree of saturation, the pore structure, and the length of the flow path to the nearest void for the water to escape (Wessman 1997).

**The ice lens growth theory** is based on the formation of ice in larger pores during the cooling of concrete. Water will then be withdrawn from the smaller neighbouring pores to make the ice crystal grow. The process continues as long as the energy level of the ice is lower than the energy level of the water in the finer pores. Microscopic ice lenses inside individual pores will develop, causing damage. Ice lenses will grow in all pores where ice is present. Lens growth is favoured by the increased duration of the freezing period. (Laugesen 1996 and Wessman 1997)

**The osmotic pressure theory** stated that during freezing water moves from the gel pores to the capillary pores according to the theory of osmosis (diffusion along concentration gradients). Water flow along ion concentration gradients can also occur during freezing. The water in capillary pores is not pure water but a solution of various ions dissolved in water. Ice, on the other hand, is pure water. Therefore, when ice forms in a capillary the concentration of the remaining unfrozen pore solution increases and a concentration gradient is developed. Even if the capillary is full of ice, water will flow from the gel (less concentrated) to the capillary (more concentrated) to equalise the pore solution concentration. This osmotic movement of water generates pressure towards the capillary pores. The total pressure required to force the capillary water out of the pores will be a combination of hydraulic pressure and osmotic pressure, which would contribute to stressing the concrete. (ACI 201.2R-08 2008)

**The thermodynamics and surface force considerations theory** is based on the movement of water during freezing from the gel pores to the capillary pores according to the laws of

thermodynamics (diffusion from high to low free energy). The freezing temperature of the water depends on the size of the pore. The water in the largest pores freezes first and the water in the small pores cannot freeze or would freeze at a very low temperature as a result of the high surface forces. The water in the gel pores (1-30 nm) cannot freeze at temperatures above  $-78^{\circ}\text{C}$ . At temperatures below  $0^{\circ}\text{C}$  the water has a higher free energy than ice; therefore water will flow from the gel to the capillaries along a free energy gradient in order to freeze. If sufficient water flows to the capillaries and freezes, the capillary will become full and pressure will develop. This pressure increases the free energy of the ice (or ice and water) in the capillary. Water will continue to flow to the capillary until the free energy of the ice and water in the capillary equals the free energy of water in the gel pores. As a result drying shrinkage or cracks occur in the gel structure, while ice accumulates in the large pores, leading to the formation of new cracks or the extension of old ones. (Yang et al. 2004)

**The hindered movement mechanism (Litvan's theory)** is an assumption that the water in capillary pores does not freeze in situ when the temperature of the concrete decreases below  $0^{\circ}\text{C}$ . This water is super-cooled, which tends to cause drying of the paste because the vapour (or saturation) pressure over super-cooled water is higher than over ice. The forced movement of water is caused by the vapour pressure difference. The forced movement of water creates significant internal stresses. Frost action on saturated hardened cement paste thus creates a non-equilibrium situation which lasts as long as the pressure of water vapour in the capillary pores has not decreased sufficiently, i.e. as long as it has not reached the value corresponding to that of ice. (Pigeon and Pleau 1995)

### **Factors that affect the frost damage to concrete**

As shown in Table 2.7, Schulson (1998) summarised the factors that affect the freezing-thawing damage to concrete as internal factors that depend on the properties of the concrete and external factors that depend on the environment it is exposed to.

Table 2.7: Summary of the factors that affect the freezing and thawing damage to concrete.

<b>Internal factors (Properties of concrete)</b>	Water-to-cement ratio (Major effect)
	Entrained air (Major effect)
	Aggregate
	Type of cement
	Silica fume
	Pore size distribution
<b>External factors (Environmental factors)</b>	Degree of saturation (Major effect)
	Freezing rate
	Minimum temperature
	Freezing holding time
	Curing temperature
	Freezing and thawing cycles

The dominant material properties that affect the freezing and thawing durability of concrete are the amount of freezable water, the availability of empty space, the permeability of the concrete, and the strength of the concrete.

The water-to-cement ratio determines not only the total capillary porosity, but also the pore size distribution. The lower the ratio, the lower the porosity and permeability and the greater the resistance to freezing-thawing damage (Laugesen et al. 1996).

Entrained air is another major factor affecting the freezing and thawing damage of concrete. When it is intentionally incorporated to around 5-7% of the volume of the concrete and appropriately distributed, ice damage can be greatly suppressed (Pigeon and Pleau 1995).

The freezing point of water in a pore is lower if the pore diameter is small. The water in the capillary pores of concrete structures starts to freeze at a temperature of  $-5^{\circ}\text{C}$  when the ambient relative humidity is 95%. At freezing temperatures of  $-10^{\circ}\text{C}$  to  $-20^{\circ}\text{C}$  neither the water in the gel pores nor the water in the finest capillaries freezes. Table 2.8 shows some examples of the relation between the pore diameter and the freezing point (Fagerlund 2001).



Table 2.8: Relation between the pore diameter, the corresponding relative humidity when capillary condensation takes place in the pore, and the freezing point (Fagerlund 2001).

<b>Pore diameter</b>	<b>Relative humidity</b>	<b>Freezing point</b>
<b>(nm)</b>	<b>RH (%)</b>	<b>(°C)</b>
45	95	-6
28	92	-10
20	88	-15
16	85	-20
11.5	80	-30
9.5	76	-40

The degree of saturation is the ratio between the absorbed, freezable water and the total available space (volume of water plus available air-filled capillary pores and air voids). The critical degree of saturation is the limit above which the amount of water causes damage on freezing. Fagerlund (1977), cited in Laugesen et al. (1996), recommended a range from 0.75 to 0.90 as the critical degree of saturation for ordinary concrete.

### **Dilation of concrete during freezing and thawing**

The thermal dilation upon a change of temperature in any uniform isotropic linear-elastic material can be directly calculated using the thermal coefficient of linear expansion. However, such a generalisation is not valid for concrete because of its porosity and composite nature. Thermal dilation in concrete upon a change of temperature depends on the thermal expansions of the individual components and that in the presence of other components. (Bishnoi 2004) In general, thermal dilation in concrete is dependent on three components: the response of the solid skeleton to thermal change, the response of the aggregates, and the response of the internal moisture (Grasley 2003).

Miura and Lee (1991), cited in Bishnoi (2004), reported experimental results dividing the variations in thermal dilation with temperature into four major zones.

- i) At temperatures higher than  $-20^{\circ}\text{C}$  concrete was found to follow an almost linear contraction. This was explained by

the accommodation of the relatively small amount of frozen water in the available void spaces.

- ii) In the range between  $-20^{\circ}\text{C}$  and  $-50^{\circ}\text{C}$  expansion was found to occur in concrete, reportedly as a result of the formation of ice in most micro-pores and the initiation of micro-cracks.
- iii) At temperatures lower than  $-50^{\circ}\text{C}$  since most of the freezable water is already frozen and concrete is reported to again exhibit a linear contraction.
- iv) Upon heating back to higher temperatures strains in the concrete were found to increase along a different path than during cooling and hysteresis in the strain-temperature curve was observed.

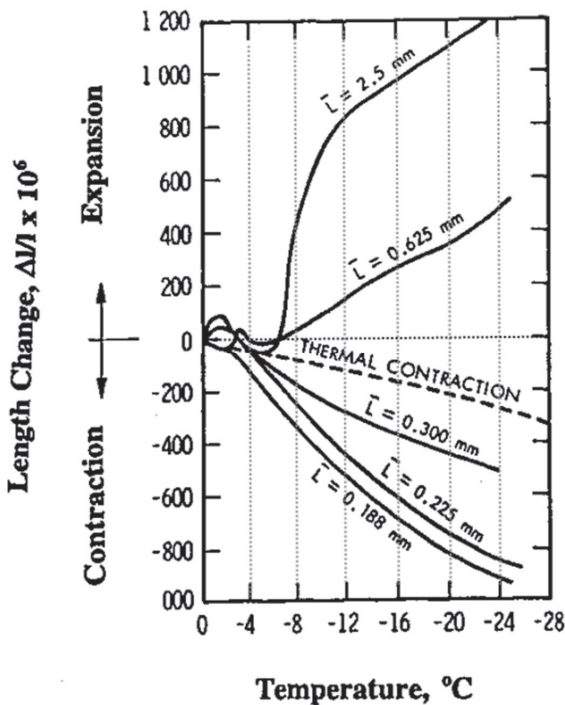


Figure 2.20: Length changes as a result of freezing of cement pastes of different entrained air contents ( $L$  spacing factor) (Ramachandran and Beaudoin 2001).

The effect of the air void system (air content) on the thermal dilation of concrete is shown in Figure 2.20. For length change measurements on cooling ( $0.25^{\circ}\text{C}/\text{min}$ ) relatively thick specimens with different air-void spacing, but with similar porosity, shrinkage occurred in specimens with a pore spacing factor of  $0.30\text{ mm}$  or lower. These

specimens were saturated (except for the entrained space) and, therefore, the existence of closely-spaced air pores provided sites for water to migrate and for ice crystals to grow without the imposition of stress. (Ramachandran and Beaudoin 2001)

Sakyi-Bekoe (2008) pointed out that the coefficient of thermal expansion of concrete is an important fundamental property of concrete, and one which is used in the analysis and design of concrete structures. The coefficient of thermal expansion can influence the early-age cracking, fatigue cracking, faulting, and joint spalling that occur in concrete structures.

#### **2.6.4 Mould growth on concrete building facades**

Mould growth has mostly been associated with organic materials such as wood and materials with organic components such as gypsum boards with paper surfaces (Hyvärinen et al. (2002), as cited in Li (2007)). Mould growth can also be found on inorganic materials such as concrete and brickwork. The reasons might be dust or some other particles containing organic fragments that have gathered on the surface of such materials, which provide nutrition for mould growth. There might also be other nutrients, such as nitrogen, in the materials, which provide an extra trigger for mould growth. (Li 2007)

Johansson et al. (2010) found out that many facades made with thin rendering on thermal insulation have problems with biological growth. The problem of mould growth on concrete building facades is a complex phenomenon involving a number of interacting factors related to both the organic and non-organic conditions of the facade system. The interacting factors affecting mould growth are biological factors, such as organic nutrition and organisms, and non-biological factors, such as temperature and relative humidity.

The exterior corners of concrete building facades are common locations for mould growth in hot climates and in poorly insulated buildings in cold climates. They tend to be closer to the outdoor temperature than other parts of the building surface for one or more of the following reasons:

- poor interior air circulation
- exterior wind-washing

- low insulation levels
- greater surface area of heat loss

As shown in Figure 2.21, organic building materials such as paper and wood are sensitive to mould growth when exposed to high humidity conditions or a water damage situation (relative humidity greater than 97%). Stone-based materials such as concrete and bricks are more tolerant of mould growth but the organic dust or material accumulated on their surfaces will change the properties of those surfaces and make it suitable for mould to grow. Under lower humidity conditions of around RH 90% mould growth in mineral wool and concrete is very low (Viitanen et al. 2009).

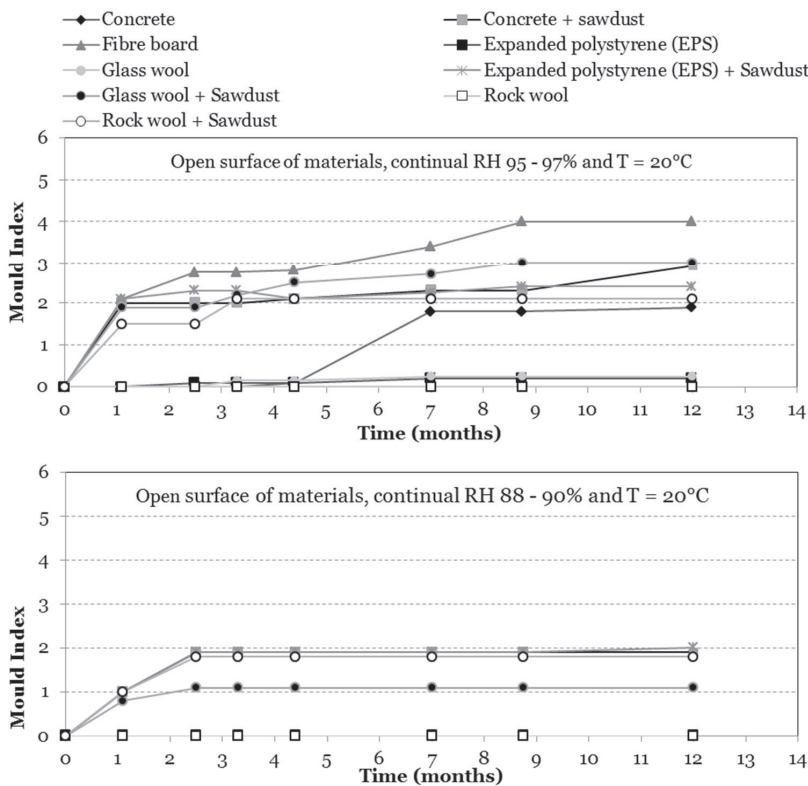


Figure 2.21: Response of building material to mould growth at 88-97% relative humidity and a temperature of 20°C. (Viitanen and Ojanen 2007)

### 2.6.5 Alkali-Silica Reaction

Alkali-aggregate reactions result when alkalis normally present in cement react with siliceous aggregates in concrete that is exposed to moisture. The reaction produces a gel that develops over years or

decades until the forces created expand and crack the concrete. (Lemieux and Totten 2010) The Alkali-Silica Reaction (ASR) is a chemical reaction between the alkalis in concrete pore solutions and certain siliceous aggregates. These aggregates, when placed in a highly alkaline solution and in the presence of water and calcium, will expand and a gel will begin to form. As the aggregate particle expands, it causes the concrete to crack. As the concrete deteriorates, more water enters to fuel the reaction. This cycle continues until the concrete deteriorates past the point of serviceability.

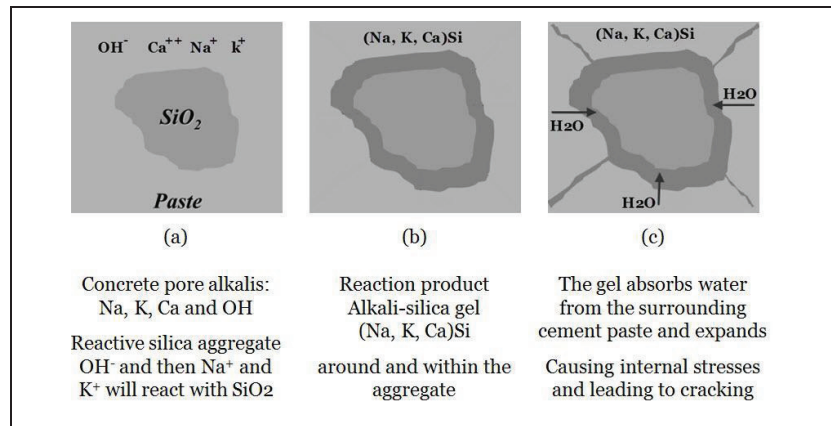


Figure 2.22: Sequence of Alkali-Silica Reaction (ASR) in concrete.

Folliard et al. (2003) summarised the factors that affect the rate and severity of the Alkali-Silica Reaction (ASR) as:

- the alkali content of the cement,
- the potential alkali reactivity of the aggregate,
- the amount of water present in the concrete and
- the number of wet/dry cycles.

The alkalis present in cement are in the form of potassium oxide ( $K_2O$ , molecular weight 94.196) and sodium oxide ( $Na_2O$ , molecular weight 61.979). The quantity of alkalis in cement is typically expressed as a total sodium oxide equivalent (or equivalent soda) in terms of per cent by mass of cement. The total sodium oxide equivalent is calculated with the following formula:

$$Na_2O_{eq}(\%) = Na_2 + 0.658 * K_2O$$

A cement with a total sodium oxide equivalent content less than or equal to 0.6% by mass is considered to have a low alkali content.

The Alkali-Silica Reaction can occur only in moist environments. It has been observed that in environments with a relative humidity below 80 and 90% alkalis and reactive aggregates can co-exist without any damage being caused. The temperature influences the reaction, by favouring it as the temperature increases. (Bertolini et al. 2004)

The Alkali-Silica Reaction is a significant cause of damage to concrete structures in many countries around the world, for instance in the UK, Denmark, Norway, Sweden, France, Belgium, the Netherlands, Canada, and the USA. As concrete is usually made with aggregate from local sources, the experience in each of these countries is based on a particular range of aggregates. (Nijland et al. 2002)

### **3 Monitoring and prediction system (RHT-MAPS)**

This chapter provides an overview of the relative humidity and temperature monitoring and concrete facade deterioration prediction system (RHT-MAPS). In section 3.1, a system from an adjacent research field is reviewed and the motivation for developing the RHT-MAPS system is discussed. In the other sections, the components, the developing process, testing, expenses and evaluation of the RHT-MAPS are covered.

#### **3.1 Review of monitoring and prediction related research**

The development of the RHT-MAPS was motivated by an existing system called COMSY (Condition Oriented ageing and plant life Monitoring System) developed by Framatome ANP GmbH. The COMSY system has been developed to provide a software tool for nuclear power plants ageing management and service life extension activities. It was designed to efficiently establish a virtual data model for nuclear power plant systems, focusing on piping and vessels (Zander and Nopper, 2003).

The COMSY system acquires, manages and evaluates component and operating parameters relevant to ageing management of nuclear power plants. The data related to individual vessel elements, piping elements and systems are stored in a “virtual power plant database model”. Based on these plant data, the program conducts a condition-oriented service life analysis for various degradation mechanisms which are commonly experienced in power plants. Those are for example, material fatigue (transient, stratification and cycling), strain-induced cracking, erosion corrosion, cavitation erosion, droplet impingement erosion, stress induced corrosion

cracking, pitting, crevice corrosion and microbiologically influenced corrosion (MIC). This process, shown in Figure 3.1, is supported via (i) a user graphic interface, (ii) analysis functions, (iii) comprehensive material libraries, (iv) a module for management and evaluation of examination results and (v) a probabilistic tool which allows to prioritize and to optimize the inspection date by means of risks and costs criteria. (Zander et al. 2007)

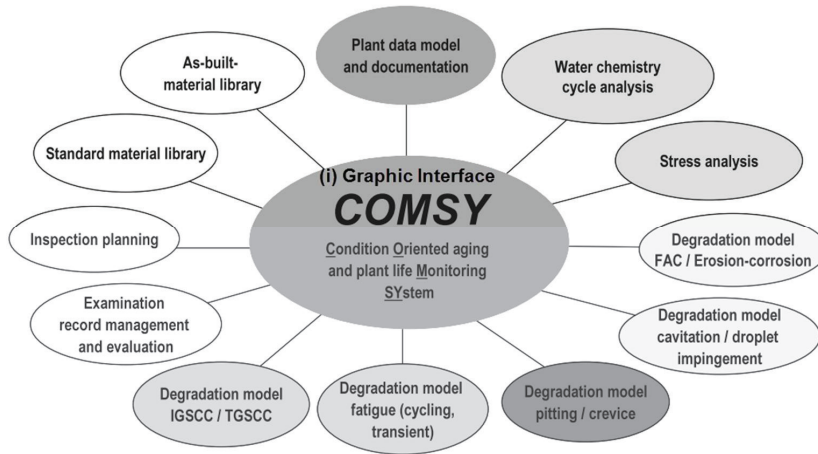


Figure 3.1: Comsy software modules (Zander, 2009).

Service life prediction is the key function of COMSY software system for ageing and service life management. On this basis, maintenance management and plant availability could be optimized and the service life of components extended. The preparation of deterioration models assumes a detailed understanding of the type of deteriorations concerned as well as the functional interactions of the relevant parameters that influence the rate of degradation progression.

Implementation of COMSY software tool for the life management of piping system requires information concerning the design of piping system and monitoring their operating conditions in site. Based on this information a prediction of the components remaining service life can be performed, if the relevant degradation mechanism has been understood.



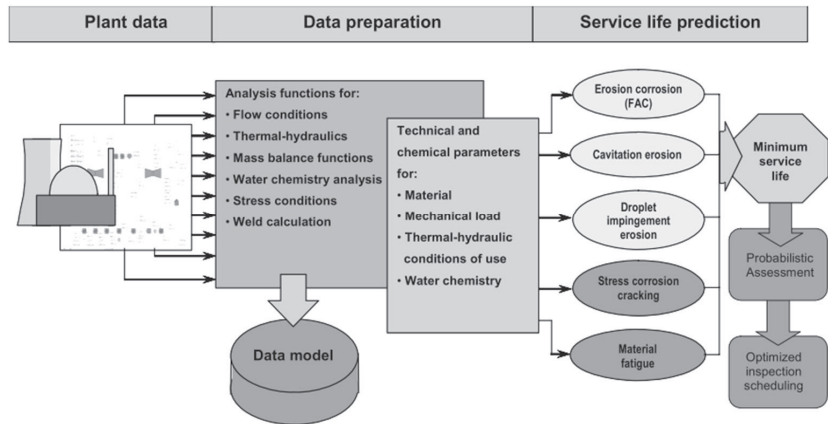


Figure 3.2: Overview of the service life prediction process using COMSY system. (Zander, 2009).

The COMSY system, which utilizes more than 25 years of experience resulting from research activities and operational experiences, was the start point for designing a new system for monitoring and predicting the service life of concrete structures, especially concrete building facades. The deterioration processes of the concrete facades occur very slowly and depend on the exposure conditions and the quality of their building materials. For the previous reasons, the developed monitoring system must include a module for monitoring of the hygrothermal behaviour of facade components, a database of the building materials, a module for evaluating the monitoring results and a module for predicting the deterioration of the concrete building facades.

### 3.2 RHT-MAPS architecture and components

The developing of the RHT-MAPS involves two parts, one concerning automated monitoring of the relative humidity and temperature of building facades, the other concerning the deterioration prediction models utilizing monitoring data. The aim of the RHT-MAPS is to provide a tool for:

- monitoring and quantifying the main environmental parameters affecting the deterioration of concrete building facades,
- analysis of the environmental hygrothermal data and the response of the concrete facade to it, and

- predicting the deterioration of concrete facades, which are reviewed in the literature review of this thesis, on the basis of their hygrothermal behaviour.

The RHT-MAPS consists of two major parts: a sensor network and monitoring and data analysis software. This section describes the design and implementation of the RHT-MAPS sensor network and the RHT-MAPS monitoring and data analysis software.

### 3.2.1 Sensory system

The RHT-MAPS sensor network was built on the LINET “Light Network System” (LINET, 2007). The LINET network is a tool for electronics designers to plan and implement application-specific control and slow data networks. The function of the LINET network was modified so as to be able to monitor the moisture and thermal performance of concrete facades continuously by means of relative humidity and temperature sensors. The components of the LINET network were also modified to be able to communicate with the relative humidity and temperature sensors. The RHT-MAPS sensor network consists of a controller and nodes where relative humidity and temperature sensors are connected. The controller provides configuration services and enables communication with computers to take place. The sensor network may contain up to 200 nodes connected to a twisted-pair CAT5 cable with a maximum total length of 1000 metres. A schematic diagram of the RHT-MAPS sensor network is provided in Figure 3.3.

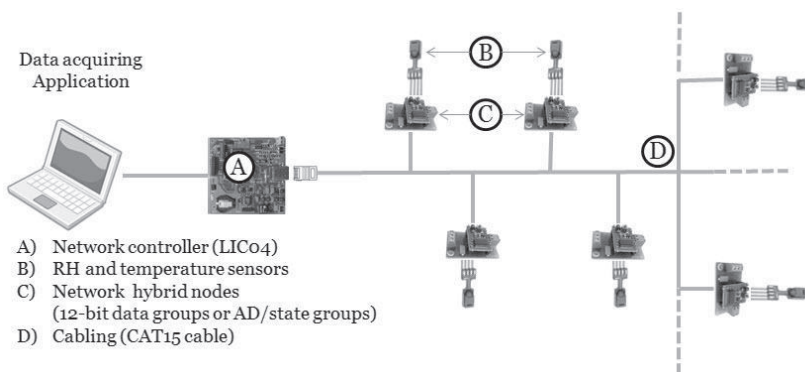


Figure 3.3: Schematic diagram of the RHT-MAPS sensor network.

A full description of the specification of the components of the RHT-MAPS monitoring sensor network and the configuration of its communication system are shown in Appendix A and Appendix B, respectively.

### **The LIC04 controller**

The LIC04 network controller is a stand-alone network power supply and controller for the monitoring network. The LIC04 controller accepts IP/UDP (Internet Protocol/User Datagram Protocol) connections and only transmits data on demand. The controller receives and sends packets in binary format. The data entities are 8- or 16-bit unsigned integers. The same data structure is used to send data to the controller and receive data from it.

The LIC04 network controller contains:

- i) an on-board RISC (Reduced Instruction Set Computer) microcontroller and firmware for running the standard network functions,
- ii) an RS232/RS485 serial interface and an Ethernet interface for connecting to industrial Ethernet or intranet systems,
- iii) an extension bus for a local computer, and
- iv) a real-time clock for stand-alone applications that require timing.

The board display of the LIC04 network controller card is shown in Figure 3.4.

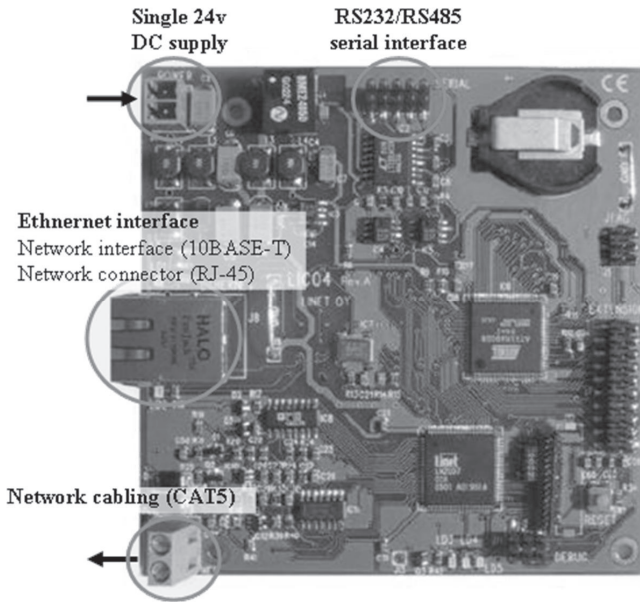


Figure 3.4: Printed circuit board display of the LICo4 network controller card

### The hybrid nodes

A node is a network adapter that incorporates fixed I/O functions for general control network applications. The nodes have a documented hardware interface and the network protocol is embedded in the system. To build distributed intelligence a microcontroller is connected to the node. The node can supply operating power and a clock signal to the microcontroller. In the RHT-MAPS sensor network, each node is configured as a data group.

The nodes used in the RHT-MAPS sensor network are hybrid nodes configured as 12-bit data and analogue-digital AD/state groups. In the data group, each node is capable of receiving and sending binary data at a constant rate. Data exchange with the network controller is handled with 12-bit words. In the AD/state groups, each node contains an integrated 12-bit A/D converter with internal 1.25-V references that convert the output into 12-bit words. The RHT-MAPS sensor network node is shown in Figure 3.5.

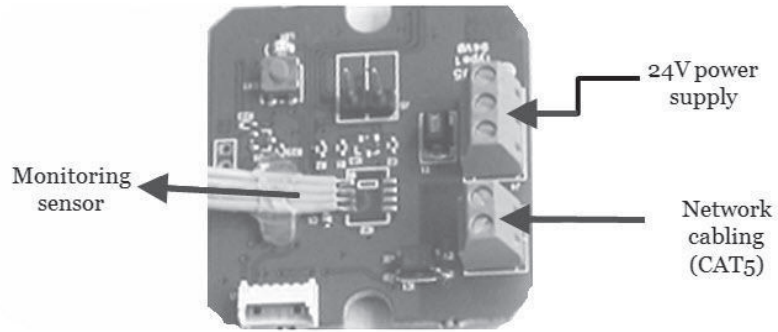


Figure 3.5: The RHT-MAPS sensor network node.

### The network cabling

The type of cable used in the RHT-MAPS sensor network is a standard type known industry-wide as "Category 5 Unshielded Twisted Pair Cable" or "CAT5" for short. Inside the jacket of any grade of unshielded twisted pair cable (UTP) are four individual pairs of wires with the wires of each individual pair twisted around each other in a spiral fashion that helps minimise and cancel out some of the problems that can disrupt data over the wire.

An Ethernet CAT5 cable with an RJ-45 connector is used to connect the controller of the RHT-MAPS sensor network to the internet. An Ethernet crossover cable is used for connecting the controller of the RHT-MAPS sensor network directly to the host computer. The difference in cable wiring between the Ethernet cable and the crossover cable is illustrated in Figure 3.6.

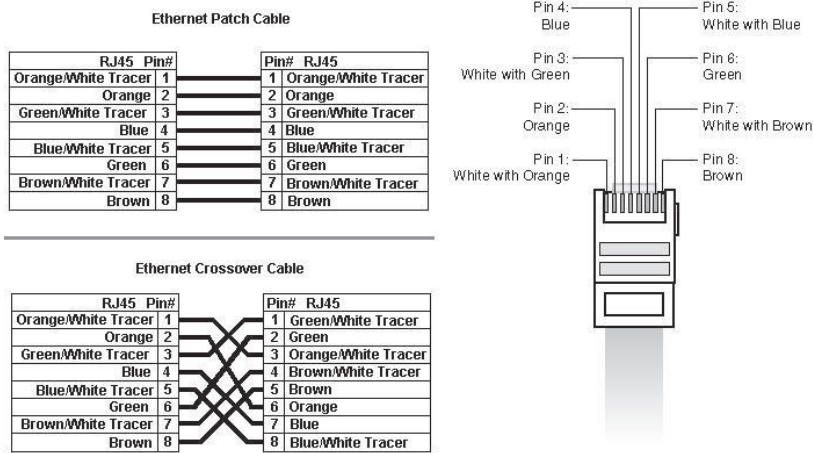


Figure 3.6: Illustration of Ethernet Cables: Straight-through cable and Crossover cable

The cabling is totally topology- and polarity-free and no terminating resistors are needed, which provides maximum flexibility in designing, installing, and modifying the network. The total length behind one network controller (all the segments added together) must not exceed 1000 metres. Furthermore, because of the resistive signal damping only a limited number of nodes per network bus segment length are allowed. Figure 3.7 shows the recommended cable branching approach and the maximum number of nodes per segment .

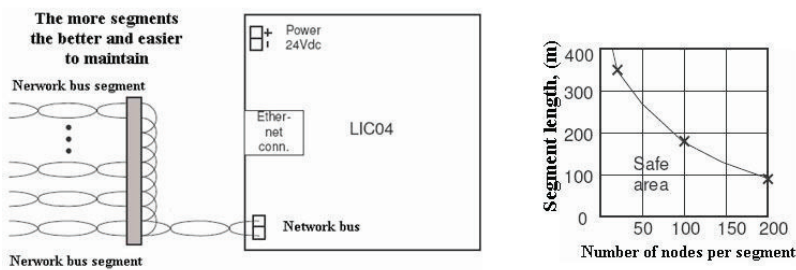


Figure 3.7: The recommended cable branching approach and the maximum number of nodes per segment.

The controller can be located anywhere in the network, as shown in Figure 3.8, but the most favourable location would be in the middle of the network so that the average distance between the nodes and the controller is at its minimum.

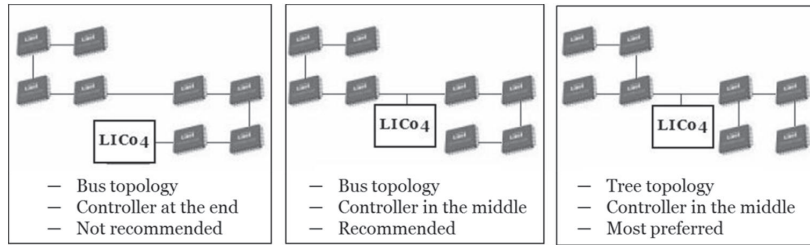





Figure 3.8: RHT-MAPS sensor network topology examples

### The relative humidity and temperature sensors

The relative humidity and temperature sensors were chosen to provide the required functionality for correct system operation. There are a number of sensors available for this type of application. For the RHT-MAPS sensor network, three different types of sensors were selected to be connected to the network nodes for measuring temperature and relative humidity: the temperature was measured using PT100 sensors and relative humidity using HMP44 and SHT15 sensors. The choice of HMP44 and PT100 sensors was made because of their stability and accuracy, along with long experience of using these sensors. SHT15 was selected for its low price and compatibility with the network nodes. The calibrations of the relative humidity sensors were confirmed by the manufacturers. Details of the sensors used in the RHT-MAPS sensor network are shown in Table 3.1.

Table 3.1: Relative humidity and temperature sensors used in the RHT-MAPS sensor network.

Sensor	Manufacturer	Output data	Data group type	
HMP 44	Vaisala Oy, Finland	RH (%)	AD / state	
SHT15	Sensirion AG Switzerland	RH (%) and T (°C)	12 bit data	
PT100	different manufacturers	T (°C)	AD / state	

### 3.2.2 Data acquisition system

The RHT-MAPS monitoring and data analysis software communicates between the host computer and the RHT-MAPS

sensor network controller collects relative humidity and temperature data and processes the monitored data. The software was developed for this thesis at the Laboratory of Structural Engineering and Building Physics using Microsoft Visual Basic 6.0 and runs on Microsoft Windows platforms. It consists of four basic modules: a system configuration module, a telnet simulation module, a data collecting module, and a data processing module. The flow chart of the RHT-MAPS monitoring and data analysis software is shown in Figure 3.9. The RHT-MAPS monitoring software is only presented visually here and more details are presented in Appendix C.

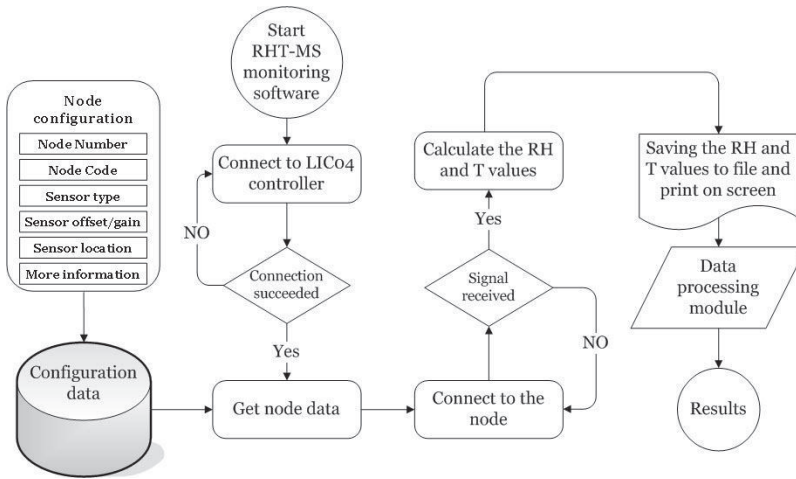


Figure 3.9: Flow chart of RHT-MAPS monitoring and data analysis software.

### System configuration module

The system configuration module contains two parts: the configuration of the monitored target cross-section as shown in Figure 3.10 and the configuration of the sensors and nodes for the RHT-MAPS sensor network as shown in Figure 3.11. The monitored target cross-section configuration includes information about the cross-section code and the numbers of the first and last nodes in the cross-section. The information on the configuration of the monitored target cross-section is stored in a configuration file, “cross-sections.cfg”, which is used by the data-processing module.



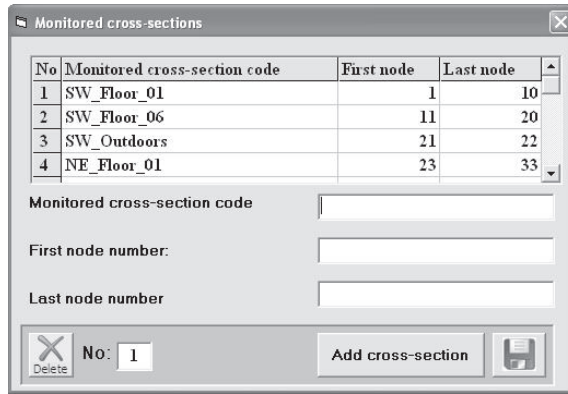


Figure 3.10: Configuration of the monitored target cross-section

The node and sensor configuration includes information such as the node number code, the sensor type, the location of the sensor connected to the node, and the monitored target cross-section code. The information for the node and sensor configuration is stored in a configuration file, “sensors.cfg”, which is used by the RHT-MAPS calculation and output module.

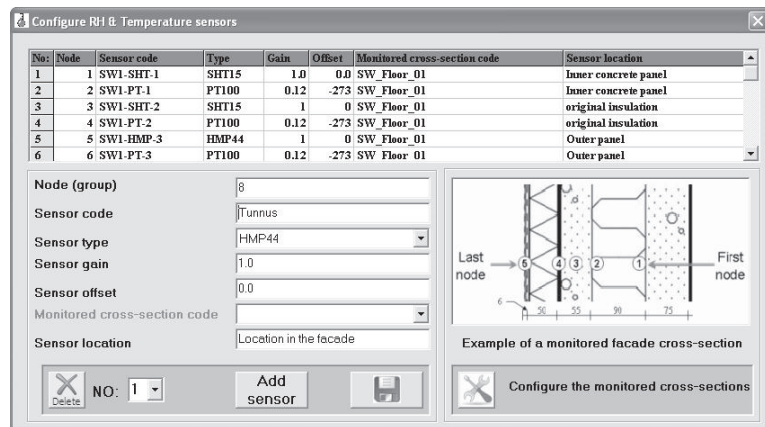


Figure 3.11: Configuration of the sensors and nodes of the RHT-MAPS sensor network.

## Telnet simulation module

The telnet simulation module is used in communication with the LICO4 controller of the RHT-MAPS sensor network. The user inputs information about the IP address of the controller (Internet Protocol address) and the communication port between the LICO4 controller and the host computer. The telnet simulation module sends and

receives data at certain intervals from the LICo4 controller. The telnet simulation module is shown in Figure 3.12.

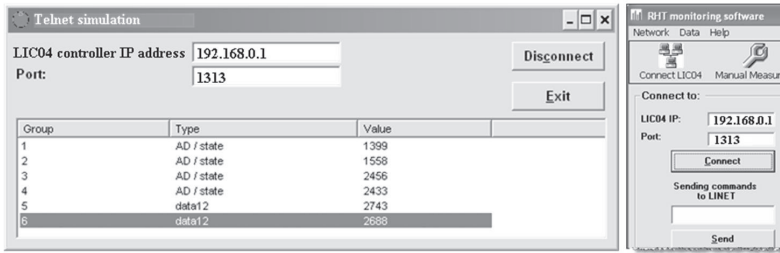


Figure 3.12: The graphical user interface of the Telnet simulation module.

### Data-collecting module

The data-collecting module is used for calculating the temperature and relative humidity monitoring values, saving the resulting values in an ASCII file, and displaying them on the screen. The data-collecting module gets the node and sensor information from the system configuration module, using the information for temperature and relative humidity, while taking into consideration the offset and gain of every sensor. The graphical user interface of the data-collecting module is shown in Figure 3.13.

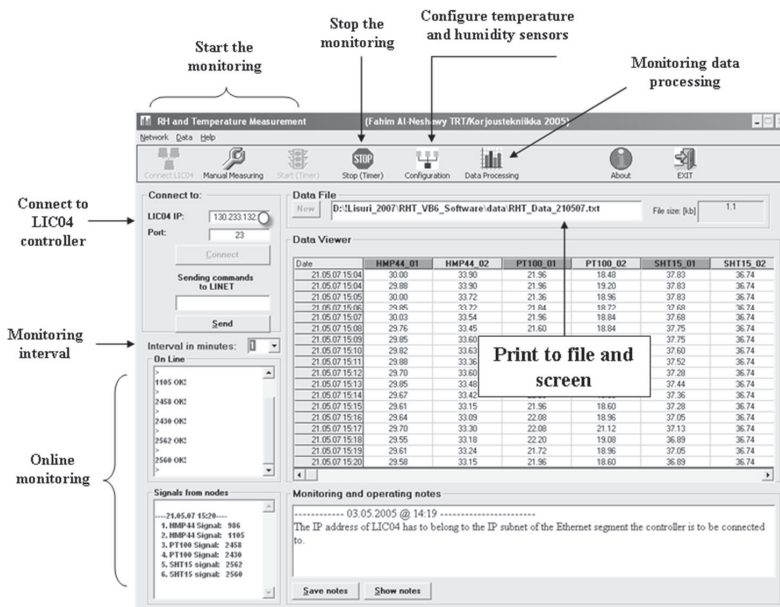


Figure 3.13: The graphical user interface of the data-collecting module.

Equations (3.1) and (3.2) are used to calculate the relative humidity and temperature. The values calculated are displayed on the screen and stored in an ASCII file for later processing.

According to the data sheet of the SHT15 sensor (Sensirion AG 2007), the non-linearity of the humidity sensor is compensated for by using the following quadratic polynomial formula to convert the readout of the sensor SHT15 to a relative humidity value.

$$RH = c_1 + 2 * c_2 * (R_{SHT} - 2048) + c_3 * (R_{SHT} - 2048)^3 \quad (3.1)$$

where

$RH$  is the calculated relative humidity value [%],  
 $R_{SHT}$  is the SHT15 output signal for relative humidity [-], and  
 $c_1$ ,  $c_2$ , and  $c_3$  are the relative humidity conversion coefficients as shown in Table 3.2.

Table 3.2: The relative humidity conversion coefficients for the SHT15 sensor

$R_{SHT}$	$c_1$	$c_2$	$c_3$
12 bit	-4.0	0.0405	$-2.8 * 10^{-6}$
8 bit	-4.0	0.6480	$-7.2 * 10^{-4}$

The relative humidity value for the HMP44 sensor is calculated from the following equation:

$$RH = (0.03 * R_{HMP}) * gain + offset \quad (3.2)$$

where

$RH$  is the calculated relative humidity value [%],  
 $R_{HMP}$  is the HMP44 sensor output signal for relative humidity [-],  
 $gain$  is the calibration gain value of the HMP44 sensor, and  
 $offset$  is the calibration offset value of the HMP44 sensor.

The values of the calibration gain and offset of the HMP44 sensor are unique and are supplied by the manufacturer for each of the sensors. The temperature value for the PT100 sensor is calculated from the following equation:

$$T = R_{PT} * gain + offset \quad [3.3]$$

where

- T is the calculated temperature value [°C],  
 $R_{PT}$  is the PT100 sensor output signal for temperature,  
 gain is the calibration gain value of the PT100 sensor, and  
 offset is the calibration offset value of the PT100 sensor.

The PT100 sensors were calibrated using temperatures of +20°C and +50°C. On the basis of the calibration, the values of the gain and the offset were calculated for each of the sensors.

### 3.2.3 Data-processing and deterioration predicting module

The data-processing and deterioration predicting module was developed using Visual Basic for Applications under Microsoft Excel. A flow chart of the data processing module is shown in Figure 3.14.

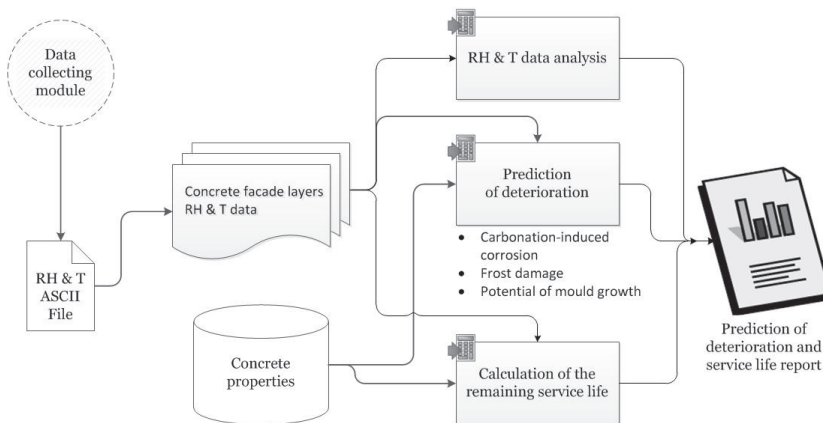


Figure 3.14: The flow chart of the data processing module

As shown in Figure 3.14, the monitored relative humidity and temperature data are processed as follows:

- i) dividing the relative humidity and temperature data being monitored into facade layers and storing the building material information for each layer;
- ii) selecting the facade layer being monitored and its building material and then opening its relative humidity and temperature data file;
- iii) analysing the relative humidity and temperature data for outdoor conditions and analysing the response from each facade layer;

- iv) predicting the deterioration and calculating the remaining service life of the facade layer on the basis of its building material and the relative humidity and temperature data;
- v) transforming the resulting data into graphical charts.

The data-processing and deterioration predicting model represents the implementation of hygrothermal analysis of the concrete facade presented in Chapter 5 and the deterioration prediction models proposed in Chapter 6. The model is composed of data windows based on the deterioration mechanisms highlighted in Figure 2.9. The data-processing model is graphically presented in five different windows as follows:

- 1) input configuration window;
- 2) hygrothermal data analysis window;
- 3) carbonation-induced corrosion window;
- 4) frost damage window;
- 5) potential mould growth window.

The data-processing and deterioration predicting model is presented visually in Figure 3.15 to Figure 3.19.

The input configuration window is where the user defines information about the monitoring data and the concrete types used in the construction of the facade.

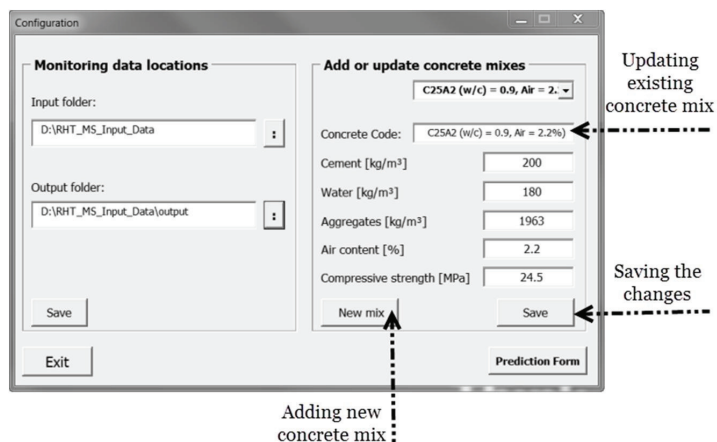


Figure 3.15: The graphical user interface of the input configuration window.

The hygrothermal data analysis window shows the results of the outdoor air analysis and the hygrothermal performance of the concrete building facades.

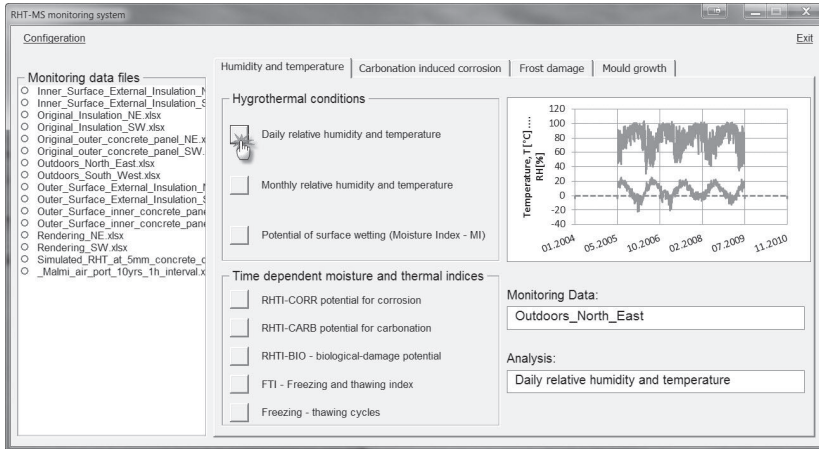


Figure 3.16: The graphical user interface of the hygrothermal data analysis window.

The carbonation-induced corrosion window is where the time-dependent carbonation-induced corrosion data are processed on the basis of the monitored relative humidity and temperature data and the concrete properties of the facade structure. The carbonation-induced corrosion data processing implements the carbonation depth model, which is presented in Chapter 6, Section 6.2.1.

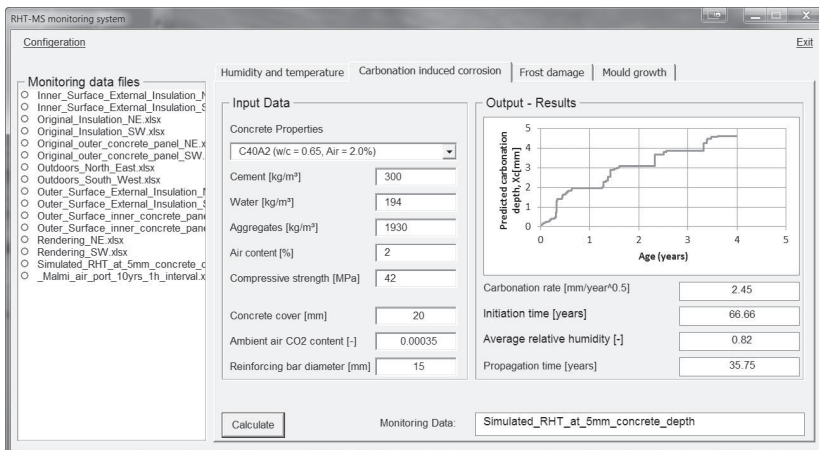


Figure 3.17: The graphical user interface of the carbonation-induced corrosion window.

The frost damage window shows the frost damage and the remaining service life results on the basis of the critical relative humidity and

the frost damage level of the concrete structure. The frost damage data processing implements the frost damage model, which is presented in Chapter 6, Section 6.3.1.

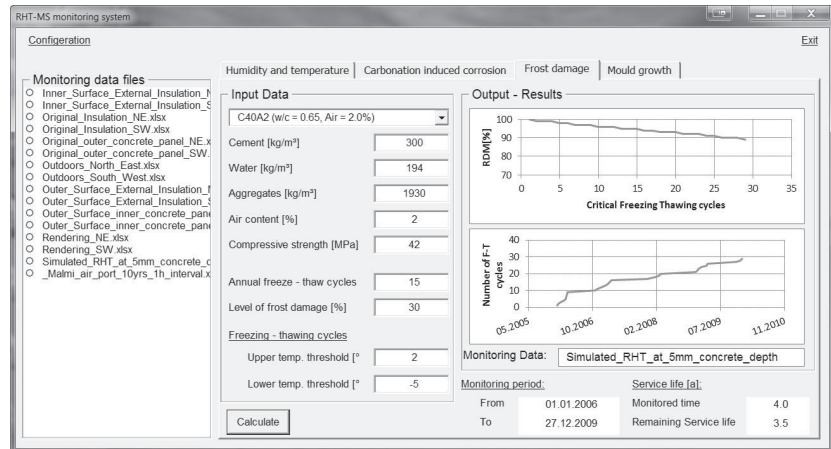


Figure 3.18: The graphical user interface of the frost damage window

The potential mould growth window shows the calculated risk of mould growth on the mineral wool insulation - layer on the basis of the monitored relative humidity and temperature data. The calculation of the risk of mould growth is presented in Chapter 6, Section 6.4.1.

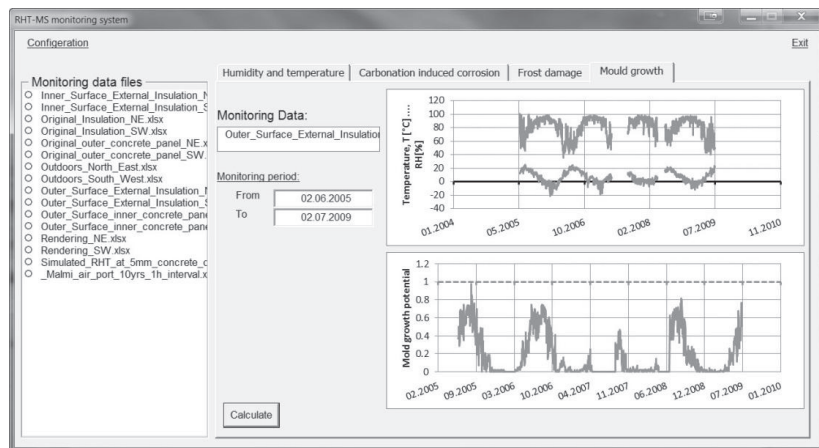


Figure 3.19: The graphical user interface of the potential mould growth window.

### 3.3 RHT-MAPS testing

The purpose of the laboratory tests was to validate and refine the requirements of the RHT-MAPS and to test the feasibility of the

suggested design. The suitability of the hardware and software for implementing the design solution was evaluated in laboratory tests and then a prototype of the RHT-MAPS was built. A list of the hardware and software functionality tests of the RHT-MAPS for the initial design is shown in Table 3.3.

Table 3.3: Testing of the RHT-MAPS monitoring system.

Testing	Description of the test
Sensors	Testing the reliability of the temperature and relative humidity the sensor provides and their output.
Data transmitting	Testing the data transmission between RHT-MAPS sensor network node and the controller, and then to the host computer.
Output	Testing that the RHT-MAPS monitoring software accurately stores the received relative humidity and temperature data.
Analysing the monitored data	Verifying the functionality of the data processing module

The prototype for the RHT-MAPS sensor network shown in Figure 3.20 was built using two HMP44 sensors, two SHT15 sensors, and two PT100 sensors. The sensors were connected to the LICo4 controller using a pair of wires from the CAT5 cable. The LICo4 controller was connected directly to the host computer using a crossover Ethernet cable. The RHT-MAPS monitoring and data analysis software was installed on a Microsoft Windows XP platform.

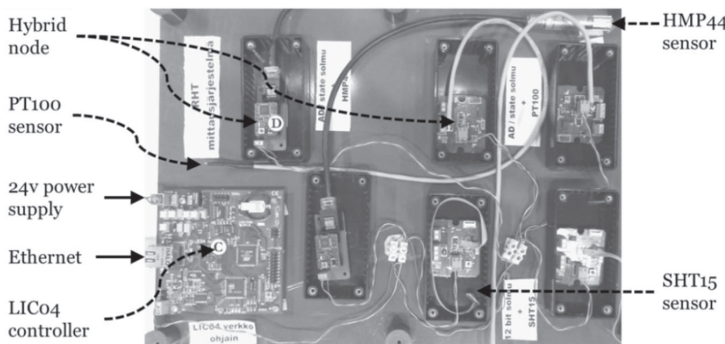


Figure 3.20: The prototype for the RHT-MAPS sensor network



### 3.4 RHT-MAPS expenses

The expenses of the RHT-MAPS consist of the sensor network components, the monitoring and data analysis software, the installation of the system on-site, and the operating costs. The calculations of the expenses exclude the development of the RHT-MAPS monitoring software and the host computer. An example of the cost of the RHT-MAPS for monitoring the hygrothermal performance of a repaired concrete facade is shown in Table 3.4.

Table 3.4: Example of the initial cost calculation of the RHT-MAPS monitoring system for a repaired facade in the year 2007

Component	units	Cost (€)	Proportion of the expense (%)
LICo4 Main Control Unit	1	400	7,3
Standard CAT5 cable	200 m	100	1,8
Hybrid nodes	44	1540	28,2
PT100 temperature sensor	22	180	3,3
HPM44 humidity sensor	6	1200	22
SHT15 humidity sensor	16	560	10,3
RHT-MAPS sensor network installation	32 h	1280	23,4
RHT-MAPS monitoring software		200	3,7
<b>Total</b>		<b>5460</b>	

The costs for the RHT-MAPS sensor network components were calculated on the basis of prices for the year 2007. The operating expenses consist of the maintenance of the system devices and the data analysis. The author of the thesis considers four person-hours monthly and the total yearly operating cost is €1900 (Statistics Finland Wage and Salary Statistics).

It is shown that the RHT-MAPS monitoring system does not represent a large additional cost to the facade expenses in comparison to the usefulness of the monitoring results.

### 3.5 RHT-MAPS evaluation

The RHT-MAPS is a new technique for monitoring the moisture and thermal performance of repaired concrete building facades. The

RHT-MAPS monitoring system is designed to fulfil the need for a simple network of relative humidity and temperature sensors. The advantages of using the RHT-MAPS are:

- easy system design, installation, network configuration, and administration;
- a network that is completely topology- and polarity-free;
- transmission of both data and power in the same twisted-pair cable;
- intensive measurement: in each network, the maximum length of the network cable is 1000 m and the maximum number of nodes is up to 200 nodes;
- low-cost components to operate.

Monitoring allows the environmental stressors on the deterioration of concrete building facades such as relative humidity, temperature, and carbon dioxide to be quantified. Continuous monitoring provides a much better understanding of how the environment and the building interact and can complement visual inspections. By measuring the relative humidity and temperature of building components, we can determine the potential for deterioration, wetting and drying patterns in building components, and the changes in moisture content.

Monitoring is especially useful when applied to the maintenance and repair sector. Documenting the performance of a repaired building through monitoring can improve the understanding of the methods and materials used for repairs and structural behaviour, which increase the durability and the service life cycle of the repaired structures.

Detailed information about the moisture and thermal performance is not sufficient for predicting the performance of building materials or building assemblies because the interaction of heat and moisture and the material is often unknown. Knowing the chemical reactions and ageing functions is important in order to get enough information about the performance of the building materials.

During the feasibility study of this thesis, the RHT-MAPS was designed to be fully capable of identifying main physical phenomena

regarding the temperature and relative humidity measurements. Meanwhile, the design of hygrothermal model of the performance of concrete building facades-brought up the need for more data about the wind, rain, water condensation, and air pressure. These data are recommended to be added as a future work to the RHT-MAPS.

One disadvantage of embedding the relative humidity and temperature sensors in the facade wall layers is that the maintenance of the sensors becomes difficult, which in turn affects the measurement accuracy. Dirtiness and the condensation of water and alkalis on the sensor probes also affect the accuracy of the relative humidity and temperature measurements. In general, one of the major challenges of the RHT-MAPS sensor network is the difficulty of examining the durability and the fixings of the embedded components of the network, as well as the need for periodic calibration of the nodes and sensors after they have been embedded in the concrete structures.

The RHT-MAPS has its limitations. Occasionally, as a result of unpredictable failure modes, the data gathered from a relative humidity and temperature sensor network could be inherently faulty. These faulty data can reduce the credibility of the prediction of the deterioration of the concrete building facade. Some filtering methods should be applied to detect these faults and the users should be able to understand and pick out the faulty data points because of their expertise.

The interpretation of the relative humidity and temperature data is the foundation upon which the RHT-MAPS deterioration prediction system is based. Inaccurate data generate erroneous results of the prediction models which could lead to wrong decisions. The RHT-MAPS user should be able to diagnose the measurements and solve the problems of data reconciliation for the prediction models. For example, as shown in Figure 3.21, knowledge of moisture transfer should tell the user that the result of relative humidity under 6 mm rendering coat is faulty measurements.

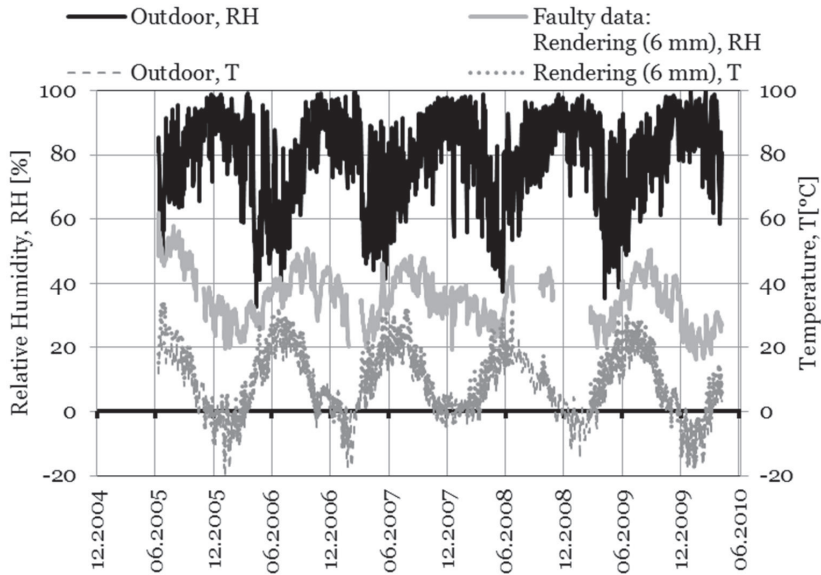


Figure 3.21: Example of faulty relative humidity measurements in the rendering system (6 mm from the surface).

### 3.6 Summary

This development of the RHT-MAPS was motivated by an existing system called COMSY developed by Framatome ANP GmbH. The COMSY system was developed to provide a tool for nuclear power plants ageing management and service life extension activities.

The moisture and thermal monitoring RHT-MAPS was developed to help understand the formation of moisture and the thermal performance of concrete building facades. The RHT-MAPS consists of a sensor network and monitoring software. The sensor network consists of a controller, smart nodes, and relative humidity and temperature sensors and may contain up to 200 nodes connected to a twisted-pair CAT5 cable with a maximum total length of 1000 metres. The monitoring software application was developed for connecting the monitoring network to the host computer in order to collect relative humidity and temperature data; these data were processed via a data-processing module developed using Visual Basic for Applications under Microsoft Excel.

There are some constraints on the use of the RHT-MAPS. The user must be aware of how to use the system and how to interpret the results, which means that the results must be checked for credibility.

The installation of the RHT-MAPS is shown in Chapter 5. The analysis of the monitored data and the response of the concrete building facades to these data are also presented in Chapter 5. The interpretation of the RHT-MAPS monitoring results and the use of the results in predicting the deterioration of concrete building facades are shown in Chapter 6.



## 4 Laboratory investigations

The motivation of the laboratory investigation was to clarify the effect of thermal and moisture gradients on different deterioration mechanisms of concrete structures and to test the quality of concrete against different exposure classes. The degradation models presented in this thesis include parameters, which have to be determined with specific laboratory tests such as carbonation rates, coefficient of thermal expansion and level of damage caused by freezing and thawing cycling.

The objective of this chapter is to investigate the effect of moisture and temperature on the deterioration of concrete building facades. The laboratory tests were selected based on the deterioration mechanisms of concrete building facades shown in Figure 2.9, except for the biological mould growth. The effects of thermal and moisture changes on the carbonation depth and the frost resistance of concrete were investigated in a laboratory environment. The laboratory tests were carried out according to the test standards shown in Table 4.1.

In the laboratory, the accelerated carbonation of concrete samples under different carbon dioxide contents was investigated. Specifically, an experiment was carried out to study the natural carbonation of concrete samples when exposed to outdoor conditions. The frost resistance of concrete was investigated by means of two different test methods. The first method measured the thermal expansion in concrete specimens when they were subjected to accelerated cyclic freezing and thawing in temperatures around  $-40^{\circ}\text{C}$ . The second method (CEN/TS 12390-9:2006), the slab test method, is based on the Swedish Standard SS137244 for measuring both the scaling and internal damage of the concrete.

Table 4.1: Standard codes for concrete laboratory tests.

<b>Laboratory test</b>	<b>Test Standard</b>
<u>Testing fresh concrete</u>	
Slump test	EN 12350-2:2009
Concrete density	EN 12350-6:2009
Air content	EN 12350-7:2009
<u>Testing hardened concrete</u>	
Compressive strength	EN 12390-4:2000
<u>Freezing thawing</u>	
Slab test (internal damage)	CEN/TR 15177-2006
Slab test (surface scalling)	CEN/TS 12390-9:2006
Thermal expansion	AASHTO TP 60-00: 2004
<u>Carbonation</u>	
Accelerated carbonation test	EN 13295:2004

The results of the laboratory tests are used for validating the deterioration models that are discussed in Chapter 6.

## **4.1 Material selection**

### **4.1.1 Cement**

Three types of cement were used in the concrete mixes. These cements were produced by Finnsementti's cement plant at Parainen. Table 4.2 shows the oxide composition and the properties of the different cement types according to their chemical analyses. These values were obtained from tests performed by the cement manufacturer.



Table 4.2: The chemical composition and the properties of the cement used.

	<b>Rapid Cement *</b>	<b>SR- Cement **</b>	<b>Ordinary Cement ***</b>
<b>Oxide</b>	<b>Content, %</b>		
CaO	60.7	65.3	63
SiO <sub>2</sub>	20.5	21.4	20
Al <sub>2</sub> O <sub>3</sub>	5	3.9	4.8
Fe <sub>2</sub> O <sub>3</sub>	2.4	4.1	2.9
MgO	3.1	3.2	2.8
K <sub>2</sub> O	0.8		
Na <sub>2</sub> O	0.85		
SO <sub>3</sub>	3.1	3	2.8 – 3.4
Ignition loss (950 °C)	3.4	2.4	
Initial setting time (min)	120	180	190
Fineness (m <sup>2</sup> /kg)	470	380	370
<b>Compressive strength (MPa)</b>			
1d	19	14	15
7d	44	41	38
28d	49	51	50

\*) Rapid cement: CEM II/A-LL 42,5 R

\*\*) Sulphate Resistant cement: CEM I 42,5 N - SR

\*\*\*) Ordinary cement: CEM II/A-M(S-LL) 42.5 N

#### 4.1.2 Aggregates

The aggregate used in these mixes was natural granite gravel, which was washed, dried, and graded by sieving. The concrete mixes were made by using the same aggregate grading. The grading of the combined aggregates is shown in Appendix D.

#### 4.1.3 Water

The water used was normal tap water provided by the water distribution system of the city of Espoo and its temperature was 20±2°C.

#### 4.1.4 Air-entraining agent

The air-entraining agent was Ilma-Parmix, manufactured by Finnsementti Oy Finland. This agent was stored in a polyethylene bottle at room temperature.

## 4.2 Mix design and sampling

For all the mix designs and specimens in the different tests, specific codes were assigned, as given in Figure 4.1.

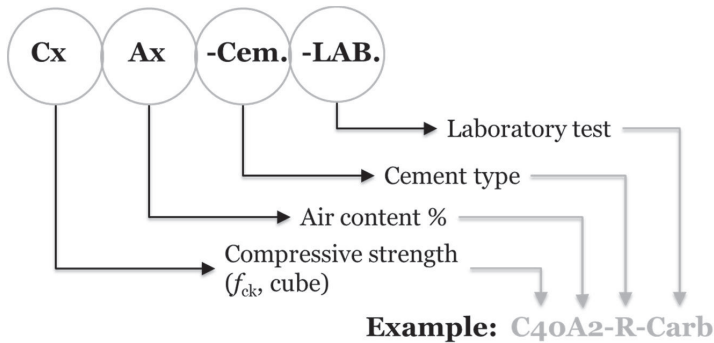


Figure 4.1: Example of the coding system used for identifying concrete specimens.

### 4.2.1 Accelerated and natural carbonation

Three concrete mixes were selected in order to measure the carbonation depth in the accelerated carbonation test. The selected concretes had a compressive strength of 40 MPa and were cast using Ordinary Portland cement and Sulphate-Resistant cement. The mix designs, the properties of the fresh concrete, and the compressive strengths are presented in Table 4.3 and Table 4.4. Details of the mix designs and the properties of the accelerated carbonation test concrete specimens are shown in Appendix D.

Table 4.3: The composition of the concrete mixes for the accelerated carbonation test.

Concrete	Concrete composition [kg/m <sup>3</sup> ]					
	Cement	Water	Aggregates			Air agent
			R 0 – 1	R 0 – 8	R 5 – 16	
C40A2-Y*	321	185	77	1083	743	-
C40A6-Y	321	192	75	1058	725	2.3
C40A2-SR**	321	192	56	103	799	-
C40A6-SR	321	191	53	988	764	3.9

\*) Y = Ordinary cement [CEM II/A-M(S-LL) 42.5 N]

\*\*) SR = Sulphate Resistant cement [CEM I 42,5 N - SR]

Table 4.4: The properties of the concrete mixes for the accelerated carbonation test.

Concrete	Basic properties of the fresh concrete				Compressive strength [MPa]	
	Slump [mm]	Temp. [°C]	Density [kg/m <sup>3</sup> ]	Air content [%]	7d	28d
C40A2-Y	12	22	2408	2.6		45
C40A6-Y	4	24	2319	5.0	25	38
C40A2-SR	42	24	2404	1.7	31	40
C40A6-SR	115	24	2308	5.4	24	36

Concrete cubes of a size 150 x 150 x 150 mm<sup>3</sup> were produced for measuring the carbonation depth of the concrete in the laboratory. After casting, the specimens were kept in their moulds and covered with a plastic sheet for one day. They were then unmoulded and stored under water for seven days, after which they were stored in a constant condition room with a relative humidity of 65% and a temperature of 20°C ± 2°C. At the age of 21 days, the concrete cubes were cut into 50-mm samples and transferred to the constant condition room. At the age of three months the accelerated carbonation was tested at 1% or 4% CO<sub>2</sub>, 60% RH, and 20°C. Moreover, the normal (non-accelerated) carbonation was evaluated for 56 days.

To monitor the natural carbonation of concrete a set of concrete prisms with dimensions of 50 × 50 × 150 mm<sup>3</sup> were cast and stored in outdoor conditions and exposed to rain and snow. The selected concretes had a compressive strength in the range 30 to 45 MPa and were cast using Rapid Portland cement (CEM II A 42.5R). The prisms were removed from the moulds seven days after casting. Thereafter, the specimens were stored for 21 days in a climate chamber (22°C, 45% RH) and then moved outdoors. The composition and the properties of the concrete are shown in Table 4.5.

Table 4.5: The composition and the properties of the concrete mixes exposed to natural carbonation.

Concrete	Concrete composition [kg/m <sup>3</sup> ]					Properties of concrete	
	Cement*	Water	Agg.	SP**	Air agent	air content [%]	$f_c$ , 28d
C30A2-R-Carb	266	206	1779	0	0	1.5	35.2
C30A6-R-Carb	250	144	1907	1.5	0.05	6	30
C35A5-R-Carb	343	167	1786	0	0.27	5	38
C40A2-R-Carb	270	204	1874	0	0	2	42
C45A6-R-Carb	428	195	1610	5.1	0.23	6.5	46.6

\*) Cement type: Rapid cement [CEM II A 42.5 R]

\*\*) SP = Plasticizer

#### 4.2.2 Thermal expansion of concrete

For measuring the thermal expansion of the concrete seven concrete mixes were selected. Concrete mixes with 28-day target cubic strengths of 25 to 45 MPa were considered. The target air content was 2% for non-air-entrained concrete and 3 to 10% for air-entrained concrete. The Rapid cement was chosen when the concrete mixes were being designed. Table 4.6 shows the composition of the concrete mixes, while Table 4.7 presents the properties of the fresh and hardened concrete.

Table 4.6: Composition of concrete mixes for thermal dilation test.

Concrete	Concrete composition [kg/m <sup>3</sup> ]				
	Cement*	Water	W/C	Agg.	Air agent
C25A2-R-TE* <sup>1</sup>	200	180	0.90	1963	0.0
C40A2-R-TE	280	180	0.64	1894	0.0
C25A3-R-TE	250	190	0.76	1867	0.0
C25A4-R-TE	250	190	0.76	1815	0.1
C45A6-R-TE	475	190	0.40	1610	0.4
C40A7-R-TE	475	190	0.40	1557	0.7
C35A9-R-TE	475	190	0.40	1502	1.2

\*) Cement type: Rapid cement [CEM II A 42.5 R]

\*\*) TE = Thermal Expansion

Table 4.7: The properties of the concrete mixes for the thermal dilation test.

Concrete	Basic properties of the fresh concrete			Hardened concrete density [kg/m <sup>3</sup> ]	28 d compressive strength [MPa]
	Temp. [°C]	Density [kg/m <sup>3</sup> ]	air content [%]		
C25A2-R-TE	25	2343	1.9		24.5
C40A2-R-TE	24	2363	2.0		38.5
C25A3-R-TE	25	2358	2.8	2315	26.5
C25A4-R-TE	25	2300	4.3	2251	28.7
C45A6-R-TE	26	2233	5.9	2241	44.4
C40A7-R-TE	27	2214	6.8	2224	40.0
C35A9-R-TE	28	2170	9.5	2163	34.0

Concrete cylinders with a diameter of 65 mm and a height of 195 mm were cast. A plastic tube with a diameter of 10 mm was cast into the concrete specimens to a depth of 60 mm for measuring the internal temperature and relative humidity. After casting, the specimens were kept in their moulds and covered with a plastic sheet for one day. They were then unmoulded and transferred to the storing room, where the specimens were stored both under water and in closed containers in which the relative humidity was kept constant at 95%, 90%, and 86% RH using a saturated salt solution. One specimen was taken from the water and dried at 105°C for one week before the test to be used as a reference sample.

#### 4.2.3 Freezing and thawing resistance of concrete

The mix design, the properties of the fresh concrete, and the compressive strength of the concrete samples used in the freezing and thawing test are similar to those of the concrete mixes tested in the accelerated carbonation test and are presented in Table 4.3 and Table 4.4.

The sample for the freezing and thawing test, shown in Figure 4.2, was a concrete slab (150 mm in length x 150 mm in width x 50 mm high) that had been sawn off from a 150-mm cube. The surfaces of the slab were sealed with neoprene sheets and then thermally insulated, while the test surface was covered in plastic film.

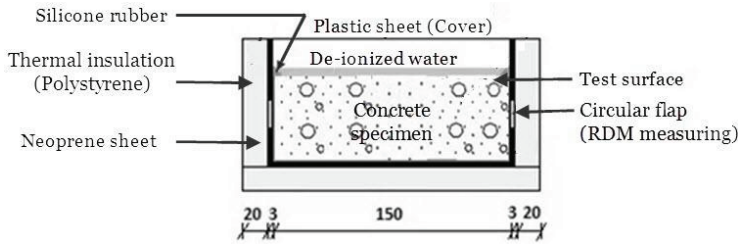


Figure 4.2: Test specimen prepared for freezing-thawing testing. Dimensions in [mm].

The curing process comprised one day in the mould and six days in water at 20°C, followed by 21 days in dry storage at 20°C with the slabs sawn off. After 14 days of dry storage, the specimens were sealed and insulated. The test liquid was poured in to a depth of 3 mm after the dry storage period and the freezing-thawing cycles were started after three days.

### 4.3 Experimental test equipment and procedures

#### 4.3.1 Accelerated and natural carbonation

An accelerated carbonation test was carried out in order to assess the carbonation of the concrete samples. The carbonation chamber shown in Figure 4.3 is an environmental chamber where air is conditioned to a CO<sub>2</sub> content of 4% or 1%, the relative humidity is 60%, and the room temperature is 20±2°C.

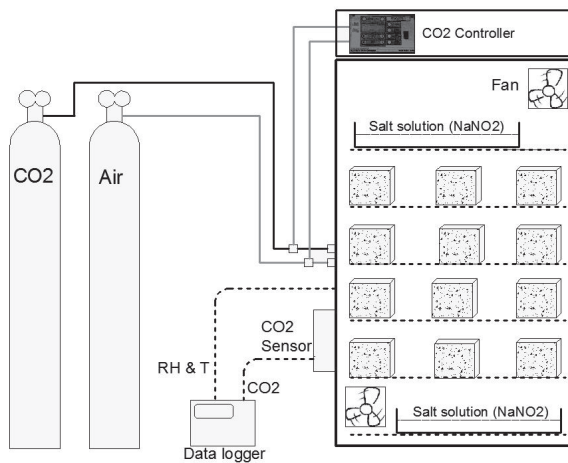


Figure 4.3: Schematic of the accelerated carbonation test chamber.

Relative humidity was controlled with multiple pans of a fully saturated salt solution composed of  $\text{NaNO}_3$  and water. Periodic checks were made to ascertain that the solutions were not under-saturated or dried out. The  $\text{CO}_2$  atmosphere was created using a compressed  $\text{CO}_2$  gas supply. An atmosphere controller was used to regulate the supply of  $\text{CO}_2$ . Examples of the  $\text{CO}_2$  content, the temperature, and the relative humidity of the environmental chamber are shown in Figure 4.4.

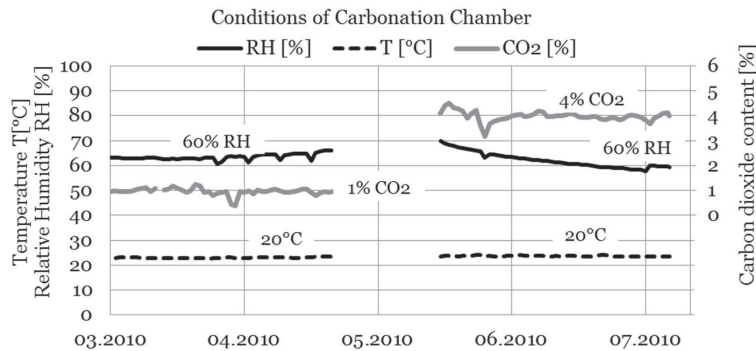


Figure 4.4: An example of the  $\text{CO}_2$  content, relative humidity, and temperature in the environmental chamber.

The outdoor conditions for the natural carbonation test of concrete prisms are illustrated in Figure 4.5. The concrete specimens were directly exposed to rain and snow in southern Finland.

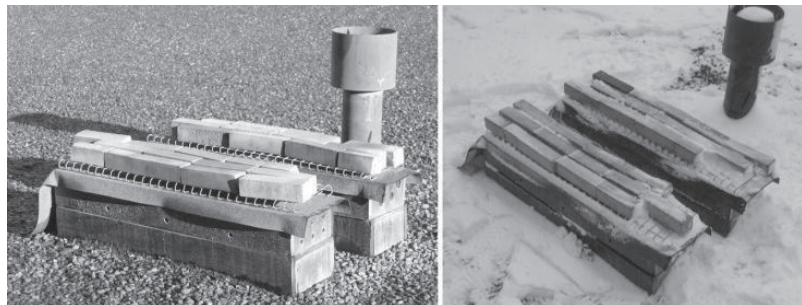


Figure 4.5: Concrete specimens stored outdoors and used for monitoring the natural carbonation.

The carbonation depth is measured using a solution of phenolphthalein indicator that appears pink in contact with alkaline concrete with pH values in excess of 9 and colourless at lower levels of pH. The test is carried out by spraying the indicator on freshly

exposed surfaces of concrete broken off from the specimens. The result of the average depth of carbonation measured at least six points perpendicularly to the faces of the broken concrete cube. The average value of the depth of carbonation is shown in Figure 4.6 and calculated using Equation (4.1).

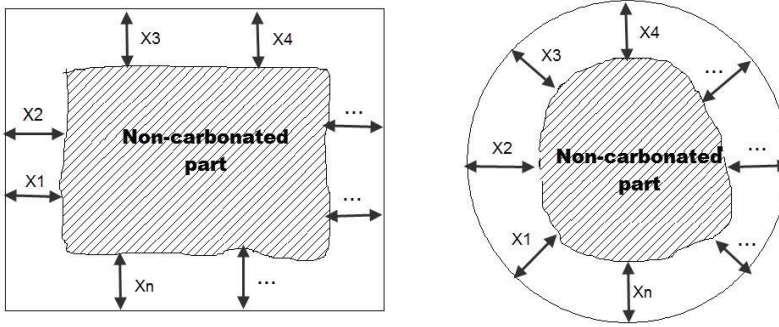


Figure 4.6: Cross-section of concrete specimens after carbonation.

$$X_{ca} = \frac{\sum_{i=1}^n X_i}{n} \quad (4.1)$$

where

- $X_{ca}$  is the average carbonation depth [mm],
- $X_i$  is the measured carbonation depth at point (i) [mm], and
- $n$  is the number of the measured points.

### 4.3.2 Thermal expansion of concrete

Figure 4.7 presents a diagram of the apparatus used for the thermal expansion test. The apparatus consists of:

- a cooling and heating chamber,
- a tight stainless steel vessel where the specimens are placed during the test, shown in Figure 4.8,
- probes for strain, temperature, and relative humidity, and
- a data acquisition system, with a network card and data acquisition software.



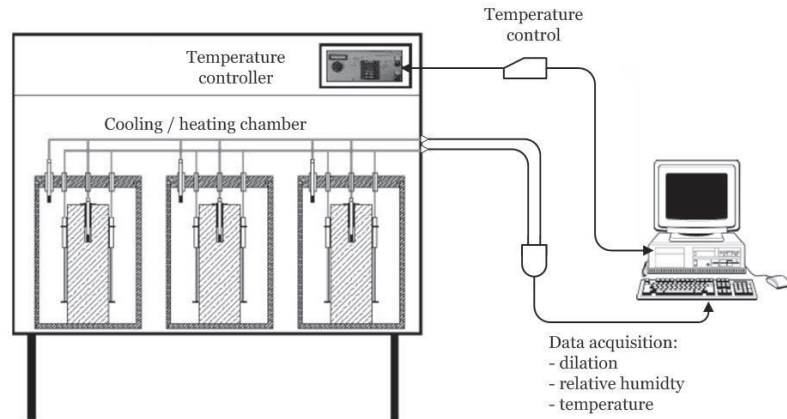


Figure 4.7: Schematics of the thermal dilation test apparatus.

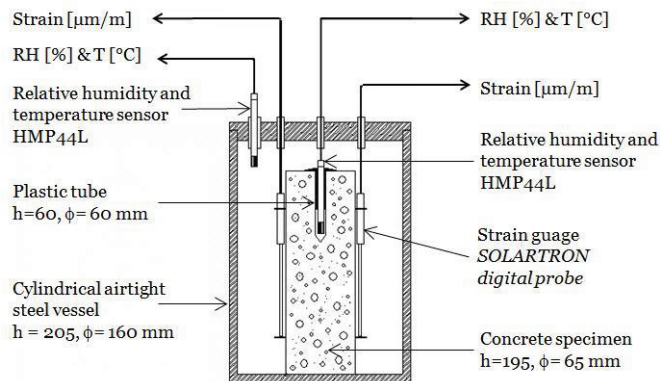


Figure 4.8: Schematics of the thermal expansion test steel vessel.

Before the thermal expansion test, the bottom end of the plastic tube was drilled through and two inductive strain gauges were mounted on the surface of the specimen so that the axial strain of the surface could be measured during the test run. The concrete specimens were placed into a cylindrical airtight steel vessel with a diameter of 160 mm and a height of 250 mm. The relative humidity and temperature of the steel vessels were measured. The test specimens in the steel vessels were cooled from 20 to  $-38^{\circ}\text{C}$  with a cooling rate of  $3.0^{\circ}\text{C}/\text{h}$ . The warming rate was  $4.2^{\circ}\text{C}/\text{h}$  and the temperature rose to  $+10^{\circ}\text{C}$ . Thereafter the cooling and warming procedure was repeated for another cycle. In the second cycle, the temperature rose to  $+20^{\circ}\text{C}$ . The cooling and warming temperatures are shown in Figure 4.9. The temperature, relative humidity, and strain data were measured every 60 s throughout the test run.

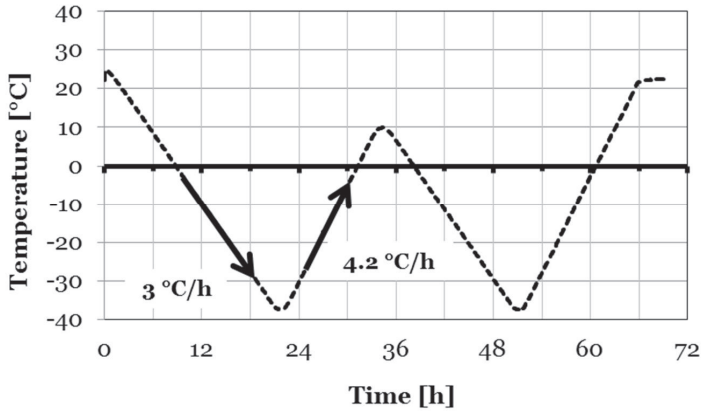


Figure 4.9: Freezing and thawing cycles in the thermal expansion test.

### 4.3.3 Slab test: freezing-thawing resistance of concrete

The cooling and heating chamber is a temperature- and time-controlled refrigerating and heating system with a capacity such that the time-temperature sequence can be monitored. The test chamber allows for the freezing and thawing of the concrete specimen according to CEN/TR 15177 (2006). The cooling and heating chamber is shown in Figure 4.10.

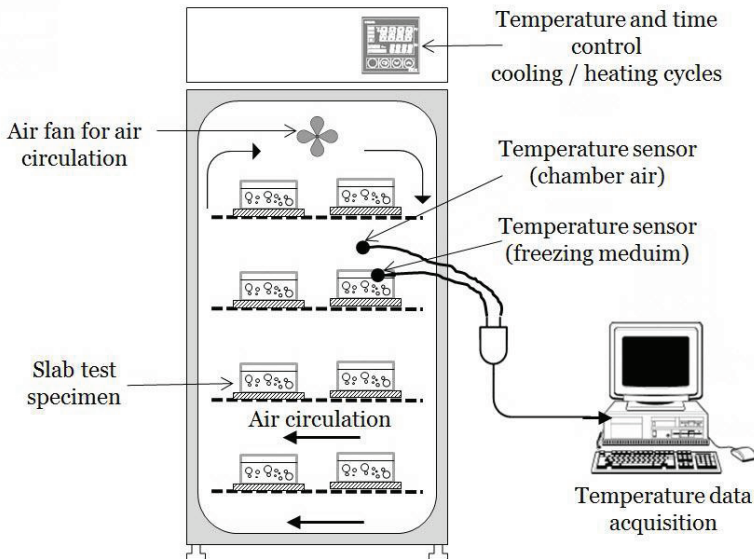


Figure 4.10: The principle of the freezing-thawing test chamber for the slab test with a freezing-thawing chest.

The freezing and thawing cycle had a temperature range of +20°C to -20°C in accordance with a specified time-temperature curve, shown in Figure 4.11.

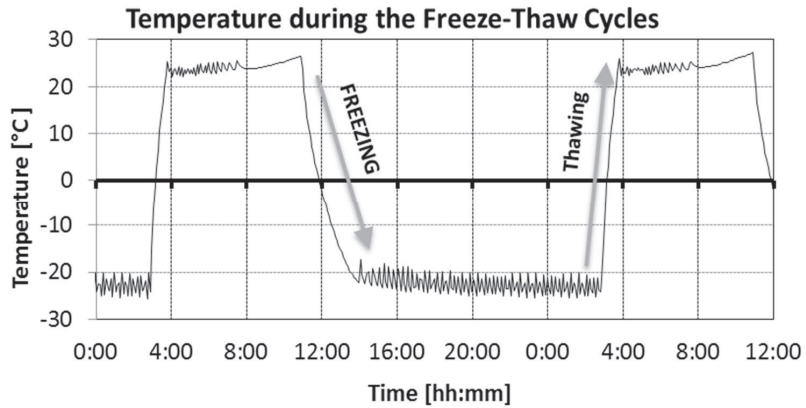


Figure 4.11: Temperature behaviour for the indoor air in the cooling and heating chamber.

The scaling and internal damage measurements were taken after 7, 14, 28, 42, and 56 cycles. The internal damage was measured according to CEN/TR 15177 (2006) and the scaling was measured according to CEN/TS 12390-9 (2006). Internal damage or cracking was measured using an ultrasound pulse velocity, after which the relative dynamic modulus percentage (RDM) could be obtained through calculations as follows:

$$RDM = 100 * \left(\frac{t_o}{t_c}\right)^2 \quad (4.2)$$

where

$t_o$  is the initial ultra-sonic pulse transit time [ $\mu$ s] and

$t_c$  is the ultra-sonic pulse transit time after ( $c$ ) cycles of freezing and thawing [ $\mu$ s]

## 4.4 Results and data analysis

### 4.4.1 Carbonation depth of concrete

The accelerated carbonation test was initiated at 70 days for 1% CO<sub>2</sub> and at 90 days for 4% CO<sub>2</sub>. Table 4.8 presents the carbonation depths for concrete specimens exposed to 1% CO<sub>2</sub> and 4% CO<sub>2</sub> accelerated testing exposures respectively. It can be seen that the air-entrained concrete has a higher carbonation depth when compared to

non-air-entrained concrete when exposed to 1% CO<sub>2</sub> and 4% CO<sub>2</sub> carbonation testing. The reason could be the faster drying of the air-entrained concretes compared with non-air-entrained concretes, which increases the carbonation rate for the air-entrained concrete samples.

Table 4.8: Accelerated carbonation depth of concrete specimens placed in 1% CO<sub>2</sub> and 4% CO<sub>2</sub>.

Concrete code	Accelerated carbonation			
	1 % CO <sub>2</sub>		4 % CO <sub>2</sub>	
	28d	56d	28d	56d
C40A2-Y	3.6	5.4	7.8	9.5
C40A6-Y	5.2	8	9.5	10.7
C40A2-SR	3.6	6.6	5.5	7.5
C40A6-SR	5.5	6.8		

The natural carbonation depth of the concrete specimens was determined after thirteen years of outdoor exposure in the southern part of Finland and the results are presented in Figure 4.12. The results indicate that the non-air-entrained concrete had a greater carbonation depth than the air-entrained concrete after thirteen years of outdoor exposure. The reason as a result of frost action, which leads to an increased depth of carbonation near the surface and internal cracks.

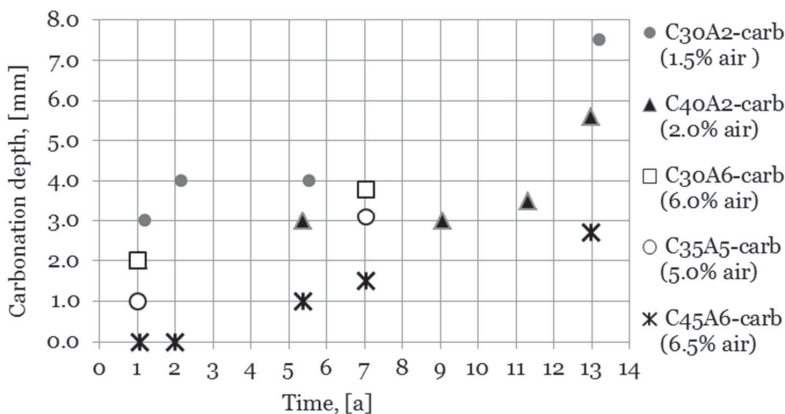


Figure 4.12: Natural carbonation depth of concrete specimens stored in outdoor conditions and exposed to rain.

The carbonation rates of the naturally carbonated concrete specimens are shown in Table 4.9. The results of the naturally

carbonated concrete show that an increase in the compressive strength and the air content of the concrete reduces the carbonation rate.

Table 4.9: Carbonation rates of concrete specimens placed in outdoor conditions.

Age [a]	Carbonation rate [mm/a <sup>0.5</sup> ]				
	C30A2-carb	C30A6-carb	C35A5-Carb	C40A2-carb	C45A6-carb
1.2	2.7	2.0	1.0	2.0	
2.2	2.7				
5.5	1.7			1.3	0.4
7.0		1.4	1.2		0.6
9.1				1.0	
11.3				1.0	
13.2	1.1			1.6	0.7
AVG	2.4	1.7	1.1	1.3	0.5
CV (%)	34	25	11	30	31

The results of both the accelerated and natural carbonation tests are used to validate the carbonation depth model in Chapter 6.

#### 4.4.2 Thermal expansion of concrete

As this study focuses on measuring the strains in concrete specimens when they are subjected to accelerated cyclic freezing and thawing in different moisture states, the following is an overview of the results obtained. Figure 4.13 shows an example of the moisture state and temperature during the freezing and thawing cycles inside the thermal expansion test vessel.

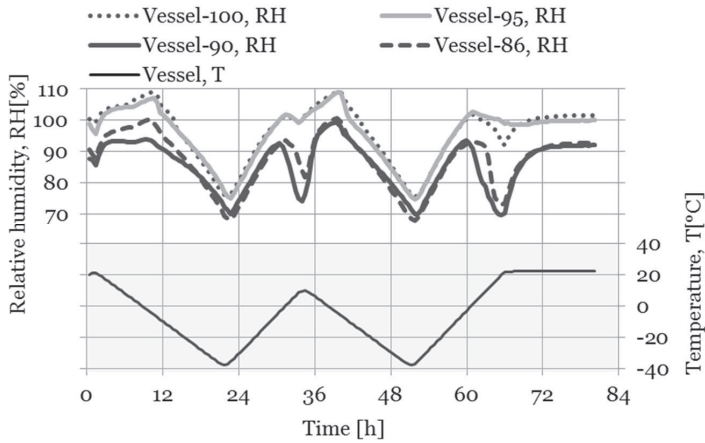


Figure 4.13: Relative humidity and temperature during the freezing and thawing cycles inside the thermal dilation test vessel.

A literature review was conducted to validate the results of the thermal expansion test for calculating the coefficient of thermal expansion (CTE) of concrete. Most of the literature emphasises that the CTE of Portland cement concrete ranges from about  $8$  to  $12 \cdot 10^{-6}/^{\circ}\text{C}$ . The range of CTE values for different concretes reflects the variation in CTE of the component materials of the concrete. The aggregate type has the greatest effect on the CTE of the concrete. For example, concrete containing granite aggregate has a CTE that varies from  $6.8$  to  $9.5 \cdot 10^{-6}/^{\circ}\text{C}$ , while concrete containing quartz sands and gravels has a CTE that varies from  $10.8$  to  $15.7 \cdot 10^{-6}/^{\circ}\text{C}$  (Shin and Chung, 2011). The CTE of hardened cement paste, which is a function of factors such as the water-to-cement ratio and the fineness, composition, and age of the cement, also affects the CTE of the concrete.

The results of the thermal expansion test for the concrete samples subjected to freezing and thawing cycles at different moisture levels are shown in Table 4.10 and Table 4.11.

The CTE of concrete is calculated by the following equation:

$$\alpha_L = \left( \frac{\Delta L}{L_0} \right) / \Delta T \quad (4.3)$$

where

- $\alpha_L$  is the coefficient of thermal expansion [ $(\mu\text{m}/\text{m})/^{\circ}\text{C}$ ],
- $\Delta L$  is the change in length during temperature change [ $\mu\text{m}$ ],

$L_0$  is the length of the specimen at room temperature [m], and  
 $\Delta T$  is the measured temperature change [°C].

Table 4.10 shows the effect of the compressive strength and air entrainment on the CTE values of concrete samples stored in different moisture conditions. Viewing the results shows that the values of CTE for air-entrained concretes are higher than those for non-air-entrained concretes. The compressive strength of the concrete has little effect on the CTE. The CTE of the dry specimens was always smaller than that of the wet specimens. However, the effect of the moisture state (86% to 100% RH) of each specimen on the value of the CTE varied for different concretes, depending on the compressive strength and the air content of the specimens. The CTE values ranged from 4.2 to 5.8  $\cdot 10^{-6}/^{\circ}\text{C}$  for the dried specimens and from 5.2 to 10.0  $\cdot 10^{-6}/^{\circ}\text{C}$  for the wet specimens.

Table 4.10: The coefficient of heat expansion of concrete mixes.

Moist curing condition of specimen	Coefficient of heat expansion [ $\cdot 10^{-6}$ (m/m)/°C]				
	Dry*	86%	90%	95%	100%**
C25A2-R-TE	4.2	5.9	5.7	5.8	5.7
C40A2-R-TE	4.4	6.4	5.5	6.1	7.5
C25A3-R-TE	4.5	5.2	5.8	5.5	6.8
C25A4-R-TE	4.6	5.7	6.0	5.5	5.8
C45A6-R-TE	5.2	6.6	9.8	10.0	7.4
C40A7-R-TE	4.9	6.2	7.1	9.3	7.6
C35A9-R-TE	5.8	9.7	10.0	10.0	7.4

\* Specimen was taken from the water and dried at 105°C for one week then cooled one day before the thermal expansion test

\*\* Specimen was stored under water

Mensinga et al. (2010) suggested that thermal expansion greater than 100  $\mu\text{m}/\text{m}$  (equivalent to approximately 0.01 mm) is considered a reliable indicator of frost damage. To compare the results from the thermal expansion test and the frost damage indicator, the residual thermal deformations after two freezing and thawing cycles are calculated as shown in Table 4.11. The results show that the air-entrained concrete resisted the frost action better than the non-air-

entrained concrete in the case of the fully saturated concrete specimens. For concrete specimens stored in 86% RH moisture conditions, there was also slight frost damage in the air-entrained concrete.

Table 4.11: The residual strain of concrete samples subject to two cycles of freezing and thawing.

Moist curing condition of specimen	Residual strain after 2 cycles [ $\mu\text{m}/\text{m}$ ]				
	Dry	86%	90%	95%	100%
C25A2-R-TE	55	51	80	38	224
C40A2-R-TE	92	57	108	68	129
C25A3-R-TE	63	105	86	44	32
C25A4-R-TE	79	109	96	55	27
C45A6-R-TE	95	141	92	30	9
C40A7-R-TE	66	117	92	36	14
C35A9-R-TE	54	83	79	38	29

\* Specimen was taken from the water and dried at 105°C for one week then cooled one day before the thermal expansion test

\*\* Specimen was stored under water

Examples of the impact of the moisture state of the concrete specimens during the test of the thermal expansion of concrete are shown in Figure 4.14 and Figure 4.15. The results of the thermal expansion test for different concrete mixes are shown in Appendix D. The freezing dilation in the most saturated specimen (100% RH) of the non-air-entrained C40A2-TE concrete caused a much larger freezing dilation and residual expansion when compared to the specimen that was stored in 86% relative humidity. For the air-entrained C40A7-TE concrete, the dilation of the specimens stored in water before the test (moisture state 100%) showed no residual expansion after two cycles of freezing and thawing. Interestingly, the dilation of the specimens stored in relative humidity from 86% to 95% showed residual expansion of about 100  $\mu\text{m}/\text{m}$  after two cycles of freezing and thawing for the air-entrained C40A6-TE concrete.

For the fully saturated C40A2-TE specimen, contraction was clearly seen before ice formation increased to too high a level at around -3 to



-5°C during freezing. For the specimens stored in relative humidity 86% to 95% RH, contraction was perceivable all the way down to the minimum temperature that was reached, -37°C. It can be seen that the fully saturated C40A2-TE specimen accounts for the obvious freezing and thawing hysteresis and the residual deformation. This suggests that the sample was damaged under freezing and thawing loading. For the air-entrained C40A7-TE specimens subjected to freezing and thawing loadings, there was either no deformation or only a slight deformation followed by continual contraction and/or slight expansion when the temperature cooled down to -37°C.‰

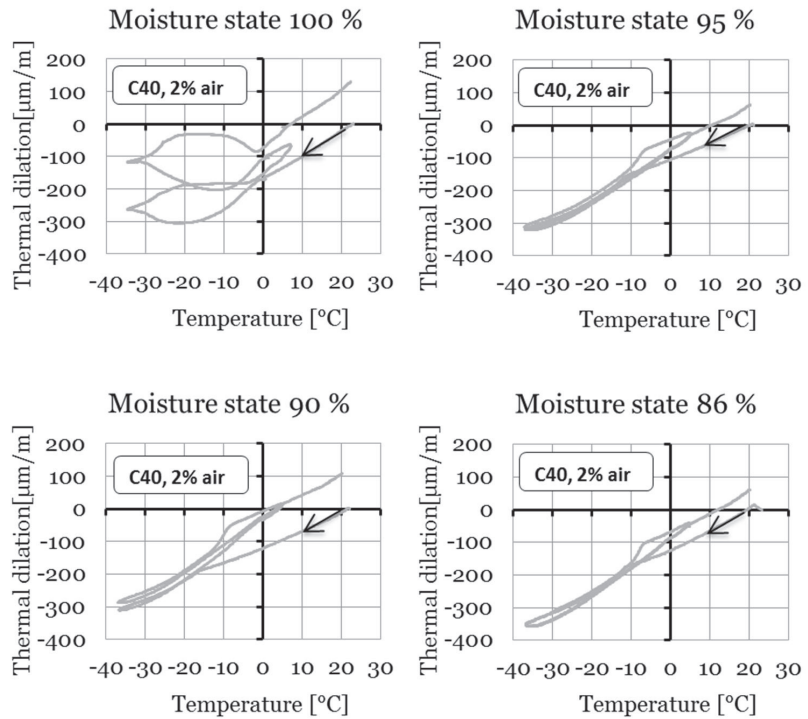


Figure 4.14: Length changes resulting from the freezing and thawing of C40A2-R-TE concrete.

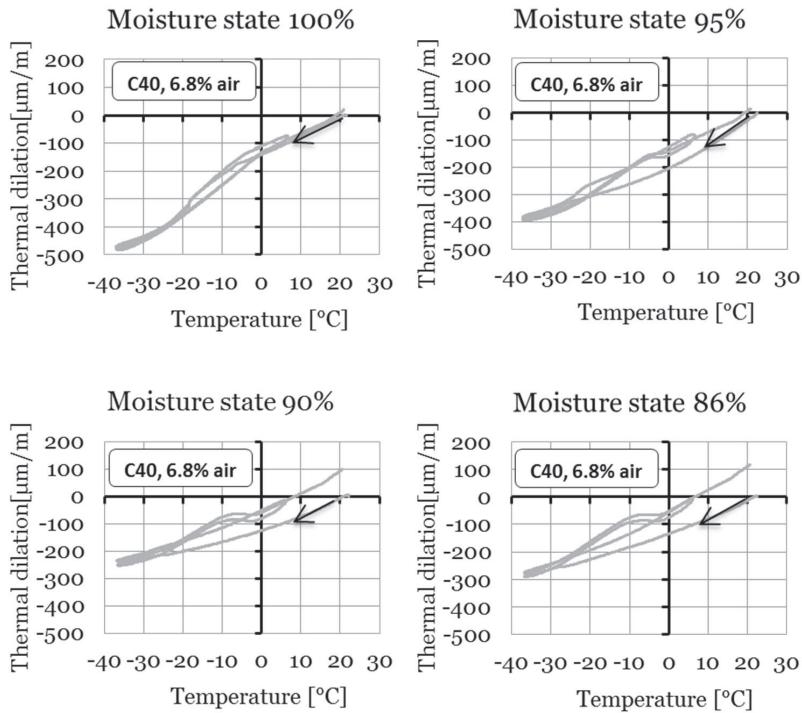


Figure 4.15: Length changes resulting from the freezing and thawing of C40A7-R-TE concrete.

The total deformation of porous materials under freezing and under free stress loading is made up of the deformation resulting from the pure thermal contraction of the solid skeleton and the deformation induced by internal pressure. Figure 4.16 shows the thermal contraction and deformation caused by pore pressure for concrete specimens in a moisture state of 100%. The thermal strain is the strain resulting from the pure thermal effect and the pressure strain is the strain resulting from the pore pressure induced by ice formation and the hydrothermal effect of the pore solution.

In the saturated non-air-entrained concrete specimens C40A2-TE, the thermal contraction increases as the temperature decreases, while the deformation induced by the pore pressure decreases slightly at first, then expands significantly. The first contraction may be due to the temperature-dependent density of the liquid solution. Therefore, the contraction of the liquid phase with the reduction in temperature leads to a negative liquid pressure. As cooling goes on, the liquid pressure increases significantly because of the formation of

ice, and the more ice that forms, the higher the liquid pressure will be. For the air-entrained specimens C40A7-TE, contraction is seen all the way down to the minimum temperature of  $-37^{\circ}\text{C}$ . The difference in liquid pressures between the air-entrained and non-air-entrained concrete specimens is due to their pore structures.

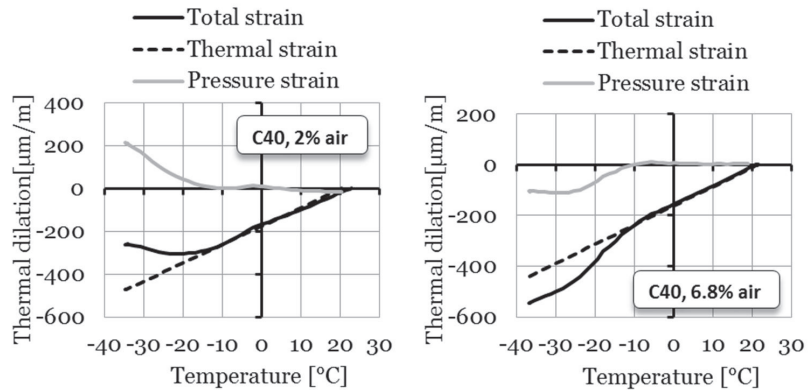


Figure 4.16: Detail of deformation in concrete specimens with a moisture state of 100% RH.

In the thermal expansion test changes in temperatures through the freezing-thawing cycles initiate the expansion and contraction of moisture absorbed by the concrete. The results of the thermal expansion test show that the concrete could be damaged as a result of the absorption of moisture and thermal expansion and contraction. The resulting mechanical action causes fractures and spalling of the concrete.

The results of the thermal expansion test are used as a preliminary test for the freezing and thawing tests to validate the frost damage model in Chapter 6. The thermal expansion test investigates the effect of the freezing and thawing cycles and the quality of the concrete on the frost damage to concrete when water is not used as a freezing medium.

#### 4.4.3 Frost damage to concrete

The internal damage caused by the freezing and thawing leads to a decrease in the dynamic modulus of elasticity (RDM), as shown in Figure 4.17. Takewaka and Sakai (2005) suggested a critical minimum value of the relative dynamic modulus of elasticity to

ensure required performance of the structure under cyclic freezing and thawing action, as shown in Table 4.12.

Table 4.12: Minimum critical level of RDM to ensure a satisfactory performance of the structure under cyclic freezing and thawing action (Takewaka and Sakai, 2005).

Exposure of structure	Minimum critical RDM level (%)			
	Severe weather or cyclic freezing and thawing action		Mild weather, atmospheric temperature rarely drops to below 0°C	
	Thin structures*	General structures	Thin structures*	General structures
(1) Immersed in water or often saturated with water	85	70	85	60
(2) Subjected to normal exposure conditions	70	60	70	60

\* Members with thickness less than 20 cm may be considered thin structures

On the basis of Table 4.12 and considering the minimum critical RDM level of 70% for the outer panels of concrete building facades, the results show that there was no indication of internal deterioration of the air-entrained concretes. Otherwise, it can be seen that for non-air-entrained concretes, the RDM level decreases to below 70% after 42 freezing and thawing cycles, which indicates that the concretes cannot ensure the satisfactory performance of the structure under cyclic freezing and thawing action.

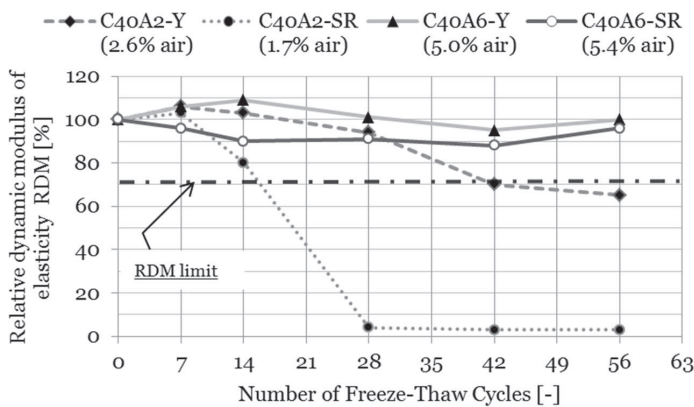


Figure 4.17: Relative dynamic modulus of elasticity vs. cycles of freezing and thawing for concrete specimens of slab test.

It is a well-known and accepted fact that air entraining minimises the damage caused by freezing and thawing in concrete. The influence of air entraining was already clear in the previous slab test results, where it was shown that internal damage in concrete was reduced significantly if the concrete had a proper artificial air pore structure.

The slab test investigates the effect of freezing and thawing cycles and the quality of the concrete on the frost damage to concrete when water is used as a freezing medium. The results of the slab test are used to validate the frost damage model in Chapter 6, Section 6.3.

#### **4.5 Summary**

The aim of the laboratory investigation of the environment-related deterioration of concrete facades was to test the durability of different concrete mixes used in concrete facade structures. The different deterioration mechanisms of concrete building facades were described in Chapter 2.

In all the experiments, the air entrainment of the concrete was used as the parameter that was tested. C40 concrete was selected as the concrete used in concrete facade structures. The experimental tests were designed to study the effect of thermal and moisture changes on the carbonation and the frost resistance of concrete.

The carbonation of concrete was tested in an accelerated CO<sub>2</sub> test in laboratory conditions and natural carbonation in an outdoor environment. To test the frost resistance of concrete, thermal expansion tests and a freezing and thawing slab test were performed.

The results of the accelerated carbonation tests showed that air-entrained concrete has a higher carbonation depth when compared to non-air-entrained concrete when exposed to 1% CO<sub>2</sub> and 4% CO<sub>2</sub> carbonation testing. For the naturally carbonated specimens, the results show that the non-air-entrained concrete had a greater carbonation depth than the air-entrained concrete after thirteen years of outdoor exposure, which could be due to the high relative humidity of the pore system of the concrete. In addition, that increment in the compressive strength of the concrete reduces the carbonation rate.

The results of the thermal expansion test show that air-entrained concrete resisted the action of frost better than non-air-entrained concrete. The influence of air entraining was clear in the results of the slab test. It was shown that the internal damage done to the concrete is reduced significantly if the concrete has a proper artificial air pore structure.

The results of the laboratory investigation of the environment-related deterioration of concrete are used to validate the suggested models in Chapter 6 for predicting the deterioration and remaining service life of concrete building facades.

## 5 Field monitoring of relative humidity and temperature

This field monitoring of relative humidity and temperature was motivated by a desire to simulate the data monitoring for COMSY system and understanding the hygrothermal behaviour of the concrete building facades over time. The aim was also to quantify the environmental factors affecting the slow deterioration of concrete building facades.

This RHT-MAPS sensor network provides a generic procedure for measuring the relative humidity and temperature and is designed for use in ambient environment and/or embedded in structures. The interpretation of the RHT-MAPS measurement results and the deterioration prediction of the structures depend on a combination of the structure and its ambient environment. For testing the RHT-MAPS in site, two building facades in the southern Finland were selected.

Field monitoring of the relative humidity and temperature at regular intervals of 15 minutes was carried out for two concrete building facades that had been repaired using different methods. Hourly values are used in this chapter because there were no significant differences in 15-minute measurements in comparison to one-hour measurements, as shown in Figure 5.1. In addition, the deterioration and remaining service life prediction models in Chapter 6 are based on values of relative humidity and temperature that were measured hourly.

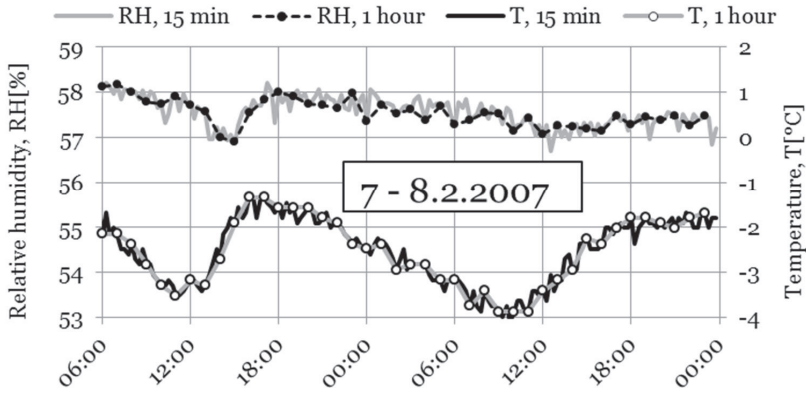


Figure 5.1: Comparing relative humidity and temperature values measured at 15-minute and one-hour intervals in the rendering coat.

In this chapter, the installation of the RHT-MAPS sensor network at two different sites is described and the monitored relative humidity and temperature data are analysed. The results of the data analysis are used as input for the deterioration prediction models in Chapter 6.

## 5.1 Installation of the RHT-MAPS sensor network

The monitoring of humidity and temperature using the RHT-MAPS was carried out in two sandwich-type concrete building facades located in southern Finland.

### 5.1.1 Concrete building facade RF1-EPS

The monitored concrete building facade RF1-EPS, shown in Figure 5.2, belongs to a six-floor apartment building and was built with sandwich elements. The facades were repaired in the year 2005 by adding a 50-mm layer of external expanded polystyrene (EPS) insulation and a 6-mm rendering coat. The RHT-MAPS sensor network was installed during the repairing of the facades on the north-eastern and south-western sides of the building.



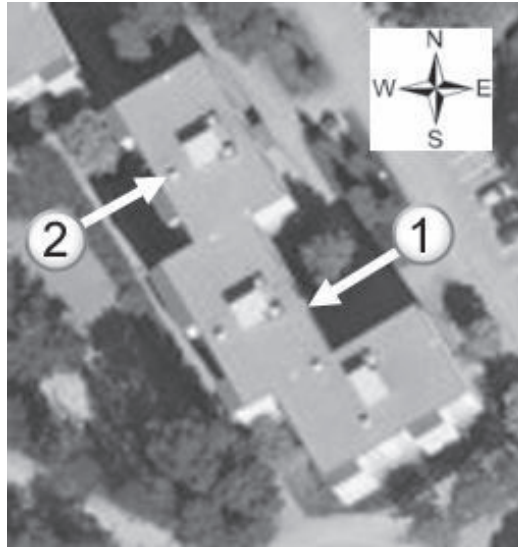


Figure 5.2: Location of the building that was monitored. Relative humidity and temperature were monitored in: 1. the north-eastern facade wall and 2. the south-western facade wall

The sensors were installed through the cross-sections of the facade wall assembly as shown in Figure 5.3.

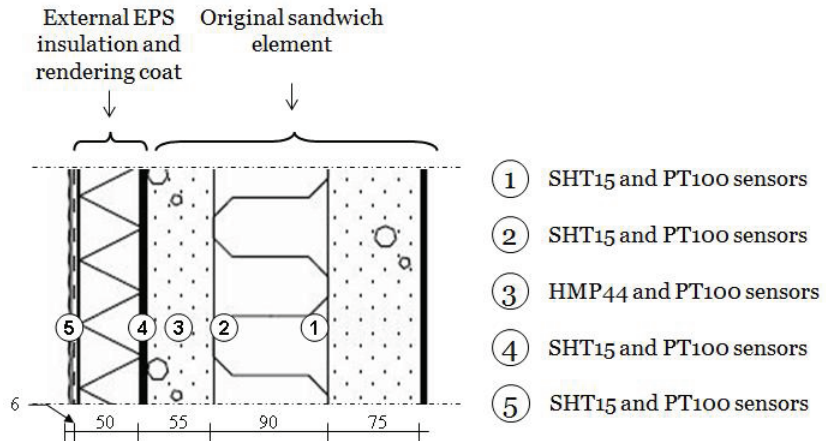


Figure 5.3: Cross-section and location of the monitoring sensors in the concrete building facade RF1-EPS

The proper locations of the relative humidity and temperature sensors were selected to evaluate the hygrothermal performance of the concrete building facade and predict the potential for deterioration of the different facade materials. In order to do that, temperature and relative humidity profiles are measured within the

facade wall. The sensors measure the temperature and relative humidity of different material layers and their contact surface, which allows the moisture problems within each material in the contact areas to be deduced. The different sensor types and their purpose, locations, and quantity are shown in Table 5.1.

Table 5.1: Relative humidity and temperature sensors installed in the concrete building facade RF1-EPS.

Point	Purpose	Sensor type	Monitored parameters	Total / Location
1	Monitoring the surface of the original inner concrete panel.	SHT15	Relative humidity	4
		PT100	Temperature	4
2	Monitoring the layer between original insulation and the original outer concrete panel.	SHT15	Relative humidity	4
		PT100	Temperature	4
3	Evaluation the wetting/drying patterns of the original outer concrete panel.	HMP44	Relative humidity	4
		PT100	Temperature	4
4	Monitoring the layer between the externally added insulation and the original facade.	SHT15	Relative humidity	4
		PT100	Temperature	4
5	Response of the new rendering system.	SHT15	Relative humidity	4
		PT100	Temperature	4
Outdoors	Monitoring the outdoor condition.	HMP44	Relative humidity	2
		PT100	Temperature	2
<b>Total / Facade</b>				<b>44</b>

### 5.1.2 Concrete building facade RF2-MWOOL

The monitored concrete building facade RF2-MWOOL, shown in Figure 5.4, belongs to a three-storey apartment building built with sandwich elements. The facade was repaired by adding 70 mm of external mineral wool insulation and a 6-mm rendering system. The

RHT-MAPS sensor network was installed in the north-eastern and south-western parts of the building.

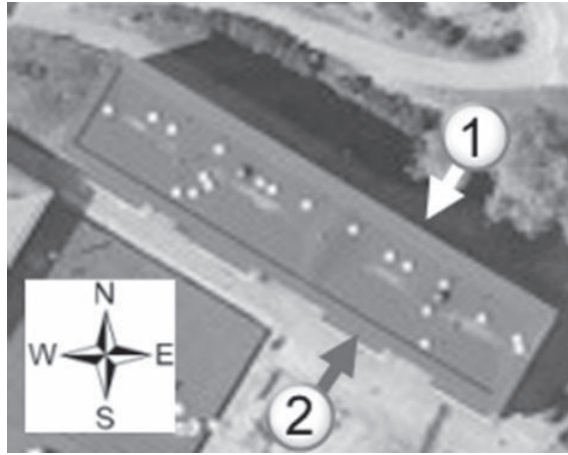


Figure 5.4: Location of the monitored locations of the building facade RF2-MWOOL: 1. north-eastern facade wall and 2. south-western facade wall.

In the repaired facade RF2-MWOOL, the relative humidity and temperature sensors were installed on the first and third floors and facing northeast and southwest, respectively. The sensors were installed through the cross-sections of the walls as shown in Figure 5.5. The list of the different relative humidity and temperature sensor types, the purpose of their use, the locations that were monitored, and the total number of sensors for every location are similar to the list shown in Table 5.1.

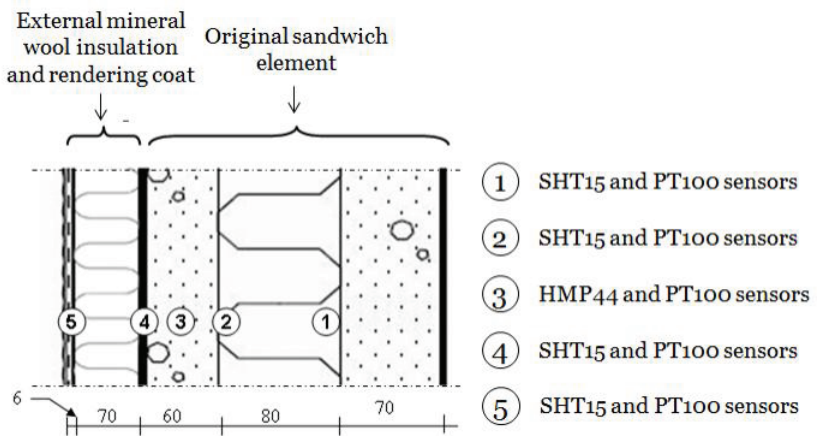


Figure 5.5: Wall cross-section and installation of nodes and sensors in the repaired facade (RF1-EPS)

## 5.2 Reliability and accuracy of the measurements

Reliability and accuracy of the relative humidity and temperature measurements is essential for the assessment of the hygrothermal performance of concrete building facades. The reliability and the accuracy of the data depend on the reliability of the RHT-MAPS components and the accuracy of the monitoring sensors. The operating temperature range for the RHT-MAPS node is between  $-40^{\circ}\text{C}$  and  $+85^{\circ}\text{C}$ , which makes it reliable for use in outdoor conditions. The sensors were additionally coated with epoxy varnish. The coating offers protection against moisture and condensation. As mentioned in Chapter 3, the calibration of the relative humidity and temperature sensors was confirmed by the manufacturers. The reliability and accuracy of the sensors used in the RHT-MAPS sensor network are shown in Table 5.2.

Table 5.2: Reliability and accuracy of the relative humidity and temperature sensors.

	Relative humidity sensor		Temperature sensor
	HMP44	SHT15	PT100
Measurement range	0 - 100%	1 - 100%	$-50$ to $+200^{\circ}\text{C}$
Accuracy			$< 0.25^{\circ}\text{C}$
Accuracy 0...90%RH	$\pm 2\%$ RH	$\pm 2\%$ RH	
Accuracy 90...100%RH	$\pm 3\%$ RH	$\pm 2$ to $4\%$ RH	
Response time	15 s - 30 min	4 s	$< 0.7$ sec
Operating temperature range for electronics	$-40$ to $+60^{\circ}\text{C}$	$-40$ to $+124^{\circ}\text{C}$	$-50$ to $+200^{\circ}\text{C}$

The relative humidity and temperature data obtained during a five-year field monitoring period from the summer of 2005 up till the summer of 2010 had some interruptions as a result of data acquisition hardware-related failures and power outages. The data loss in the long-term field monitoring of the concrete building facades RF1-EPS and RF2-MWOOL is shown in Table 5.3.

Table 5.3: Relative humidity and temperature monitoring data loss durations.

Year	RF1-EPS			RF2-MWOOL		
	From	To	Period (days)	From	To	Period (days)
2005	3.1.2005	6.10.2005	3	25.10.2005	17.11.2005	22
2006	31.10.2006	3.11.2006	3			
2007	4.5.2007	7.9.2007	126	11.2.2007	2.3.2007	19
2008	20.4.2008	17.6.2008	58	7.7.2008	1.10.2008	86
2009	17.1.2009	18.1.2009	1	10.11.2009	6.3.2010	116

The data losses were compensated for by the hourly relative humidity and temperature data from the Helsinki-Malmi Airport weather station history database, as shown in Figure 5.6.

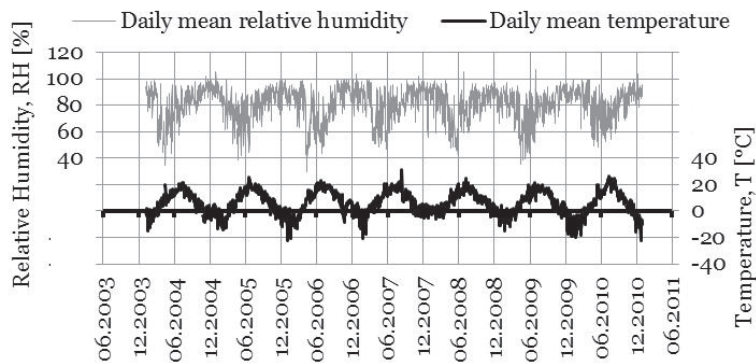


Figure 5.6: Daily mean of the air relative humidity and temperature at Helsinki-Malmi airport. (Weather Forecast, 2013)

### 5.3 The climate exposure parameters

Different climates can be classified according to various climatic parameters, such as amounts of precipitation or temperature averages. For engineering purposes, such categorisation is useful when designing outdoor structures. Climate parameters may also be combined in indices providing more complete climatic definitions, for example a moisture index. Variations in relative humidity and temperature, liquid water from precipitation and condensation, and frost influences, either separately or combined, may result in the degradation of material. Defining the coexistence of the outdoor

temperature and relative humidity provides input for determining the deterioration of the concrete building facades under consideration.

### 5.3.1 Relative humidity and temperature

The yearly weather conditions in terms of monthly mean variations in air temperature around the concrete building facades RF1-EPS and RF2-MWOOL and the statistical data from the southern Finland area during the years 1981-2012 are shown in Table 5.4 and Table 5.5 respectively.

Table 5.4: Monthly temperature of the monitored location RF1-EPS.

	Measured data					Statistical data		
	2005	2006	2007	2008	2009	1980 - 2010*	2011**	2012**
January	-4.5	-2.3	-3.5	-3.9		-5.0	-4.4	-3.4
February	-8.7	-9.3	-6.1	-4.8		-5.7	-9.9	-6.8
March	-5.8	-2.9	-2.5	-1.6		-1.9	-1.0	0.8
April	3.9	5.5	6.0	4.7		4.1	5.6	4.1
May	11.2	10.5	10.6	11.7		10.4	9.9	10.9
June	15.4	16.9	15.4	14.6	13.5	14.6	16.7	13.7
July	20.0	19.8	17.2	17.9		17.7	20.6	17.7
August	16.7	18.9	17.1	15.1		15.8	17.5	16.0
September	13.0	14.0	11.1	9.8		10.7	13.6	12.5
October	7.6	7.7	6.5	8.2		5.6	8.5	6.7
November	3.9	1.7	1.0	2.4		0.4	5.3	4.2
December	-3.2	1.0	1.4	0.2		-3.2	3.4	-5.3

\*) Source: (Pirinen et al. 2012)

\*\* ) Source: (The Finnish Meteorological Institute, 2013)

Table 5.5: Monthly temperature of the monitored location RF2-MWOOL.

	Measured data					Statistical data		
	2005	2006	2007	2008	2009	1980 - 2010*	2011**	2012**
January		-5.0	-2.8	-1.8	-3.5	-5.0	-4.4	-3.4
February		-9.1	-9.1	-6.1	-4.4	-5.7	-9.9	-6.8
March		-6.4	2.8	-3.8	-2.9	-1.9	-1.0	0.8
April		3.4	4.9	5.8	4.1	4.1	5.6	4.1
May		10.5	11.2	11.0	11.1	10.4	9.9	10.9
June		16.5	16.1	14.8	14.2	14.6	16.7	13.7
July	19.3	19.2	17.3	17.4	17.2	17.7	20.6	17.7
August	16.1	18.4	17.1	15.1	16.2	15.8	17.5	16.0
September	12.1	13.5	11.0	9.7	12.5	10.7	13.6	12.5
October	6.9	7.3	5.9	7.8	2.9	5.6	8.5	6.7
November	3.4	1.5	-0.6	2.3	2.2	0.4	5.3	4.2
December	-4.0	2.7	1.3	0.8	-5.9	-3.2	3.4	-5.3

\*) Source: (Pirinen et al. 2012)

\*\*\*) Source: (The Finnish Meteorological Institute, 2013)

Comparing the measured mean of the outdoor ambient temperature for both facades and the statistical values of the monthly average temperature shows a strong positive linear correlation between the measured and the statistical temperature data. The values of the correlation coefficient ( $r$ ), shown in Table 5.6, varied from 0.92 to 0.99.

Table 5.6: Linear correlation coefficient between measured and statistical values of the monthly average temperature.

Statistical data	Measured data			
	2006	2007	2008	2009
<b>RF1-EPS</b> 1981 - 2010	0.98	0.97	0.99	
2011	0.98	0.98	0.98	
2012	0.95	0.95	0.96	
<b>RF2-MWOOL</b> 1981 - 2010	0.96	0.97	0.98	0.98
2011	0.98	0.96	0.97	0.92
2012	0.93	0.95	0.95	0.98

Changes in the relative humidity of the ambient air around the concrete building facades RF1-EPS and RF2-MWOOL are apparent in Figure 5.7 and Figure 5.8 respectively. The monthly mean relative humidity drops during the spring from about 85% RH and continues through the summer to 60% RH, then rises again by the end of the

summer to a value of 90% during the autumn and the winter. Comparing the monthly mean relative humidity and the values of the monthly average relative humidity in the southern Finland area during the years 1981-2012 shows a strong positive linear correlation between the measured and the statistical relative humidity data. As shown in Table 5.7, the values of the correlation coefficient varied from 0.76 to 0.98.

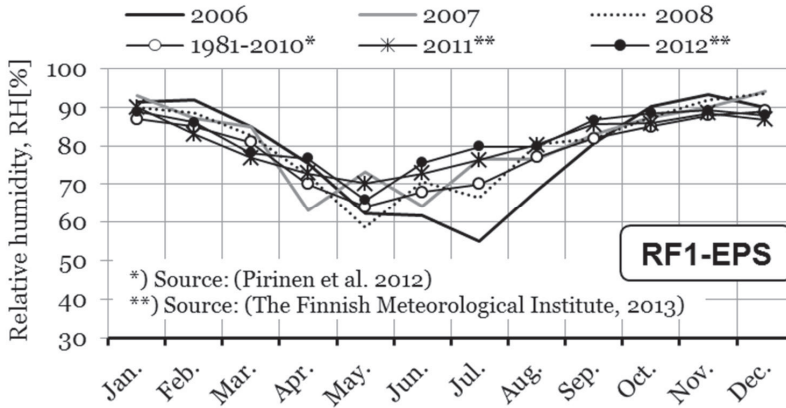


Figure 5.7: Monthly mean of the ambient air relative humidity for the facade RF1-EPS.

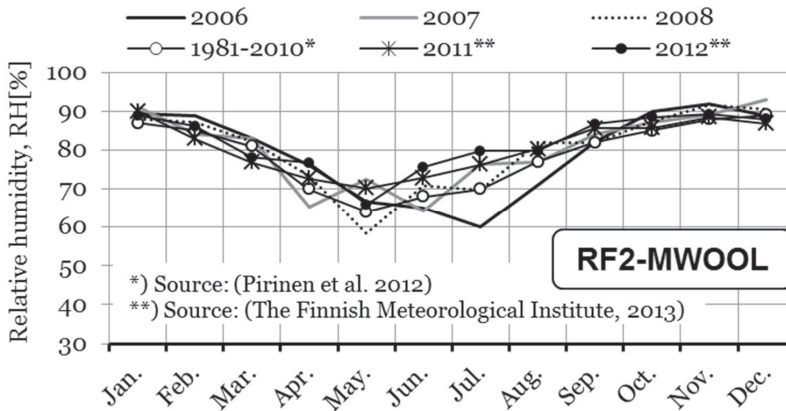


Figure 5.8: Monthly mean of the ambient air relative humidity for the facade RF2-MWOOL.



Table 5.7: Linear correlation coefficient between measured and statistical values of the monthly average relative humidity.

Statistical data		Measured data			
		2006	2007	2008	2009
RF1-EPS	1981 - 2010	0.91	0.91	0.98	
	2011	0.79	0.87	0.90	
	2012	0.77	0.76	0.90	
RF2-MWOOL	1981 - 2010	0.92	0.91	0.97	0.98
	2011	0.81	0.90	0.90	0.93
	2012	0.78	0.79	0.92	0.90

A typical pattern of the daily relative humidity of the outdoor ambient air, as shown in Figure 5.9, is nearly a mirror image of the corresponding temperature. Both in summer and winter, it is clear that as the temperature increases there is a fall in relative humidity and that when the temperature goes down the relative humidity goes up.

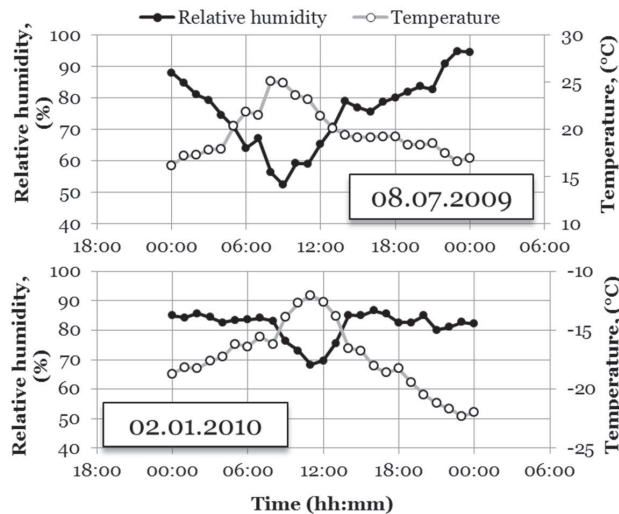


Figure 5.9: Examples of the daily variation in outdoor ambient relative humidity and temperature of the concrete building facade RF2-MWOOL (hourly measured data).

### 5.3.2 Moisture index

As mentioned in Section 2.3.1, the moisture index (MI) describes the environmental moisture and thermal load. The moisture index is a function of the amount of annual wetting and the annual potential for evaporation. The amount of wetting inside the surface of the concrete facades is assumed to be similar to the amount of rainfall around

them. The monthly mean precipitation ( $\text{kg}/\text{m}^2$ ) in southern Finland during the years 1981-2010 is shown in Figure 5.10.

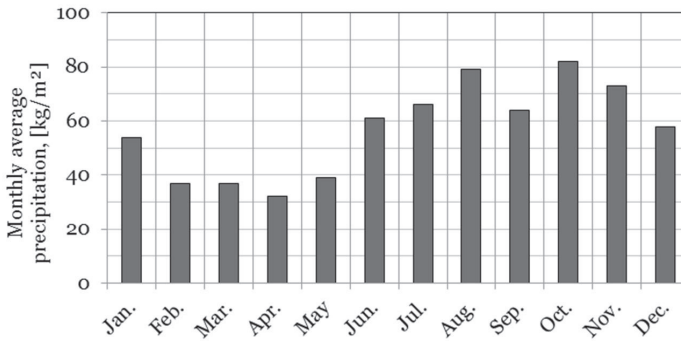


Figure 5.10: The monthly mean precipitation in Helsinki. Source: Climatological statistics of Finland 1981–2010 (Pirinen et al. 2012).

The monthly moisture index is calculated based on the monthly mean of relative humidity, temperature, and precipitation for the ambient outdoor conditions around the concrete building facades RF1-EPS and RF2-MWOOL. Figure 5.11 and Figure 5.12 show the monthly moisture index for the concrete building facades RF1-EPS and RF2-MWOOL respectively. The hypothesis is that the higher the value of MI, the greater the potential risk of moisture-related damage. The values show that the highest potential for the moisture load ( $\text{MI} \geq 1.00$ ), in both facades, RF1-EPS and RF2-MWOOL, covers the period from October to March, while the lowest potential for the moisture load ( $\text{MI} \leq 0.70$ ) is around May and July yearly.

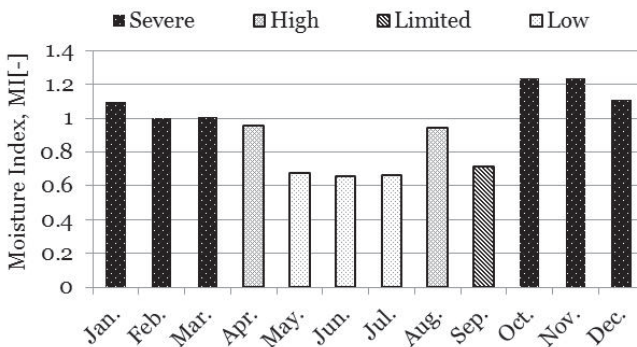


Figure 5.11: The monthly-normalised moisture index for the outdoor conditions around the concrete building facade RF1-EPS.

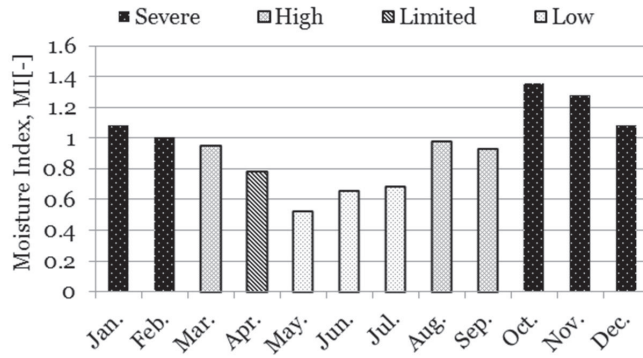


Figure 5.12: The monthly-normalised moisture index for the outdoor conditions around the concrete building facade RF2-MWOOL.

### 5.3.3 Freezing and thawing

The impacts of the regional climates on the durability of structures and their materials vary according to the materials used and construction practices. One of the most potentially destructive weathering factors on concrete building facades in the northern countries is freezing and thawing. In this thesis, the environmental factors affecting the frost resistance of concrete building facades are the cooling and warming rates and the number of freezing and thawing cycles.

The cooling and warming rates were calculated on the basis of hourly temperatures below 0°C. The maximum cooling and warming rates of the outdoor ambient air are shown in Table 5.8. The maximum cooling rate for the air during the monitoring period varied from -1.8 to -6.8°C/h and the maximum warming rate varied from 4.3 to 10.4°C/h during the monitoring period.

Table 5.8: The maximum cooling and warming rates of the outdoor ambient air of the concrete building facades RF1-EPS and RF2-MWOOL.

Facade wall direction	Cooling rate (°C/h)				Warming rate (°C/h)			
	2006*	2007	2008	2009	2006	2007	2008	2009
RF1-EPS, Southwest	-6.4	-6.0	-3.8	-6.8	6.9	8.6	6.5	7.1
RF1-EPS, Northeast	-2.4	-2.7	-1.8	-2.5	4.3	4.3	4.9	5.1
RF2-MWOOL, Southwest	-4.8	-5.7	-2.6	-3.7	6.3	6.3	6.2	10.4
RF2-MWOOL, Northeast	-3.7	-3.2	-2.6	-3.7	8.4	5.5	7.3	8.5

\*) Winter 2005/2006

The freezing and thawing cycle as defined for this thesis occurs when the temperature crosses +2°C, drops down below at least -5°C, and then returns above +2°C again. By selecting these values of temperatures, the freezing and thawing of free water in the pores of the concrete is ensured.

The numbers of freezing and thawing cycles outdoors are shown in Table 5.9. As for the ambient outdoor conditions during the monitoring period, the number of freezing and thawing cycles is higher in the south-west than in the north-east. The larger number of cycles in the south-western parts of the building is due to the solar radiation that warms up the air in the south-west part of the facade wall during the colder months of the year.

Table 5.9: Number of freezing and thawing cycles outdoors.

Direction	Number of freezing- thawing cycles outdoors				
	2006*	2007	2008	2009	2010
RF1-EPS, Southwest	21	15	22	21	
RF1-EPS, Northeast	9	11	10	9	
RF2-MWOOL, Southwest	23	12	15	13	11
RF2-MWOOL, Northeast	11	12	14	12	9

\*) Period from June 2005 to May 2006

## 5.4 Response of concrete building facades to the outdoor conditions

This section investigates how the concrete building facades respond to changes in the outdoor ambient temperature and relative humidity. When reviewing these results, it should be considered that the monitoring system measurements were not received from May to September 2007 for the RF1-EPS facade and from July 2008 to March 2009 for the RF2-MWOOL facade.

The response of the concrete building facades is assessed by (i) presenting the variation in the relative humidity and temperature within the facades, and (ii) estimating the risk of damage to the building facade on the basis of the temperature, moisture content, RHTI index, and freezing-thawing cycles as described in Sections 2.3.2 and 2.3.3.

The RHTI and FTI indices represent the intensity of the hygrothermal level in the rendering coat by which the critical conditions are exceeded. The critical temperature and relative humidity vary depending on the nature of the construction material and the moisture damage involved. In this thesis, RHTI-Bio, RHTI-Corr, RHTI-Carb, and FTI indices were calculated. The descriptions and the critical relative humidity and temperature values for these indices are shown in Table 5.10.

Table 5.10: The critical relative humidity and temperature values for the moisture indices

<b>Index</b>	<b>Temperature, T [°C]</b>	<b>Relative humidity, RH [%]</b>
RHTI-BIO	$T \geq 0^{\circ}\text{C}$	$\text{RH} \geq 75\%$
RHTI-CORR	$T \geq 0^{\circ}\text{C}$	$\text{RH} \geq 80\%$
RHTI-CARB	$T \geq 0^{\circ}\text{C}$	$65 \leq \text{RH} \leq 75\%$
FTI	$T \leq 0^{\circ}\text{C}$	$\text{RH} \geq 95\%$

### 5.4.1 Hygrothermal conditions at different locations in the facade wall

Examples of the relative humidity and temperature in the rendering system during the winter and summer are shown in Figure 5.13 and Figure 5.14 respectively. It can be seen that the relative humidity and temperature in the rendering system vary because of the solar radiation. During the hours of daylight, solar radiation will raise the temperature of the surface significantly, while it is reduced during the night; this will have a direct effect on the relative humidity in the rendering system. The relative humidity of the rendering system decreases during the daylight period but then increases during the night.

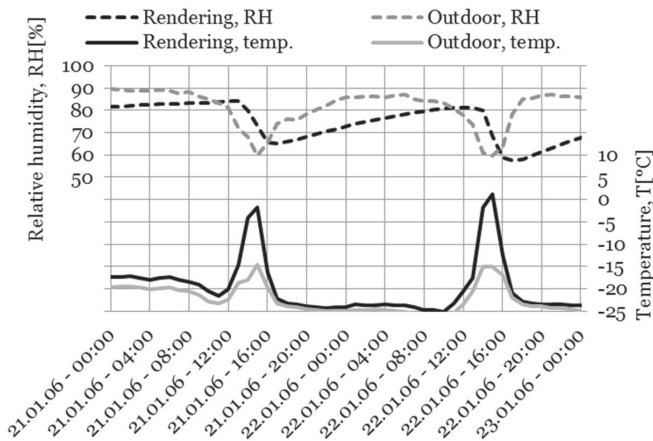


Figure 5.13: Example of the relative humidity and temperature in the rendering system of the facade RF1-EPS during cold winter conditions (data measured hourly).

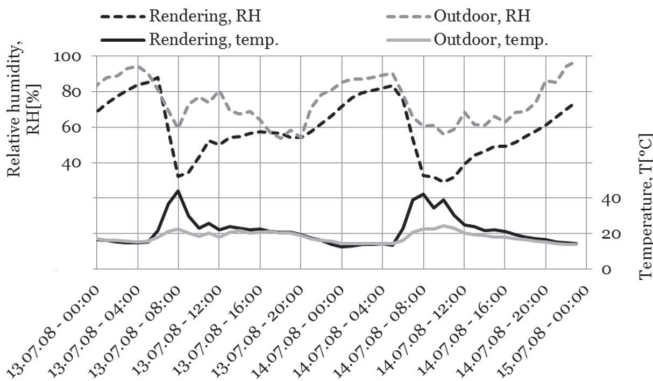


Figure 5.14: Example of the relative humidity and temperature in the rendering system of the facade RF1-EPS during a hot summer day (data measured hourly).

The monitoring results for the moisture behaviour in the concrete building facade RF2-MWOOL are presented in Figure 5.15. Differences in the relative humidity between different layers of the facade were clear. The results show that the variation in the daily average relative humidity in the rendering coat (5) follows the variation in the outdoor ambient relative humidity. At the interior surface of the new mineral wool insulation layer (4), the variations in relative humidity were smaller and the relative humidity values were always in the range from 20% to 70% RH. The relative humidity in the original facade layers was lower than 65% RH during the year.

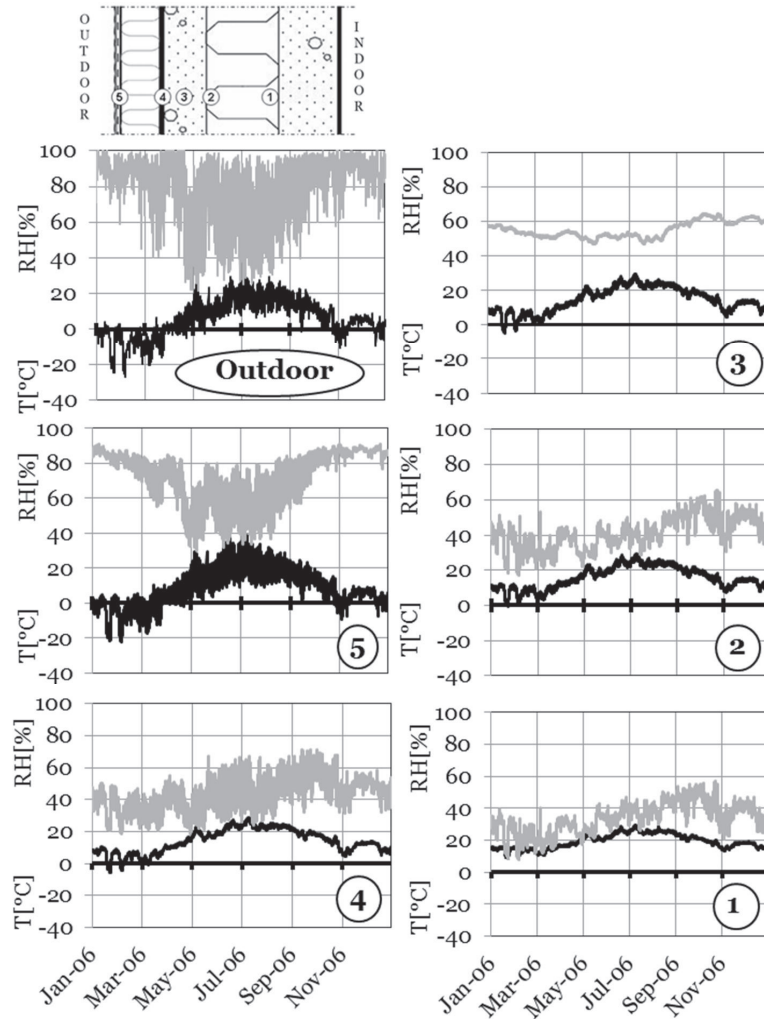


Figure 5.15: Variations in the relative humidity and temperature of the facade RF2-WOOL during the year 2006 (hourly data).

During the year 2006, the results indicate that the temperature of the rendering coat follows the outdoor ambient air temperature. The temperature under the new insulation layer (4) dropped below 0°C during January to March and then was higher than 0°C till the end of the year. The temperature inside the original outer concrete panel (3) and on the surface of the original mineral wool insulation (2) was always above 0°C.

#### 5.4.2 Time-dependent moisture and thermal indices

Examples of the calculated values of the RHTI-CORR and the RHTI-CARB indices for the rendering coat of the concrete building facade RF2-MWOOL are shown in Figure 5.16 and Figure 5.17 respectively. The values of the RHTI-CORR index indicate the low potential for corrosion damage to the metal parts of the rendering system in the period from January to July; the risk increases from then to the end of the year.

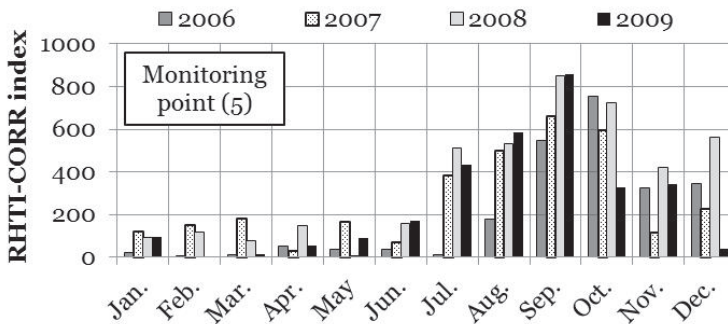


Figure 5.16: The corrosion potential of the metal parts of the rendering coat on the north-eastern side of the concrete building facade RF2-MWOOL.

The values of the RHTI-CARB index show a higher potential for the carbonation of the rendering coat during the summer and autumn as a result of the increase in the temperature and decrease in the relative humidity and lower potential during the winter and the springtime.



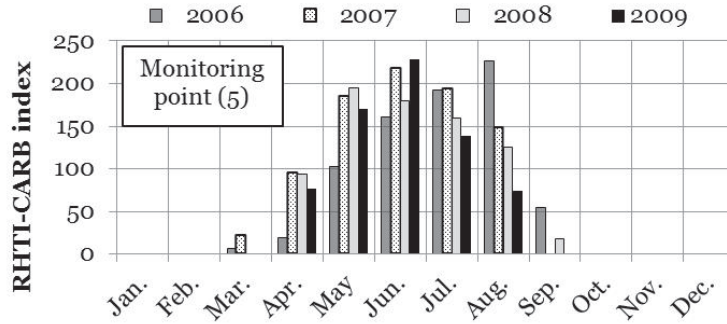


Figure 5.17: The carbonation potential of the rendering coat on the north-eastern side of the concrete building facade RF2-MWOOL.

The calculated values of the RHTI-BIO index for the external surfaces of the external mineral wool insulation of the concrete building facade RF2-MWOOL are shown in Figure 5.18. The results show that the biological growth risk increases during the end of the summer and the autumn. The risk is very low during the winter and the spring as a result of the low temperature values.

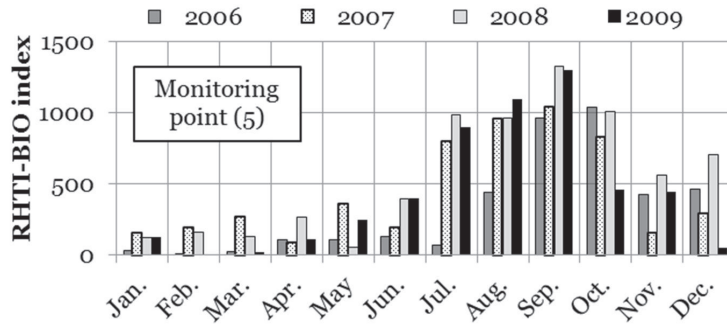


Figure 5.18: The potential of biological damage inside the external surface of the external mineral wool insulation on the north-eastern side of the concrete building facade RF2-MWOOL.

The results indicated that the risk of biological growth inside the internal surface of the mineral wool insulation did not exist because the relative humidity was below 80% RH through the year.

The freezing and thawing indices for the north-eastern rendering coat of the concrete building facades RF1-EPS and RF2-MWOOL are shown in Figure 5.19 and Figure 5.20 respectively. The results show that the potential for frost damage in the concrete building facades

that were monitored exists yearly from October, increases during December and January, and continues until the end of March.

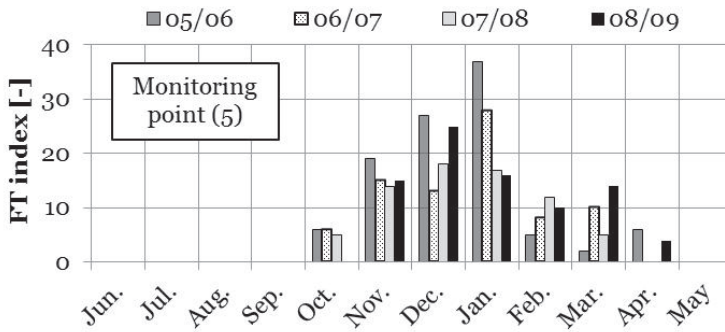


Figure 5.19: FTI index for the north-eastern rendering coat of the concrete building facade RF1-EPS.

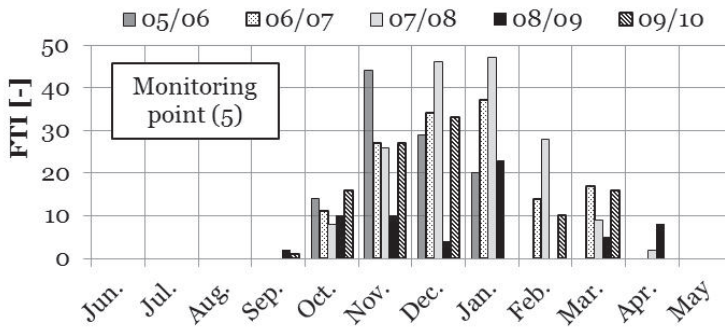


Figure 5.20: FTI index for the north-eastern rendering coat of the concrete building facade RF2-MWOOL.

The acceptable values for RHTI indices for various building materials are not available at this moment. The important features of the RHTI index include the fact that the relative humidity, temperature, and duration effects are all reflected in a single value indicator. In addition, higher RHTI index values indicate an increased severity of the hygrothermal response and greater damage potential.

### 5.4.3 Freezing and thawing cycles

The total yearly number, duration, and the lowest temperature of the freezing and thawing cycles in the facades that were monitored are shown in Table 5.11. The freezing and thawing cycle that is considered is defined in Section 5.3.3.

The results showed that the yearly freezing and thawing cycles in the rendering coat in the south-western side were always higher than those on the north-eastern side of the building. The reason is that the solar radiation warms up the rendering coat layer in the south-west and thus increases the number of freezing and thawing cycles. It was also seen that the duration of the freezing and thawing cycles and the lowest temperature of the cycles were very similar every year.

The numbers of freezing and thawing cycles in the rendering coat layer of the concrete building facades that were monitored are used in the prediction model of frost damage to concrete as shown in Chapter 6, Section 6.3.

Table 5.11: The number of critical freezing and thawing cycles in the rendering coat.

Facade wall direction		Freezing- thawing cycles in the rendering system			
		2006*	2007	2008	2009
RF1-EPS, Southwest	Number of cycles	57	41	40	49
	Duration (d)	123.6	78.8	67.8	98.5
	Lower temp. (°C)	-26.5	-27.9	-15.5	-20.5
RF1-EPS, Northeast	Number of cycles	19	16	21	25
	Duration (d)	121.8	72.7	57.7	91.5
	Lower temp. (°C)	-24.0	-25.0	-13.9	-17.6
RF2-MWOOL, Southwest	Number of cycles	73	30	31	9
	Duration (d)	93.5	40.6	35.8	90.0
	Lower temp. (°C)	-24.6	-24.6	-13.2	-23.6
RF2-MWOOL, Northeast	Number of cycles	35	13	20	6
	Duration (d)	102.5	43.9	44.5	88.3
	Lower temp. (°C)	-22.7	-23.0	-11.4	-23.6

\*) Period from June 2005 to May 2006

## 5.5 Summary

Field research was carried out to test the RHT-MAPS that was developed and to demonstrate its benefits. The RHT-MAPS was installed in the north-eastern and south-western parts of two repaired concrete building facades which are exposed to the outdoor

weather in southern Finland. The relative humidity and temperature were monitored every 15 minutes during a five-year period from the summer of 2005 up until the summer of 2010. Hourly values are used in the data analysis because there were no significant differences between the 15-minute measurements and the one-hour measurements.

The monitored outdoor ambient relative humidity and temperature were statistically analysed to determine the climatic parameters affecting the concrete building facades. Relative humidity and temperature were also combined in the moisture index and freezing and thawing, which provide more climatic definitions. The results show that the monthly averages of relative humidity and temperature in the locations that were monitored during the years 2006-2008 are close to the climatological average monthly relative humidity in the southern part of Finland during 1981-2010. The values of the moisture index show that the highest potential for moisture problems is from October to March, while the lowest potential for moisture problems is only around May and July every year.

The response of the concrete building facades to the surrounding climate was assessed by (i) presenting the variation in their relative humidity and temperature and (ii) estimating the risk of damage caused by moisture and changes in temperature within their different layers. The results show that the external insulation and rendering system reduce the risk of the deterioration of the original concrete facades, as their temperature remains above zero and the relative humidity was lower than 65% RH.

The hygrothermal field monitoring of concrete building facades is useful for: (i) documenting and analysing the relative humidity and temperature data within the concrete facades and the surrounding environmental conditions; (ii) integrating the effects of these relative humidity and temperature data into different indicators for calculating the potential for deterioration, and (iii) working as an early warning alarm to ensure appropriate renovation and maintenance measures by setting different threshold values for the deterioration indicators.

The field-monitored relative humidity and temperature data for the outdoor ambient air and the wall layers of the concrete building facades will be used in prediction models of the corrosion of reinforcement, carbonation, and frost damage to concrete and the potential of biological growth in the insulation layers in Chapter 6.



## 6 Deterioration and service life prediction

This chapter outlines the prediction of deteriorations and the remaining service life calculations of concrete building facades. The deterioration mechanisms of concrete building facades, along with the different models representing their interaction with the environment, are discussed. Data from in situ and laboratory investigations are used to validate the deterioration prediction models.

### 6.1 Overview of the durability and service life of concrete structures

The durability of a concrete structure is its capability to resist deterioration, particularly deterioration as a result of weather exposure, chemical exposure, surface abrasion, or any other deterioration process (Abdovies 2003). The deterioration of concrete typically occurs when the concrete is exposed to ambient outdoor conditions over an extended period. The deterioration of concrete, along with the reinforcement steel, during their service lives means a loss of 100% performance, and it may be due to a variety of mechanical, physical, chemical, or biological processes, as shown in Figure 6.1.

Physical	Temperature differences				
	Shrinkage				
	Early frost action	Late frost action			
Chemical				Acid, Sulphate, Alkali attack	
				Reinforcement corrosion	
Biological				Microgrowth	
				Hydrogen Sulphide (H <sub>2</sub> S) attack	
	Day	Week	Month	Year	Century

**Age of concrete structures**

Figure 6.1: Concrete deterioration mechanisms and possible time of appearance of cracking or damage (Apostolopoulos et al. 2008).

The EN 1990 (2002) defined the service life as the period of time after construction during which all properties exceed the minimum acceptable values when routinely maintained. In general, the service life of reinforced concrete depends on the time it takes for corrosion to initiate and the propagation time that is required for corroding steel to cause sufficient damage as to necessitate repairs to the concrete structures. According to Hovde (2004), the typical designed service lives for buildings are divided into five categories, which are related to the use of the building, to its cost, and to the extent of maintenance, replacements, and repairs, as shown in Table 6.1.

Table 6.1: Categories of design service life for buildings (Hovde 2004).

Category	Design service life for building	Examples
Temporary	Up to 10 years	- Non-permanent construction buildings, sales offices, bunkhouses - Temporary exhibition buildings
Short life	10 to 24 years	- Temporary classrooms
Medium life	25 to 49 years	- Most industrial buildings - Most parking structures
Long life	50 to 99 years	- Most residential, commercial, and office buildings - Health and educational buildings - Parking structures below buildings designed for long life category
Permanent	Minimum period 100 years	- Monumental buildings (e.g. National museums, art galleries, archives) - Heritage buildings



The remaining service life of concrete structures is defined as the number of years until repairs are required. Clifton et al. (2000) considered that the methods for predicting the remaining service life of existing concrete structures are the same as those for new structures. In addition, the existing structures can have the benefit of additional information being available, such as the derived material properties and the environmental loading effects. Methods for predicting the remaining service lives of concrete structures usually include the following general procedures:

- i. determining the condition of the concrete,
- ii. identifying the causes of the degradation of the concrete,
- iii. determining the continuing condition and the end of the service life of the concrete and
- iv. making a time estimation from the present state of the concrete to the end-of-service life state to establish the remaining service life.

With the development of computer techniques and the accumulation of data, mathematical simulation and modelling have been widely proposed as a solution for more reliable service life prediction. This kind of prediction requires knowledge about the dominant mechanisms, the relevant parameters, and the current stage of deterioration.

In this thesis, the prediction of the remaining service lives of concrete building facades considers carbonation-induced corrosion and frost damage as relevant deterioration mechanisms of concrete building facades and then determines the criteria which define the remaining service life of the element or structure in a quantitative way.

## **6.2 Heat and moisture transport modelling**

For predicting the deterioration of concrete building facades caused by moisture and changes in temperature, hygrothermal modelling was performed using the WUFI computer-based moisture analysis tool (Künzel et al. 2001). WUFI predicts moisture transfer by diffusion and capillary flow. The input data for the WUFI simulation were:

- the geometry and the wall assembly of the original concrete building facade RF2-MWOOL before being repaired, shown in Figure 6.2. The external surface of the facade is considered to be a surface which is not coated and thus as the worst case in terms of the risk of deterioration,
- the monitored relative humidity and outdoor temperature of the facade RF2-MWOOL in the north-easterly and south-westerly directions, and
- the properties of the building materials from the WUFI inbuilt material database.

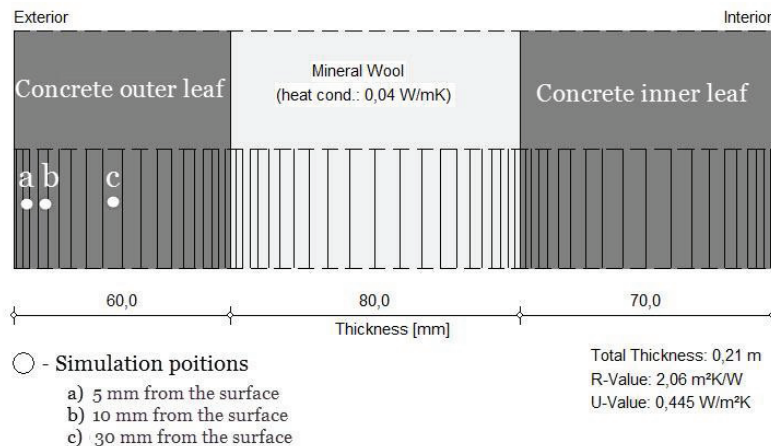


Figure 6.2: The assumed sandwich element of the concrete building facade and the relative humidity and temperature simulation positions.

The results of the relative humidity and temperature simulation are shown in Figure 6.3 to Figure 6.5 and are based on the outdoor conditions of the concrete facade RF2-MWOOL in the south-westerly direction. The simulated relative humidity and temperature values are used as follows:

- simulation position (5 mm from the surface): the values are used in the prediction of the initiation period of the carbonation-induced corrosion;
- simulation position (10 mm from the surface): the values are used in the prediction of the frost damage;
- simulation position (30 mm from the surface): the values are used in the prediction of the propagation period of the corrosion of the reinforcement.

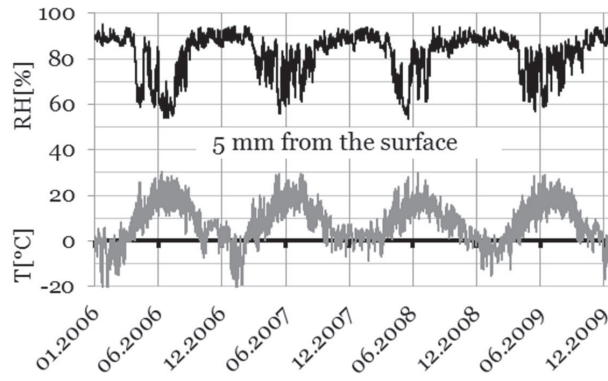


Figure 6.3: Simulated relative humidity and temperature 5 mm from the concrete facade surface.

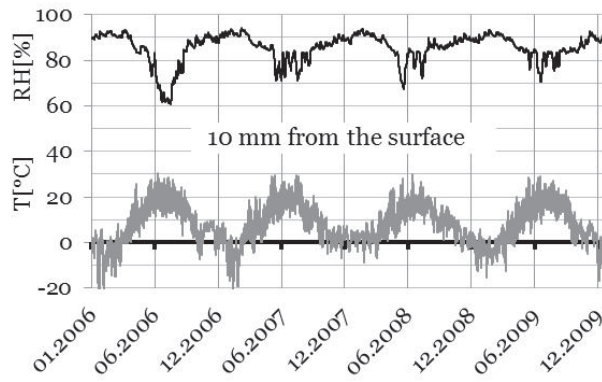


Figure 6.4: Simulated relative humidity and temperature 10 mm from the concrete facade surface.

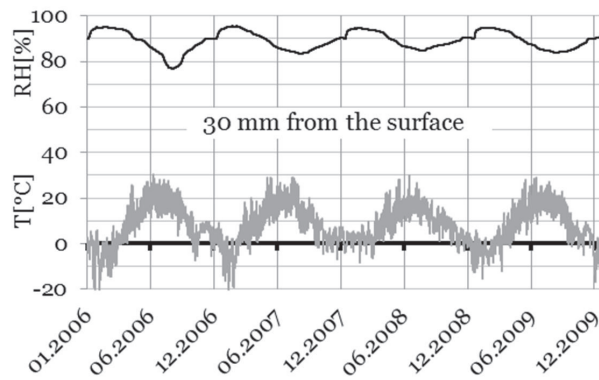


Figure 6.5: Simulated relative humidity and temperature 30 mm from the concrete facade surface.

### 6.3 Carbonation-induced corrosion

The carbonation-induced corrosion rate of the concrete is variable and highly dependent on the exposure conditions and properties of the concrete. Carbonation-induced corrosion proceeds at slower rates than chloride-induced corrosion. The carbonation of concrete leads to uniform steel corrosion, which accelerates crack formation and reduces the remaining service life of the structure. (Moreno and Sagues 1998) In this section we present: (i) the model for predicting the carbonation depth of concrete; (ii) validation of the model using the laboratory test and field monitoring results, and (iii) evaluation of the service life of carbonated concrete structures.

#### 6.3.1 Carbonation model

The carbonation process is a complicated one as it is a combination of the movement of gases and liquids. The carbonation of concrete is, in general, a diffusion process. The penetration rate of carbon dioxide depends mainly on the quality of the concrete and on the exposure conditions. The mathematical models of the carbonation of concrete introduced here are based on the diffusion of CO<sub>2</sub> in the pore system of concrete, which can be derived from Fick's second law:

$$\frac{\partial C}{\partial t} = D_{eff} \cdot \frac{\partial^2 C}{\partial X^2} \quad (6.1)$$

where

- $C$  is the concentration of the diffusing agent [mol/m<sup>3</sup>],
- $D_{eff}$  is the diffusion coefficient of carbon dioxide [m<sup>2</sup>/s],
- $t$  is the time factor [a], and
- $X$  is the distance from the surface of the concrete [m].

A lot of concrete carbonation models have been formulated by applying suitable modifications to Fick's second law of diffusion. The models generally contain parameters that relate to environmental factors involved in the carbonation process and others which describe the capacity of the cement paste matrix to bind the carbon dioxide. Typically, the concrete carbonation models take the format shown in Equation (6.2) (DuraCrete: Modelling of Degradation 1998).

$$X_{ca} = k_{ca} * \sqrt{t} \quad (6.2)$$

where

- $X_{ca}$  is the carbonation depth at time  $t$  [mm],  
 $k_{ca}$  is the carbonation rate [mm/a<sup>0.5</sup>], and  
 $t$  is the age of the concrete [a].

This thesis uses a model of the time-dependent carbonation depth of concrete, as shown in Equation (6.3). The carbonation depth model is based on the model developed by Papadakis (1992) and takes into consideration the effect of the composition of the concrete and the history of the relative humidity and temperature on the carbonation depth of concrete, as described in Ann et al. (2010), Kari (2009), Vesikari (2009), Saelta (2005), and Carlsson (2003).

$$X_{ca} = k_{con} * k_{cur} * k_T * k_{RH} * k_{CO_2} * \sqrt{t} \quad (6.3)$$

where

- $k_{con}$  is the quality of concrete related coefficient,  
 $k_{cur}$  is the concrete curing factor,  
 $k_{RH}$  is the relative humidity related coefficient,  
 $k_T$  is the temperature related coefficient, and  
 $k_{CO_2}$  is the square root of the carbon dioxide content in air.

Papadakis (1992) summarised the main composition parameters of concrete that affect the carbonation process as the water-to-cement ratio and aggregate-to-cement ratio. A simplified expression of the effect of the composition of the concrete on the depth of the carbonation with time is shown in Equation (6.4) (Papadakis (1992) and Saelta (2005)).

$$k_{con} = 350 * \frac{\rho_c}{\rho_w} * \left( \frac{\frac{w}{c} - 0.3}{1 + \frac{\rho_c}{\rho_w} * \frac{w}{c}} \right) * \sqrt{1 + \frac{\rho_c}{\rho_w} * \frac{w}{c} + \frac{\rho_c}{\rho_a} * \frac{a}{c}} \quad (6.4)$$

where

- $\rho_c$  is the mass density of the cement [kg/m<sup>3</sup>],  
 $\rho_w$  is the density of the water [kg/m<sup>3</sup>],  
 $\rho_a$  is the mass density of the aggregates [kg/m<sup>3</sup>],  
 $w/c$  is the water-to-cement ratio [-], and  
 $a/c$  is the aggregate-to-cement ratio [-].

According to Duracrete (2000), the values of the concrete curing coefficient ( $k_{cur}$ ) for the carbonation resistance are 1.0 for 7 days' curing and 0.76 for 28 days' curing of the concrete.

The influence of the ambient temperature history of the concrete surface on the carbonation depth is shown in Equation (6.5). (Kari, 2009 and Sietta 2005)

$$k_T = EXP \left( \frac{Q}{R} * \left( \frac{1}{273 + T_0} - \frac{1}{273 + T} \right) \right) \quad (6.5)$$

where

- $Q$  is the activation energy of the carbonation process,  
 $Q = 2.7$  [kJ/mol]
- $R$  is the gas constant,  $R = 0.008314$  [kJ/mol.K]
- $T_0$  is the reference temperature,  $T_0 = 25$  [°C]
- $T$  is the actual temperature in the concrete [°C].

Carlsson (2003) and Sietta (2005), cited in Kari (2009), quantified the effect of the history of the ambient relative humidity on the carbonation depth of the concrete according to Equation (6.6).

$$k_{RH} = \left( 1 - \frac{RH}{100} \right)^n \text{ for } RH \geq 65\% \quad (6.6)$$

Where:

- $RH$  is the relative humidity in the concrete cover [%], and
- $n$  is an exponent of range (1 – 2.5)

For this thesis, the value of the exponent ( $n$ ) is considered to be 1.1 on the basis of comparing the model results with the natural carbonation depth results as shown in the following section.

The carbonation process has an ongoing need for carbon dioxide from the atmosphere. The carbon dioxide content of the atmosphere by volume is considered to be 0.035% (350 ppm) and the value of  $k_{CO_2}$  is considered to be 0.0187.

### 6.3.2 Validation of the carbonation model

For predicting the carbonation depth of the concrete building facades, some assumptions were made, as follows:

- i. the concrete cover of the reinforcement is selected according to the EN 1992-1-1 (2004) for the corrosion induced by carbonation exposure;
- ii. the properties of the outer panel concrete of the sandwich element are similar to those of the concretes used in the natural carbonation tests, shown in Table 4.5;
- iii. the values of the relative humidity and temperature factors are calculated from the simulated relative humidity and temperature at a depth of 5 mm from the surface, as shown in Figure 6.3 and Figure 6.5.

The applicability of the carbonation model was validated by comparing the predicted carbonation depth with the accelerated and natural carbonation test results. A comparison between the accelerated carbonation test results and the predicted carbonation depths is shown in Figure 6.6.

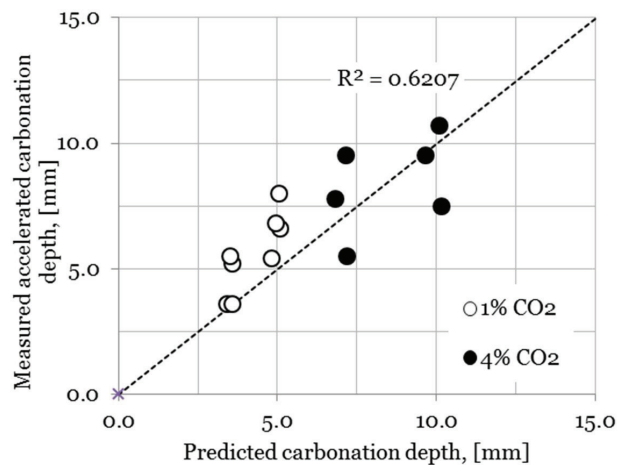


Figure 6.6: Correlation between the predicted and the measured carbonation depth from accelerated carbonation tests.

The predicted carbonation depths were calculated using the carbonation model described in Equation (6.3]. The input for the carbonation model was: (i) the properties of different concrete types (shown in Table 4.3 and Table 4.4); (ii) relative humidity of 65%; (iii)

a temperature of  $20 \pm 2^\circ\text{C}$ , and (iv) a carbon dioxide content of 1% or 4%. The relative humidity, temperature, and carbon dioxide input data are based on the accelerated carbonation chamber conditions shown in Figure 4.4. The results show that the measured carbonation depth correlates with the predicted carbonation depth with an R-squared value of 0.62.

The results for the predicted carbonation depth are shown in Figure 6.7.

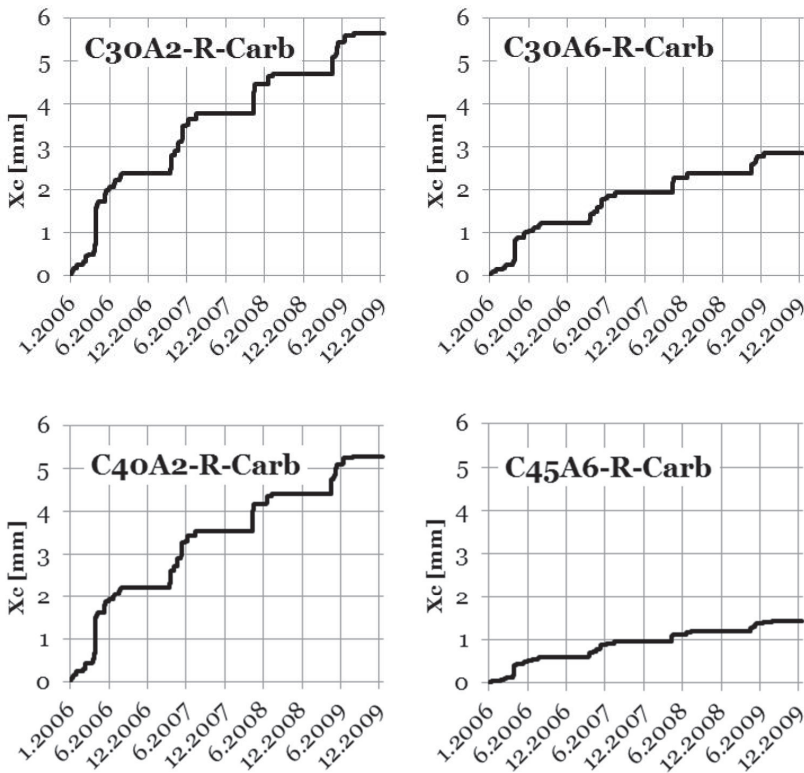


Figure 6.7: Predicted carbonation depth based on the relative humidity and temperature data for different concrete mixes.

The results show the effect of air entrainment on the carbonation depth for different concrete mixes for the same relative humidity and temperature conditions. It is clear that air entrainment helps to reduce the carbonation depth by reducing the water-to-cement ratio and the aggregate-to-cement ratio and then enhances the time taken by the carbonation front to reach the reinforcement level of the concrete.



A comparison of the predicted and measured carbonation depths for the different concrete mixes is shown in Figure 6.8. The results show that the predicted carbonation depth is closer to the measured carbonation depth for the air-entrained concretes than the non-air-entrained concretes, which is also shown in Figure 6.9.

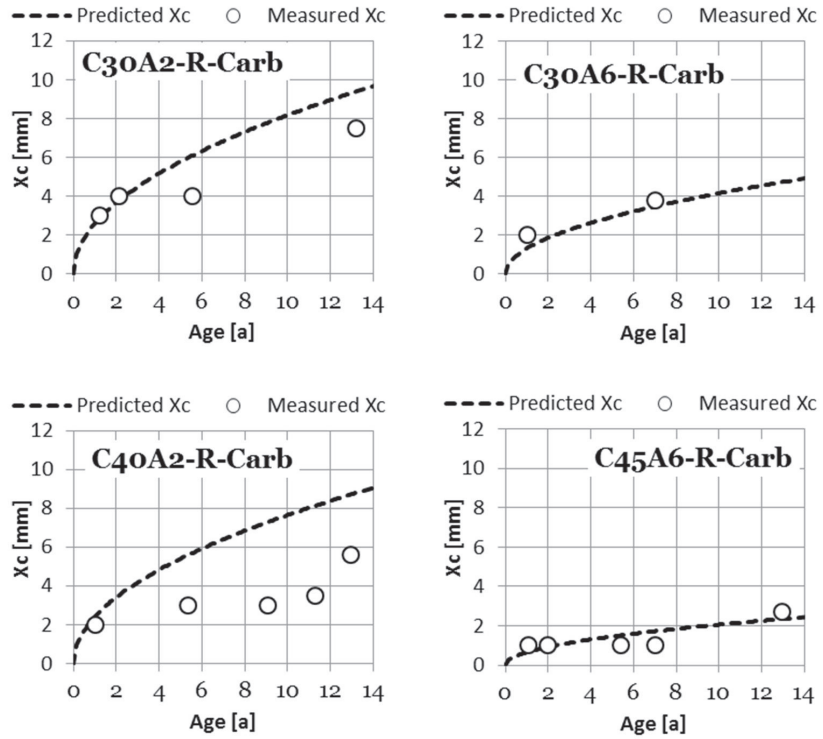


Figure 6.8: Comparison of the predicted and measured carbonation depths for different concrete mixes.

As shown in Figure 6.9, the results show that the natural carbonation depth of the concrete samples that were exposed to rain correlates with the predicted carbonation depth with an R-squared value of 0.71.

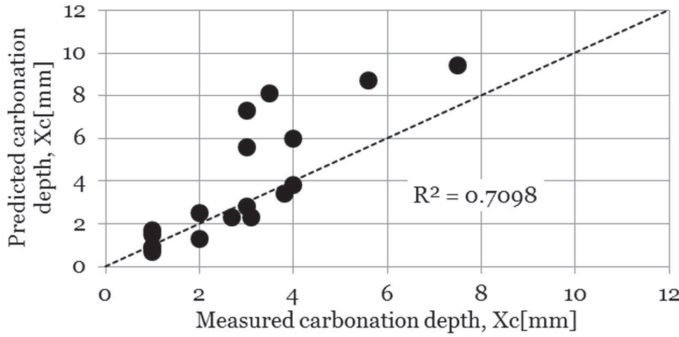


Figure 6.9: Correlation between predicted and naturally carbonated carbonation depths.

On the basis of the correlation between the measured and predicted carbonation depth results, we can ensure that the carbonation depth model is representative of the actual carbonation of in-service concrete structures.

### 6.3.3 Service life of carbonated concrete

The deterioration of a concrete structure as a result of the corrosion of the reinforcement proceeds in two phases, as shown in Figure 6.10: the initiation stage and the propagation stage. The first stage describes the time to the onset of corrosion as a result of the carbonation of the concrete or the ingress of chloride. The second stage is the actual deterioration stage. The main focus of this thesis was the initiation of the corrosion of the reinforcement by carbonation in concrete building facades.

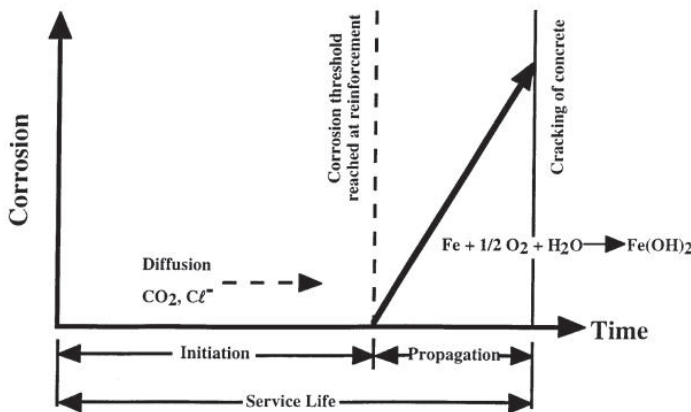


Figure 6.10: Schematic of conceptual model of corrosion of steel reinforcement in concrete (Tuutti 1982, cited in Clifton et al. 2000).

## Initiation time

The initiation time for corrosion as a result of carbonation ( $t_i$ ) is the period required for the carbonation front to reach the reinforcement rebar. The initiation time of corrosion resulting from carbonation was calculated using Equation (6.2). The carbonation rate is calculated on the basis of the composition of the concrete and the simulated relative humidity and temperature of the concrete panel, as shown in Figure 6.3.

The values of the carbonation rates for different concrete types are shown in Table 6.2. The maximum values of the carbonation rates for the facade concrete panel exposed to rain are used in the calculation of the initiation time for carbonation-induced corrosion as a worst-case condition.

Table 6.2: The rates of carbonation of different concrete types.

Concrete code	Carbonation rate		
	$K_{ca}$		
	Max. [mm/a <sup>0.5</sup> ]	Mean [mm/a <sup>0.5</sup> ]	CV* [%]
C30A2-R-Carb	3.0	2.6	21.5
C40A2-R-Carb	2.5	2.4	21.5
C30A6-R-Carb	1.7	1.3	21.5
C35A5-R-Carb	1.0	0.8	21.5
C45A6-R-Carb	0.8	0.7	21.5

\*) CV = Coefficient of Variation

The influence of the depth of the concrete cover on the initiation time of corrosion resulting from carbonation has been studied with different concrete mixes by varying the cover thickness from 10 to 40 mm. The variations in initiation time resulting from the cover depth are presented in Figure 6.11. For example, with an element made from a C30A2-R-Carb concrete mix exposed to rain with a concrete cover depth of 30 mm, the time required for the initiation of corrosion caused by carbonation is 100 years, while the initiation period for the air-entrained C30A6-R-Carb concrete is about 300 years.

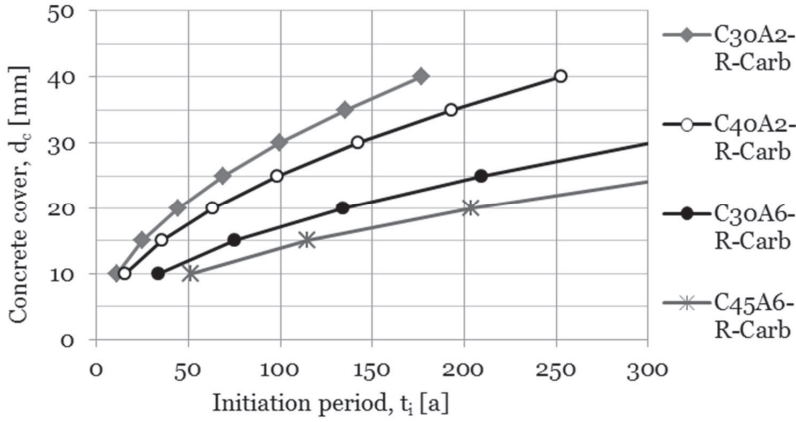


Figure 6.11: Initiation time of corrosion resulting from carbonation.

### Propagation time

Bouquet (2002) has defined the propagation period as the time interval between the initiation of corrosion and the moment when visible cracks appear along the reinforcement (e.g. crack widths greater than 0.3 mm).

Siemes et al. (1985), cited in Parameswaran et al. (2008), suggested the following formula for estimating the propagation time of corrosion on the basis of the cracking of the concrete cover.

$$t_p = \frac{80}{\phi} * \left( \frac{d_c}{V_{\text{corr}}} \right) \quad (6.7)$$

where

- $t_p$  is the propagation time [a],
- $V_{\text{corr}}$  is the corrosion rate [ $\mu\text{m/a}$ ],
- $d_c$  is the cover thickness [mm], and
- $\phi$  is the diameter of the reinforcement [mm].

As shown in Figure 6.12, the corrosion rate is calculated by data fitting based on the results obtained by Page (1992), which are shown in Figure 2.18.

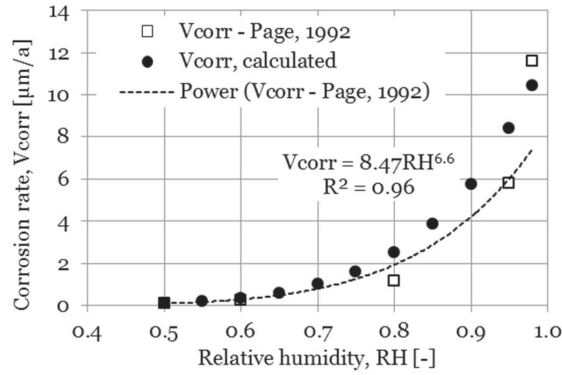


Figure 6.12: Corrosion rate calculation as a function of relative humidity

For fitting the calculated corrosion rate and the result data from Page (1992), Equation (6.8) is introduced and used in the propagation time calculation.

$$V_{corr} = 12.0 * \left(\frac{RH}{100}\right)^{7.0} \tag{6.8}$$

where

- $V_{corr}$  is the corrosion rate [ $\mu\text{m/a}$ ] and
- $RH$  is the relative humidity [%]

An example of the corrosion rate in carbonated concrete as a function of relative humidity is shown in Figure 6.13.

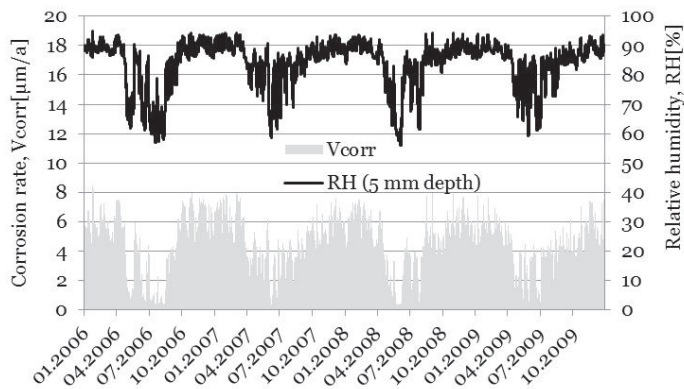


Figure 6.13: Corrosion rate in carbonated concrete as a function of relative humidity

The thickness of the concrete cover is one of the important parameters in calculating the propagation time of carbonation-induced corrosion. The minimum required concrete cover depth for

exposure classes XC2 and XC3, corrosion induced by carbonation, is 25 mm (CEN, 2004). This is valid for concrete with a normal weight, normal reinforcement, and a service life of 50 years. The minimum cover should be increased by 10 mm for a service life of 100 years. Lahdensivu (2012) concluded that the depths of the concrete cover in some concrete facades do not meet the minimum requirements set in the design and durability guidelines and stated that there is a considerable share of 20-mm concrete cover depths in all facade surfaces.

For calculating the propagation period of the corrosion of the reinforcement in concrete building facades built of pre-fabricated sandwich elements, (i) concrete cover depths of 20 mm and 35 mm were selected and (ii) the maximum diameter of the steel bars is 10 mm. The propagation time of carbonation-induced corrosion based on the values of corrosion rates for different relative humidity and concrete cover depth values is shown in Figure 6.14.

On the basis of the relative humidity monitoring data, the average relative humidity for the walls of the concrete facades during the monitoring period was 84%. As shown in Figure 6.14, the corrosion propagation time for the concrete building facades that were monitored in the event of corroding steel bars with a diameter of 10 mm varied from 45 to 79 years when the depths of the concrete cover were 20 and 35 mm respectively.

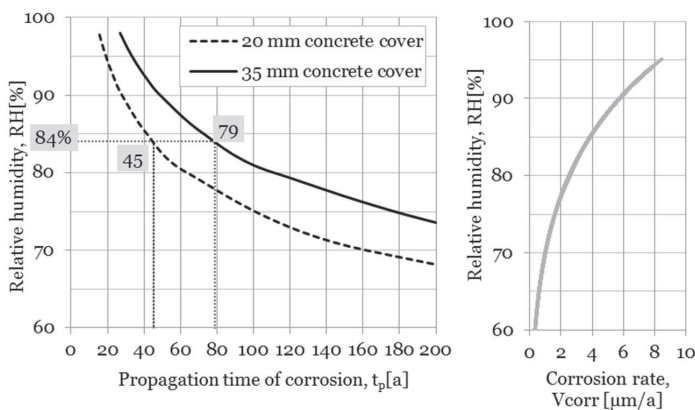


Figure 6.14: Propagation periods for different values of relative humidity in carbonated concrete structures with reinforcement steel bars of a diameter of 10 mm.

## 6.4 Frost damage to concrete

Fagerlund (2004) summarised two basic types of frost attack on concrete structures: (i) an internal frost attack caused by the freezing of moisture inside the concrete, and (ii) surface scaling that is normally caused by the freezing of water that comes in contact with the surface of the concrete. This section deals only with the internal damage to concrete structures expressed by the relative dynamic modulus of elasticity. In this section, (i) the model for predicting the frost damage to concrete is presented, followed by (ii) the validation of the model using the freezing and thawing laboratory test and the field results of the freezing and thawing cycles, and (iii) evaluation of the remaining service life of concrete structures as a result of frost damage.

### 6.4.1 The frost damage model

The frost damage model is based on the models of Walton et al. (1990) for the freezing-thawing durability of concrete structures. This model involves the effect of the compressive strength, the entrained air content, the water-to-cement ratio, and the number of freezing-thawing cycles on the relative dynamic modulus of elasticity of the concrete. The calculated relative dynamic modulus RDM (%) of the concrete can be expressed by the following equation:

$$\text{Calculated RDM} = 100 - \left( \frac{N_{FT}}{C_a * C_b - 100} \right) * 100 \quad (6.9)$$

where

- $N_{FT}$  is the number of freezing-thawing cycles [cycle],
- $C_a$  is a coefficient dependent on the air content [-], and
- $C_b$  is a coefficient dependent on the water-to-cement ratio [-].

The air content coefficient is a parameter to account for the effect of the air content of the concrete in reducing the dynamic modulus of the elasticity of the concrete. It is calculated using Equation (6.10).

$$C_a = \begin{cases} 275 * w_a + 118.25 * w_a^2 & \text{for } w_a \geq 4\% \\ 118.25 * w_a^2 & \text{for } w_a < 4\% \end{cases} \quad (6.10)$$

where

$w_a$  is the air content of the fresh concrete [%].

The water-to-cement ratio coefficient is a parameter to account for the effect of the concrete's water-to-cement ratio on the reduction of the dynamic modulus of elasticity of the concrete and is calculated using Equation (6.11).

$$C_b = 4.2 - 8.0 * \left(\frac{W}{c}\right) + 3.2 * \left(\frac{W}{c}\right)^2 \quad (6.11)$$

where

$w/c$  is the water-to-cement ratio [-].

The applicability of the dynamic modulus of elasticity model was validated by comparing the calculated RDM and the measured RDM from freezing and thawing resistance laboratory tests. As shown in Figure 6.15 and Figure 6.16, the small number of freezing-thawing cycles (56 cycles) is not enough to validate the model.

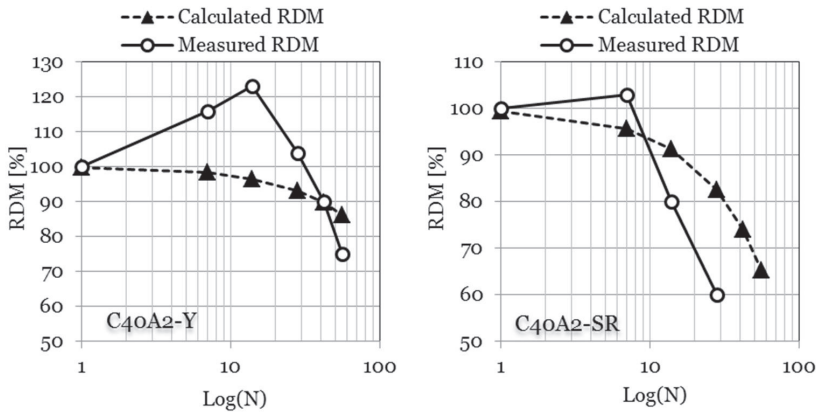


Figure 6.15: Comparison of the measured and the calculated RDM for C40A2-Y and air-entrained C40A6-Y concretes. (N = Number of freezing-thawing cycles)



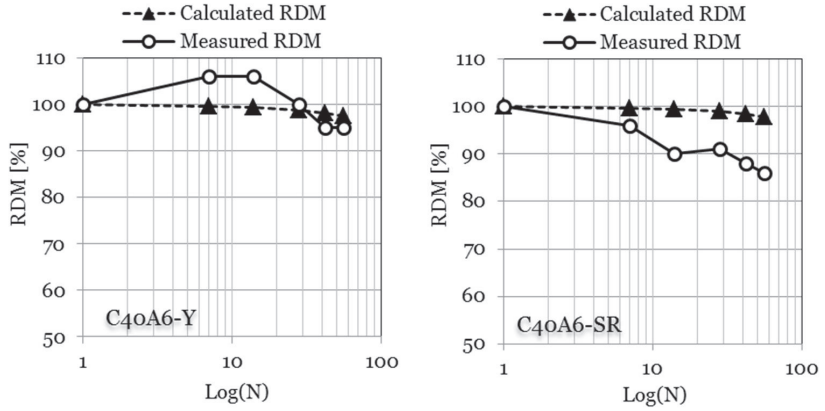


Figure 6.16: Comparison of the measured and the calculated RDM for C40A2-SR and air-entrained C40A6-SR concretes. (N = Number of freezing-thawing cycles)

For more validation of the dynamic modulus of elasticity model, the results of the freezing-thawing test conducted by Tanesi and Meininger (2006) are used. Details of Tanesi and Meininger’s frost resistance test data are shown in Appendix D. Examples of the comparison between the calculated and measured RDM are shown in Figure 6.17 and Figure 6.18. The results show that the correlation between the calculated and the measured RDM was higher for the air-entrained C45A2 concrete. For the C40A2 and C45A5 concretes, the measured RDM correlates with the calculated RDM with R-squared values of 0.89 and 0.92 respectively.

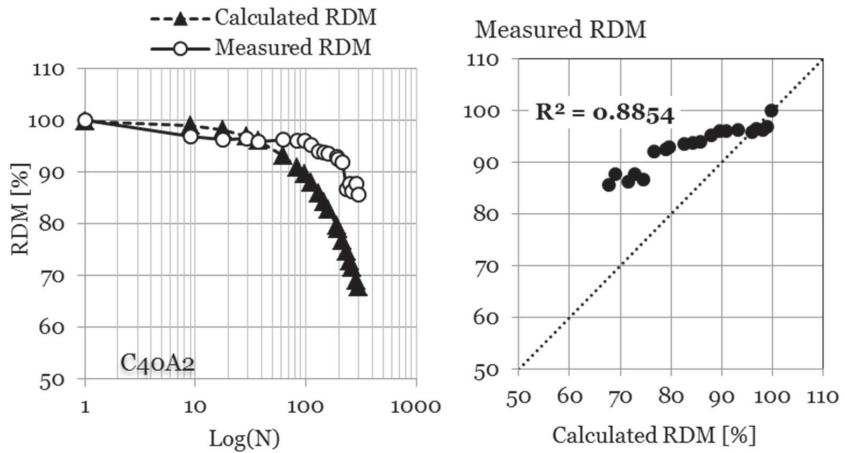


Figure 6.17: Comparison of the measured and the calculated RDM for the C40A2 concrete. (N = Number of freezing-thawing cycles)

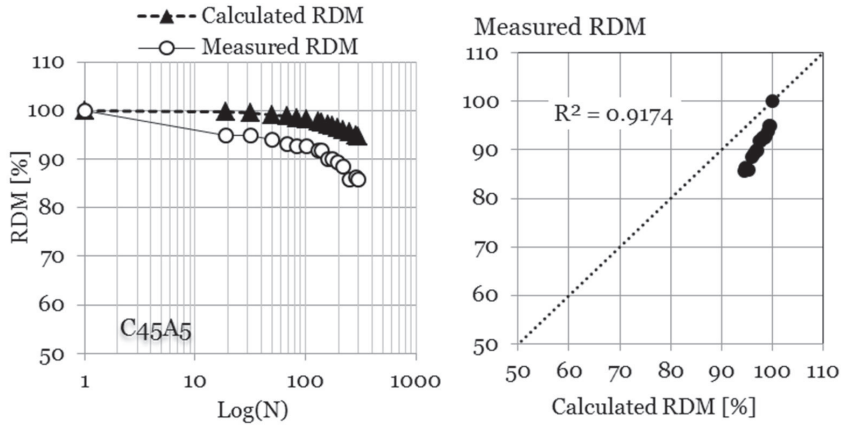


Figure 6.18: Comparison of the measured and the calculated RDM for the air-entrained C40A5 concrete. (N = Number of freezing-thawing cycles)

On the basis of the comparison between the measured and calculated RDM, it can be seen that the correlation varied, depending on the air content of the concrete. Some representative results of the model are found to describe the actual frost damage to in-service concrete structures, but more long-term research is needed to validate the frost damage model.

#### 6.4.2 Predicting the frost damage to concrete

For predicting the frost damage to the outer walls of the concrete building facades, the properties of the outer panel concrete of the sandwich element are assumed to be similar to those of the concretes shown in Table 4.3 and Table 4.4. Figure 6.19 shows that the deterioration of the non-air-entrained concretes reaches an RDM level of 70% in around 50 cycles for the C40A2-SR concrete and 100 cycles for the C40A2-Y concrete. The air-entrained concretes reach an RDM level of 70% after more than 700 freezing and thawing cycles for both C40A6-Y and C40A6-SR concretes.

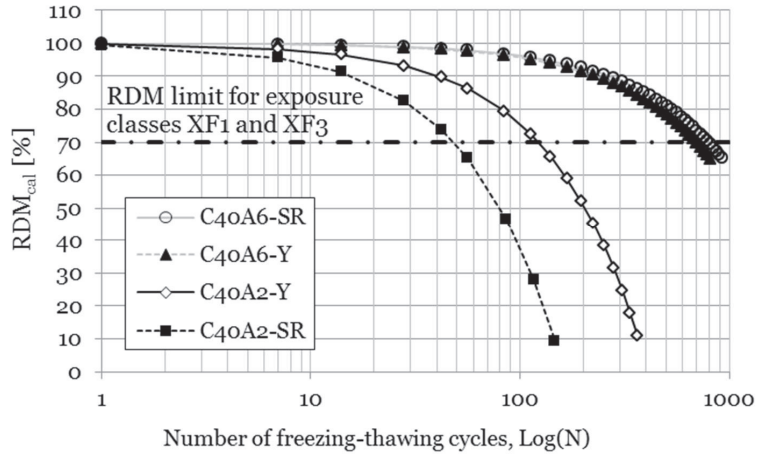


Figure 6.19: Calculated RDM for different air-entrained and non-air-entrained concretes.

### 6.4.3 Remaining service life as a result of frost damage

The frost damage level is taken as the point of significant cracking and deterioration of the concrete as a result of freezing-thawing action. The minimum critical level of RDM to ensure the satisfactory performance of the structure under cyclic freezing and thawing action is shown on Table 4.12. An RDM level of 70% is considered the minimum critical RDM for the outer panels of concrete building facades.

The remaining time required to reach a certain level of frost damage, according to the experimental work of Walton et al. (1990), is given by Equation (6.12).

$$t_d = \frac{N_{\text{tot}}}{N_a} = \frac{1}{N_a} * \left( \frac{D_l}{100} * (C_a * C_b - 100) \right) \quad (6.12)$$

where

- $t_d$  is the time required to reach the  $D_l$  level of frost damage [a],
- $D_l$  is the allowed frost damage level [%],
- $N_{\text{tot}}$  is the total number of freezing-thawing cycles needed to reach the ( $D_l$ ) level of frost damage [cycle],
- $N_a$  is the annual number of freezing and thawing cycles [cycle/a]
- $C_a$  is a coefficient dependent on the air content [-], and
- $C_b$  is a coefficient dependent on the water-to-cement ratio [-].

The annual freezing and thawing cycles are counted as the average number of yearly freezing and thawing events in the outdoor air in the southern part of Finland during 10 years of measurement, as shown in Figure 6.20. Effective freezing is considered to take place when the temperature drops to  $-5^{\circ}\text{C}$  or less and effective thawing is counted at  $+2^{\circ}\text{C}$  or more. In this thesis, the figure of 15 cycles is considered as the annual number of freezing and thawing events.

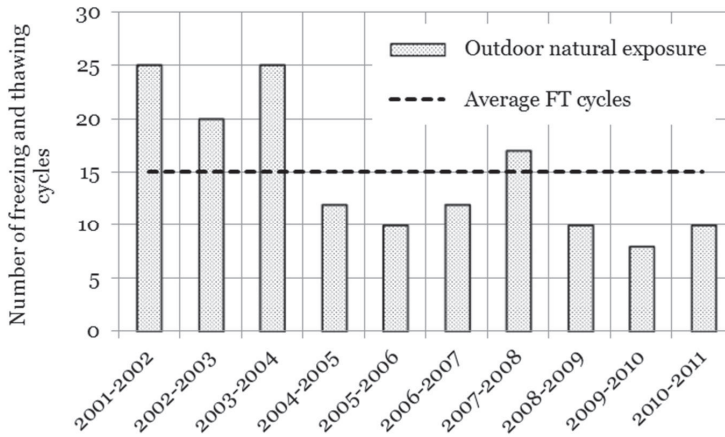


Figure 6.20: Number of freezing and thawing cycles outdoors in the southern part of Finland (Weather Forecast, 2013)

The remaining service life of different concrete mixes before they reach a frost damage deterioration level of 30% on the basis of the number of freezing and thawing cycles is represented in Figure 6.21.

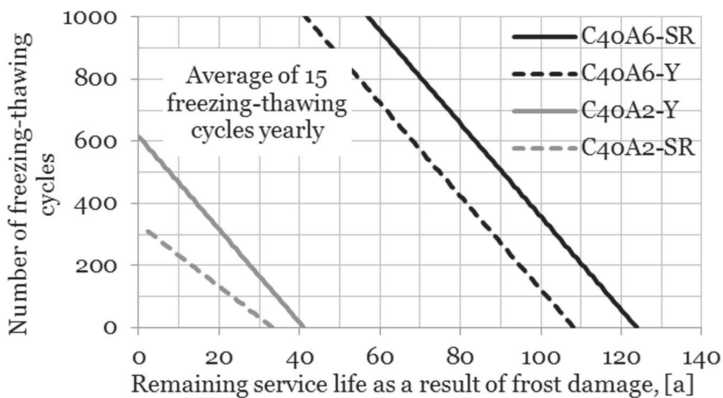


Figure 6.21: The remaining time of the concrete structures before they reach a frost damage deterioration level of 30%.

The results show that the remaining service life after exposure to frost depends on the air content of the concrete. An example of the calculation of the remaining service life after 100 freezing and thawing cycles shows that the non-air-entrained concretes C40A2-SR and C40A2-Y will resist frost action for 23 and 35 years respectively. The air-entrained concretes C40A2-SR and C40A2-Y will resist after 100 critical freezing thawing cycles for 117 and 102 years respectively before they reach a frost damage deterioration level of 30%.

## 6.5 Estimation of mould growth

Moulds and mildew are fungi that grow on the surfaces of objects, within pores, and in materials that have deteriorated. The following conditions are necessary for mould growth to occur on surfaces: (i) a temperature range above 0°C and below 50°C; (ii) mould spores, (iii) a nutrient base (most surfaces contain nutrients), and (iv) moisture (Hukka et al. 1999). Mould growth is initiated by the condensation of moisture as a result of serious panel cracks. In this section, the risk of mould growth in the mineral wool insulation of concrete building facades is evaluated on the basis of their hygrothermal condition. This section introduces (i) the model for predicting mould growth in the insulation layers of concrete building facades and (ii) estimation of the risk of mould growth on the basis of the long-term field measurements of relative humidity and temperature.

### 6.5.1 Mould growth potential model

According to Johansson (2011), the critical relative humidity for mould growth varies with changes in temperature. On the basis of experiments, the critical relative humidity is calculated using the following polynomial function:

$$RH_{cr,m} = \begin{cases} 100\% & (T < 0^\circ C) \\ f_T & (0 \leq T \leq 20^\circ C) \\ 80\% & (T > 20^\circ C) \end{cases} \quad (6.13)$$

$$f_T = -0.00267 * T^3 + 0.16 * T^2 - 3.13 * T + 100$$

where

$RH_{cr,m}$  is the critical relative humidity for mould growth [%] and  
 $T$  is the measured temperature [°C].

The mould growth potential is a ratio of the measured and critical relative humidity that takes temperature dependencies into consideration. A modification of the mould growth potential, Equation (6.14), was calculated on the basis of the research work of Sedlbauer (2002), Thelandersson et al. (2009), Johansson et al. (2010), and Johansson (2011).

$$m = \frac{RH_{\text{act}}}{RH_{\text{cr,m}}} \quad (6.14)$$

where

- $m$  is the mould growth potential [-],
- $RH_{\text{act}}$  is the current measured relative humidity [%], and
- $RH_{\text{cr,m}}$  is the critical relative humidity for mould growth [%].

Theoretically, mould growth is possible only when ( $m > 1$ ). Hence, the probability of mould growth may be illustrated by the development of the risk of mould as a function of time in the insulation layer of concrete building facades.

### 6.5.2 Estimating the risk of mould growth

For estimating mould growth in the insulation layers of concrete building facades, some assumptions were made, as follows:

- i. the concrete building facade RF2-MWOOL, shown in Figure 5.5, is the target facade for mould growth calculations;
- ii. the relative humidity and temperature were monitored at point (2) in the original mineral wool insulation and points (4) and (5) inside the internal and external sides of the externally added mineral wool insulation respectively, as shown in Figure 5.5.

To estimate the potential for mould growth in the mineral wool insulation, the monitoring data of the relative humidity, temperature, and critical relative humidity for mould growth of the RF2-MWOOL facade, shown in Figure 6.22 to Figure 6.24, are used.

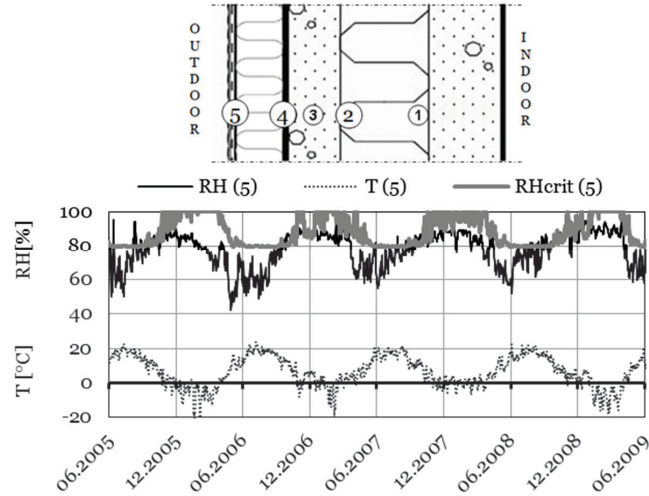


Figure 6.22: The relative humidity and temperature distribution inside the outer surface of the externally added insulation of the RF2-MWOOL façade.

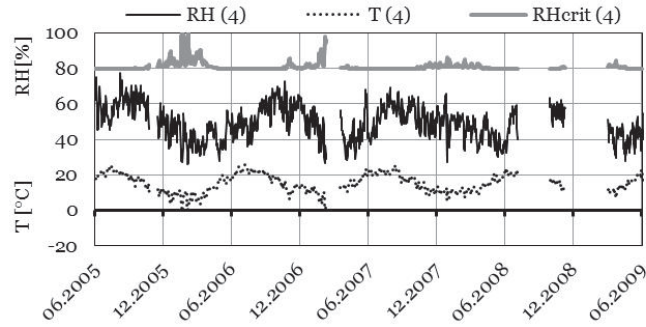


Figure 6.23: The relative humidity and temperature distribution inside the inner surface of the externally added insulation of the RF2-MWOOL façade

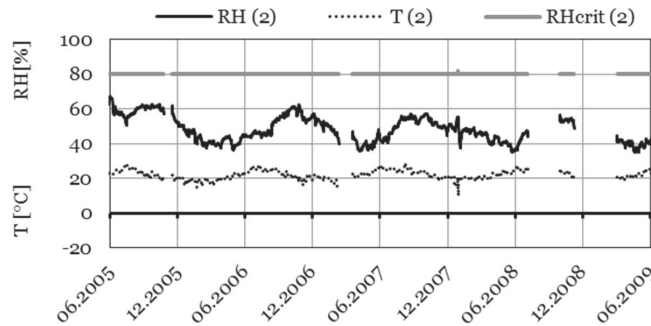


Figure 6.24: The relative humidity and temperature distribution in the original insulation of the RF2-MWOOL façade.

Figure 6.25 shows the mould growth potential for the mineral wool insulation inside the original façade and the externally added new

insulation. There was no risk of mould growth inside the internal side of the external insulation and in the original insulation of the RF2-MWOOL facade during the monitoring period because the mould growth potential was always below the critical level ( $m < 1.0$ ). The risk of mould growth inside the external side of the external insulation was higher than was the case for the internal side and the risk exceeded the critical level ( $m > 1.0$ ) during the autumn every year.

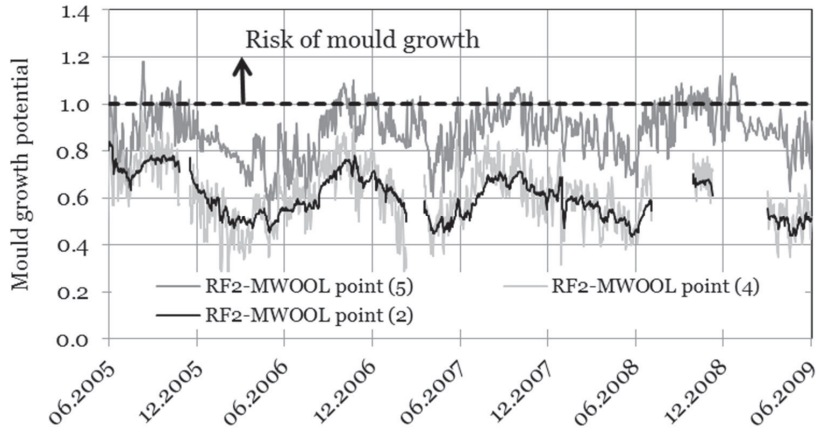


Figure 6.25: Mould growth potential for the RF2-MWOOL in the original wall and the externally added mineral wool insulation.

Thelandersson (2009) described the impact of the variation in relative humidity and temperature on the potential for mould growth by the dose-response relationship. The dose-response relationship is a proposed model for predicting the initiation of mould growth on the basis of measured data for relative humidity and temperature. For exposure during ( $n$ ) days, the total dose-response is given by:

$$D_n = \sum_{i=1}^n D_{RH} * D_T \quad (6.15)$$

where

- $D_n$  is the total dose-response during ( $n$ ) days [d],
- $D_{RH}$  is a function of the daily average relative humidity, and
- $D_T$  is a function of the daily average temperature.

The dose can be defined in relation to a reference climate period of days ( $N_{ref}$ ) with a reference relative humidity and temperature ( $RH_{ref}$



and  $T_{\text{ref}}$ ). On the basis of the experimental work of Viitanen and Ojala (2007), mould growth in rock-based mineral wool needs 38 days to be initiated in a 90% RH and at 20°C, as shown in Figure 2.21.

The functions of daily average relative humidity and temperature are given as follows:

$$D_{\text{RH}} = \text{EXP} \left( 15.53 * \ln \left( \frac{\text{RH}}{90} \right) \right) \text{ for } 80 < \text{RH} < 100\% \quad (6.16)$$

$$D_{\text{T}} = \text{EXP} \left( 0.74 * \ln \left( \frac{T}{20} \right) \right) \text{ for } 30 > T \geq 0.1 \text{ } ^\circ\text{C} \quad (6.17)$$

where

$\text{RH}$  is the average daily relative humidity [%] and

$T$  is the average daily temperature [°C].

In order to evaluate the risk of mould for the relative variations in humidity and temperature, a relative dose  $D_{\text{rel}}$  is defined. The initiation of mould growth takes place when  $D_{\text{rel}} \geq 1$ .

$$D_{\text{rel}} = \frac{1}{N_{\text{ref}}} * \left( \sum_{i=1}^n D_{\text{RH}} * D_{\text{T}} \right) \quad (6.18)$$

where

$N_{\text{ref}}$  is the reference period for the initiation of mould growth [days]

$N_{\text{ref}}$ , is considered to be 38 days for mineral wool.

The relative dose values for the insulation layers of the concrete building facade RF2-MWOOL are shown in Figure 6.26. The value of the relative dose ( $D_{\text{rel}} = 1$ ) means the initiation of mould growth. The outer side of the externally added insulation reaches a relative dose of 1 in about 1.7 years.

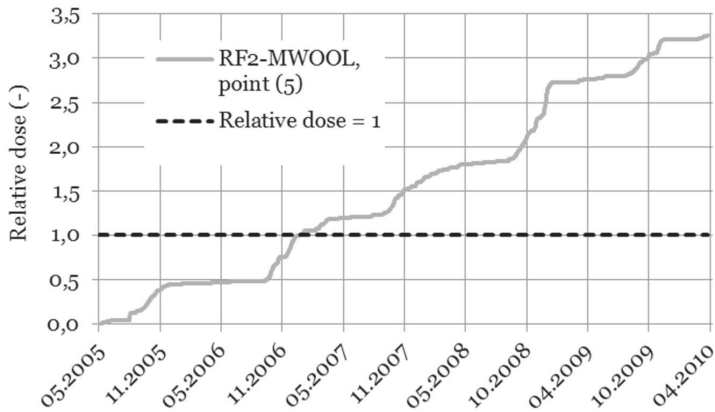


Figure 6.26: Calculated relative dose using the relative humidity and temperature data of point (5) of the RF2-MWOOL facade.

There was no risk of the initiation of mould growth inside the internal side of the externally added or original insulation of the RF2-MWOOL facade during the monitoring period because the relative humidity was lower than the relative humidity limit for mould growth ( $RH > 80\%$ ), as shown in Figure 6.24.

## 6.6 Summary

In this chapter, the deterioration of the concrete building facades as a result of changes in temperature and moisture was predicted and the remaining service lives were estimated. The focus was on the most common concrete facade deterioration mechanisms in Finland, which are corrosion caused by carbonation, deterioration resulting from freezing and thawing, and mould growth in mineral wool insulation.

The carbonation-induced corrosion rate of the concrete reinforcement is variable and highly dependent on exposure conditions and the properties of the concrete. As this work uses the model of time-dependent carbonation depth, it takes into consideration the effect of the composition of the concrete and the history of the relative humidity and temperature on the carbonation depth of the concrete.

The applicability of the carbonation model was validated by comparing theoretical accelerated carbonation tests and natural carbonation results. Based on the correlation between the measured

and predicted carbonation depth results, we can be sure that the carbonation depth model is representative of the actual carbonation of in-service concrete structures.

The service life, regarding the carbonation-induced corrosion of the concrete reinforcement, was calculated as the total sum of the initiation and propagation periods. The results showed that the initiation period of the corrosion depends on the composition of the concrete, the depth of the concrete cover, and the exposure conditions, while the propagation period depends on the depth of the concrete cover, the diameter of the reinforcement bars, and the relative humidity.

Repeated freezing and thawing cycles result in the surface and internal deterioration of the concrete structure. Presently, no well-established numerical model for the prediction of concrete damage as a result of frost attack exists. This work used a modification of the model developed by Walton et al. (1990) that was based on experimental results obtained by Tanesi and Meininger (2006). The modified model includes the effects of the entrained air content, the water-to-cement ratio, and the number of critical freezing-thawing cycles on the relative dynamic modulus of elasticity of the concrete. The applicability of the dynamic modulus of elasticity model was validated by comparing the theoretical RDM values and the results obtained from the critical freezing-thawing resistance concrete tests. The remaining service life of concrete required before it reached a frost damage deterioration level of 30% was calculated on the basis of different concrete mixes and the number of freezing and thawing cycles in the concrete of the RF1-EPS and RF2-MWOOL facades. The results show that the use of air-entrained concrete has a great effect on the durability of concrete building facades against frost damage.

The mould growth risk was evaluated by calculating the mould growth potential and the relative dose response. In order to estimate the potential for mould growth in the original and externally added mineral wool insulations, the monitoring data of the relative humidity and temperature of the RF2-MWOOL facade were used. The results show that there was no risk of mould growth inside the internal side of the externally added and original insulation of the

RF2-MWOOL facade during the monitoring period because their relative humidity was always below the limit level of relative humidity for mould growth. There was a risk of mould growth inside the outer side of the externally added insulation of the facade.

Continuous monitoring provides a much better understanding of how the environment and concrete building facades interact and complements visual inspection and planning of maintenance measures. By measuring the temperature and relative humidity of the components of the facade, we can determine the potential for their deterioration and present a justified prediction of their remaining service life.

## 7 Conclusions and discussions

### 7.1 Concluding the research objectives

The purpose of this work was to complete an in-depth investigation of the effect environmental conditions have on the deterioration of reinforced concrete structures. To narrow the aim of the study it was decided to focus on concrete building facades. The research work of this thesis consists of a literature review, the development of a thermal and moisture monitoring system for concrete building facades, laboratory and field investigation, and the development of computer-aided software for monitoring the hygrothermal performance and predicting the deterioration of concrete building facades resulting from changes in temperature and moisture.

One objective of the research was to use the possibilities offered by ICT (Information and Communication Technology) in the construction sector. For that purpose, a new thermal and moisture monitoring network system was developed. The thermal and moisture monitoring system is a tool for monitoring the hygrothermal performance of the wall assemblies of concrete building facades and a process for analysing their deterioration resulting from changes in temperature and moisture in the Finnish climatic conditions.

### 7.2 Evaluating the research work

The literature review focused on: (i) understanding the conditions that lead to the deterioration of concrete building facades; (ii) identifying the response of the facades to the surrounding conditions, and (iii) understanding the different deterioration mechanisms related to the environmental deterioration of concrete building facades.

The literature review covered: (i) the transport of heat and moisture in the concrete structure; (ii) evaluation of the environmental exposure classes and the hygrothermal response of the concrete facade, and (iii) the processes involved in the deterioration of concrete building facades. Special attention was paid to the corrosion of steel reinforcements as a result of carbonation, damage caused by repeated freezing and thawing, and mould growth on concrete building facades.

As a result of the literature review, the environmental conditions that affect the deterioration of the concrete facade were shown to be mainly the weathering conditions, such as temperature and moisture changes. Heat and moisture transfer are two connected processes and they have a great interactive impact on the performance of the facade. Heat can be transported by conductivity, convection, and radiation. The transfer of moisture as vapour takes place by diffusion and convection and its transfer as liquid water by capillarity suction and gravity flow through pores, cracks, and openings.

The hygrothermal response of concrete facades to the surrounding environment was expressed in terms of environmental moisture and thermal indices, such as (i) the moisture index; (ii) the relative humidity and temperature index, and (iii) the freezing and thawing index.

Most of the deterioration of concrete structures can only occur in the presence of water, since aggressive agents will penetrate concrete and react harmfully with the cement paste only when dissolved in water. The deterioration of a concrete facade may occur for two principal reasons: corrosion of the reinforcement as a result of carbonation, and degradation of the concrete itself. Reinforcement corrosion caused by carbonation is usually related to moisture, and is typically in the form of cracking and delamination of the concrete structure. Internal tensile stresses caused by expansion processes inside the concrete may result in internal cracking and, therefore, degradation of the concrete. Concrete may also deteriorate as a result of several phenomena such as frost attacks or alkali-aggregate reaction.

As the hygrothermal performance of concrete building facades in severe environmental conditions needs to be monitored and documented, a new thermal and moisture monitoring system was developed. The RHT-MAPS is a tool for quantifying the environmental factors that affect the degradation of concrete structures and predicting the related deterioration of concrete building facades. The RHT-MAPS consists of a sensor network and monitoring software. The sensor network consists of a controller, smart nodes, and relative humidity and temperature sensors connected to a twisted-pair CAT5 cable. The monitoring software application was developed for collecting and analysing relative humidity and temperature data. The RHT-MAPS is a useful tool for: (i) monitoring and documenting the relative humidity and temperature of the wall assemblies of concrete facades; (ii) storing information about the building materials used in the construction of the facade, and (iii) predicting the deterioration and the remaining service life of the facades under consideration on the basis of the ambient climatic conditions and their material properties.

To assess the impact of environmental factors on the durability and performance of concrete building facades, laboratory investigation and field monitoring of relative humidity and temperature were carried out. The laboratory tests were conducted as part of the study to test the properties of different concrete mixes on the basis of the requirements of different exposure classes. The material tests determined the deterioration of concrete material as a function of temperature and relative humidity. The experimental tests were designed to study the effect of thermal and moisture changes on the carbonation and frost resistance of concrete. The aim of the laboratory tests was to determine the level of damage to different concrete mixes caused by changes in the temperature and moisture conditions. The results of the laboratory tests were used to validate the prediction of the deterioration and remaining service life of the concrete building facades.

The field monitoring was performed for the temperature and moisture conditions of two concrete building facades of apartment buildings in southern Finland. The responses of the concrete building

facade walls were assessed in terms of (i) the variation in the relative humidity and temperature and (ii) the potential for the moisture and temperature to cause deterioration. The field-monitored relative humidity and temperature data of the outdoor ambient air and the wall layers of the concrete building facades are used in the prediction models of corrosion of the reinforcement and carbonation and frost damage to concrete and the potential for biological growth in the insulation layers.

The prediction of the deterioration resulting from changes in temperature and moisture so as to calculate the remaining service life of concrete building facades is useful to increase the understanding of how concrete building facades behave under repeated moisture and thermal cycles. The focus throughout was on the most common types of deteriorations of concrete facades, which are corrosion caused by carbonation, deterioration as a result of freezing and thawing, and mould growth in mineral wool insulation.

The carbonation-induced corrosion rate of the concrete reinforcement is variable and highly dependent on exposure conditions and the properties of the concrete. The service lifetime, regarding the carbonation-induced corrosion of the concrete reinforcement, is calculated as the total sum of the initiation and propagation periods. The results show that the initiation period of the corrosion depends on the composition of the concrete, the thickness of the concrete cover, and the ambient environmental conditions. The results show that the propagation time for corrosion increases as the relative humidity of the concrete around the reinforcing bar decreases.

Repeated freezing and thawing cycles result in the surface and internal deterioration of the concrete structure. This work used a modification of the model developed by Walton et al. (1990) that was based on experimental results by Tanesi and Meininger (2006). The modified model includes the effects of the entrained air content, the water-to-cement ratio, and the number of critical freezing-thawing cycles on the relative dynamic modulus of elasticity of the concrete. The applicability of the dynamic modulus of elasticity model was validated by comparing the theoretical RDM values and the results



obtained from the critical freezing-thawing resistance concrete tests. The remaining service lifetime of concrete required before it reaches a frost damage deterioration level of 30% was calculated on the basis of different concrete mixes and the freezing-thawing cycles. The results show that the air entrainment has a major effect on the durability of concrete against frost.

The risk of mould growth was evaluated by calculating the mould growth potential and the relative dose response. The results show that there was no risk of mould growth in the insulation layers of the concrete building facade that was monitored during the monitoring period because their relative humidity was always below the limit level of relative humidity for mould growth.

### **7.3 Scientific and industrial contribution**

The significance of the thesis research lies in the meaning of the usefulness of the results for scientific researchers, building designers, and building owners. The research provides the scientific researchers with models for the deterioration of concrete that are based on measured data for more validation and testing. The building designers are provided with case studies and more information about the hygrothermal performance of concrete building facades that they can take into account when designing the whole building. The building owners are provided with a tool to analyse the performance of their existing building and predict its remaining service life. The tool acts as an early warning system so as to ensure appropriate renovation and maintenance programmes for the building.

In general, the continuous monitoring of temperature and relative humidity of concrete building facades provides a great understanding of their in-service behaviour. Documenting the hygrothermal performance can enhance the understanding of the deterioration of the materials and changes in the structural behaviour caused by ageing.

### **7.4 Limitations**

Although the research has achieved its aims, there were some unavoidable limitations. The research was concentrated on concrete

building materials and building facade structures of residential buildings. The monitoring system was designed for monitoring only relative humidity and temperature, while more factors could be useful for monitoring the hygrothermal performance of building structures, such as driven rain, solar radiation, and wind speed and wind direction. Finally, because of the time limit, the validation of the deterioration prediction models was tested using laboratory test results, which were performed under severe conditions in comparison to the natural conditions.

## **7.5 Future research**

This research has thrown up some questions that are in need of further investigation.

Future research is needed to address the use of wireless sensors and communication systems in monitoring the environmental factors that affect the deterioration of building components. It is also recommended that further research be undertaken in the following areas: (i) investigations of different building materials; (ii) residential and industrial building energy efficiency research, and (iii) the use of the monitoring system for bridges, tunnels, and road structures.

The deterioration models for concrete structures of this thesis are still not very satisfying. There is a considerable amount of uncertainty coming e.g. from the lack of long-term durability test results for model validation. These models are worthy of more research and development in the future.

Considerably more work will need to be done on the RHT-MAPS components and the software programming for them to be integrated into home automation systems in order to achieve the maximum benefits of the system.

## References

- AASHTO TP 60-00 (2004). Standard Method of Test for Coefficient of Thermal Expansion of Hydraulic Cement Concrete. American Association of State Highway and Transportation Officials (AASHTO). Washington, D.C., USA.
- Abdoveis, J.M. (2003). An examination of concrete durability. Master's thesis, Department of Civil and Environmental Engineering, University of Oklahoma, USA. Available online: <http://dspace.mit.edu/bitstream/handle/1721.1/29334/1/52718626.pdf> [Accessed 9.8.2012]
- ACI 201.2R-08 standard (2008). Guide to durable concrete, Report of ACI Committee 201, American Concrete Institute, Detroit.
- Ann, K.Y., Pack, S.W., Hwang, J.P., Song, H.W., Kim, S.H. (2010). Service life prediction of a concrete bridge structure subjected to carbonation. *Journal of Construction and Building Materials*, Volume 24, Issue 8, August 2010, pp. 1494-1501. doi:10.1016/j.conbuildmat.2010.01.023
- Apostolopoulos, C.A., Papakadis, V.G. (2008). Consequences of steel corrosion on the ductility properties of reinforcement bar. *Construction and Building Materials*, Vol. 22 (12), pp. 2316-2324.
- ASTM C666-97 (1997). Standard test method for resistance of concrete to rapid freezing and thawing, Book of Standards Volume 04.02, ASTM International, West Conshohocken, Pennsylvania, USA.
- Bertolini, L., Elsener, B., Pedferri, P., Polder, R.B. (2004). *Corrosion of Steel in Concrete: Prevention, Diagnosis, Repair*, Wiley-VCH Verlag GmbH & Co. KGaA, Weinheim, ISBN. 3-527-30800-8, 392 pp.
- Bishnoi S. (2004). Strain variations in concrete subjected to cyclic freezing and thawing. M.S. thesis, Department of Civil Engineering, University of Tokyo, Tokyo, Japan.
- Bouquet G.C. (2002). Carbonation induced corrosion of reinforcement, Repair, rejuvenation and enhancement of concrete. Proceedings of the international conference held at

- the University of Dundee, Thomas Telford, London. England, 2002. pp. 465-475.
- Broomfield, J., Millard, S.G. (2002). Measuring Concrete Resistivity to Assess Corrosion Rates. The Concrete Society/Institute of Corrosion Liaison Committee, February 2002, pp. 37-39.
- Buck, A.L. (1981). New equations for computing vapor pressure and enhancement factor. *Journal of Applied Meteorology and Climatology*. Volume 20, pp. 1527-1532. Retrieved from [http://www.public.iastate.edu/~bkh/teaching/505/arden\\_buck\\_sat.pdf](http://www.public.iastate.edu/~bkh/teaching/505/arden_buck_sat.pdf) [Accessed 18.01.2013]
- Carlsson, T. (2003). Definition of decisive environmental parameters and loads. LIFECON Deliverable D 4.1, VTT Building Technology, Espoo, Finland. Online at: <http://lifecon.vtt.fi/d41.pdf> [Accessed 09.08.2012].
- Carmeliet, J., Roels, S., Bomberg, M.T. (2009). Towards development of methods for assessment of moisture-originated damage. Chapter 28 in *Moisture control in buildings: The key factor in mould prevention*, MNL18-2nd, edited by Heinz R. Trechsel and Mark Bomberg-2nd ed., ASTM International: pp. 591-605.
- CEN/TR. (2006). European Standards “CEN/TR 15177 Standard” (2006). Technical report: Testing the freezing and thawing resistance of concrete – internal structural damage. Approved 1.7.2006. CEN (European Committee for Standardization), Brussels, Belgium.
- CEN/TS 12390-9. (2006). European Standards “CEN/TS 12390-9 standard” (2006). Testing hardened concrete – Part 9: freeze-thaw resistance - scaling. CEN (European Committee for Standardization), Brussels, Belgium.
- Clifton, J.R. et al. (2000). Service-life prediction – state-of-the-art report. American Concrete Institute ACI 365.1R-00. Retrieved from [http://civilwares.free.fr/ACI/MCP04/3651r\\_00.pdf](http://civilwares.free.fr/ACI/MCP04/3651r_00.pdf) [Accessed 18.10.2012]
- Concrete Code “BY 50” (2005). Concrete Code 2004, unofficial translation from Finnish Copy; Betoninormit 2004 – BY 50. Suomen Betonitieto Oy, Helsinki, Finland. 218 pp.
- Copeland, C., Newman, P., Mukhopadhyaya, P., Van Reenen, D., Kumaran, K., El Khanagry, R., Zalok, E. (2010). Assessing moisture performance of exterior wall assembly design in wood-frame construction in Beijing, China. *Journal of Building Enclosure Design: An official publication of the National Institute of Building Sciences Building Enclosure Technology and Environment Council, USA*. pp. 11-15.

- Cornick, S., Dalglish, A. (2003). A moisture index approach to characterizing climates for moisture management of building envelopes. Proceedings of the 9th Canadian Conference on Building Science and Technology, Vancouver, B.C., February 27-28, 2003, pp. 383-398.
- Cornick, S., Dalglish, A., Said, N., Djebbar, R., Tariku, F., Kumaran, M.K. (2002). Report from task 4 of MEWS project – environmental conditions, final report. IRC-RR-1130, Institute for Research in Construction, National Research Council Canada, Ottawa, Canada.
- Davies, R. D., and Buenfeld N. R. (2007). Automated monitoring of the deterioration of concrete structures. Department of Civil and Environmental Engineering, Imperial College London.
- De Castro, A., Ferreira, R.A., Lopes, M., Cascudo, O., Carasek, H. (2004). Relationship between results of accelerated and natural carbonation in various concretes. International RILEM Conference on the Use of Recycled Materials in Buildings and Structures, 8-11 November 2004, Barcelona, Spain. pp. 988-997.
- DuraCrete (2000). General guidelines for durability design and redesign. DuraCrete R17, DuraCrete final technical report, DuraCrete – Probabilistic performance based durability design of concrete structures. Document BE95-1347/ R17, the Netherlands. Retrieved from <http://www.cur.nl/upload/documents/duracrete/BE1347R17.pdf> [Accessed 9.8.2012]
- EN 1992-1-1. (2004). European Standards EN 1992-1-1:2004. Eurocode 2: Design of concrete structures - Part 1-1: General rules and rules for buildings. CEN (European Committee for Standardization), Brussels, Belgium.
- EN 206-1. (2000). European Standard “EN 206–1” (2000). Concrete – Part 1: Specification, performance, production and conformity. CEN (European Committee for Standardization), Brussels, Belgium.
- EN. 12350 (2009). European Standard “EN 12350:2002” Testing fresh concrete, CEN (European Committee for Standardization), Brussels, Belgium.
- EN. 12390 (2000). European Standard “EN 12390:2000” Testing hardened concrete, CEN (European Committee for Standardization), Brussels, Belgium.
- EN. 13295 (2004). European Standard “EN 13295:2004” Products and systems for the protection and repair of concrete structures. Test methods. Determination of resistance to carbonation, CEN (European Committee for Standardization), Brussels, Belgium.

- EN. 1990 (2002). European Standard “EN 1990:2002” Eurocode – Basis of structural design, CEN (European Committee for Standardization), Brussels, Belgium.
- Fagerlund, G. (2001). CONTECVET (IN30902I): Manual for assessing concrete structures affected by frost. Lund University, Department of Building and Environmental Technology, Sweden. 202 pp.
- Fagerlund, G. (2004). A service life model for internal frost damage in concrete. Division of Building Materials, Lund Institute of Technology, Report TVBM-3119, pp. 1-48.
- Folliard, K., Thomas, M., Kurtis, K. (2003). Guidelines for the use of lithium to mitigate or prevent ASR, US Department of Transportation, Federal Highway Administration, Publication number FHWA-RD-03-047, 2003. Retrieved from <http://www.fhwa.dot.gov/publications/research/infrastructure/pavements/pccp/03047/index.cfm> [Accessed 19.9.2012]
- Giarma, C. (2011). Estimation of carbonation depth based on hygrothermal calculations. American Concrete Institute ACI Materials Journal Volume 108, Issue 2, March 2011, pp. 209-218.
- Grasley, Z.C., Lange D.A., D’Ambrosia M.D. (2003). Internal relative humidity and drying stress gradients in concrete. Advances in cement and concrete, Copper Mountain, CO, August 10-14, 2003. DOI: 10.1617/s11527-006-9090-3
- Gudum, C. (2003). Moisture transport and convection in building envelopes – ventilation in lightweight outer walls. PhD thesis, Technical University of Denmark, Publication R 047.
- Hallberg, D. (2005). Quantification of exposure classes in The European Standard EN 206-1. Proceedings of the 10th International Conference on Durability of Building Materials and Components, Lyon, France, 17-20 April 2005.
- Hannula, P., Salonenin, M. (2007). Buildings tell – basic information for inhabitants (in Finnish: Rakennukset kertovat – perustietoa asukkaille). Helsingin Kaupunginosayhdistysten Liitto ry. Yliopistopaino, Helsinki, Finland. 52 pp.
- Harrison T.A., Dewar J.D., Brown B.V. (2001). Freezing and thawing resisting concrete: its achievement in the UK. Concrete Society, London: CIRIA, 2001. Retrieved from: [http://www.ciria.org/service/Web\\_Site/AM/ContentManagerNet/ContentDisplay.aspx?Section=Web\\_Site&ContentID=8920](http://www.ciria.org/service/Web_Site/AM/ContentManagerNet/ContentDisplay.aspx?Section=Web_Site&ContentID=8920) [Accessed 16.9.2012]
- Haughton, L., Murphy, C. (2003). Moisture exchange – performance of OSB and plywood structural panels. June 2003 issue of

- Interface magazine. Available online at: <http://www.rci-online.org/interface/2003-06-haughton-murphy.pdf>  
[Accessed 8.9.2012]
- Haukijärvi, M., Lahdensivu, J. (2005). JUKO: Technical documentation for the repairing of building facades (in Finnish: JUKO ohjeistokansio). Tampere University of Technology, Finland. Online at: <http://www.julkisivuyhdistys.fi/julkkari/juko/> [Accessed 9.8.2012].
- Haukijärvi, M., Lahdensivu, J., Pentti, M. (2006). Finnish manual for facade repair systems. Proceedings of the European Symposium on Service Life and Serviceability of Concrete Structures, ESCS2006. 12-14 June, 2006. Espoo, Finland. pp. 359-364.
- Hens, H. (2007). Building physics – heat, air and moisture transport: fundamentals and engineering methods. Wilhelm Ernst und Sohn, John Wiley Company, Berlin, Germany. 180 pp.
- Hovde, P.J. (2004). Performance based methods for service life prediction. Part a: Factor methods for service life prediction, CIB Wo80 / RILEM 175 Service life methodologies prediction of service life for buildings and components. State of the art reports retrieved from: [http://cibworld.xs4all.nl/pebbu\\_dl/resources/literature/downloads/05AdditionalThemes/01Pub294.pdf](http://cibworld.xs4all.nl/pebbu_dl/resources/literature/downloads/05AdditionalThemes/01Pub294.pdf) [Accessed 9.8.2012]
- Hukka, A., Viitanen, H. (1999). A mathematical model of mould growth on wood material. Wood Science and Technology, Volume 33, No. 6, Springer-Verlag 1999, pp. 475-485.
- Huovinen, S., Bergman, J., Hakkarainen, H. (1998). Deterioration defects and repair methods of facades, Laboratory of Structural Engineering and Building Physics, Helsinki University of Technology. Espoo, Finland. Report 78. 69 pp.
- International Standard “ISO, 9223:1992(E)” (1992). Corrosion of metals and alloys – Corrosivity of atmospheres – Classification. 1992, ISO: Geneva, Switzerland.
- Johannesson, G. (2006). Lectures on building physics, heat and moisture transfer. Royal Institute of Technology KTH, Department of Civil and Architectural Engineering. Stockholm, Sweden. 143 pp.
- Johansson, P. (2011). Assessment of the risk for mould growth in a wall retrofitted with vacuum insulation panels. Proceedings of the 9th Nordic Symposium on Building Physics, Tampere, Finland, 29 May-2 June, 2011.
- Johansson, S. (2006). Biological growth on mineral facades, Licentiate thesis, Report TVBM 3135. Department of Building

- Materials LTH, Lund University, Sweden. Retrieved from: <http://lup.lub.lu.se/luur/download?func=downloadFile&recordId=633710&fileId=1480981> [Accessed 9.8.2012].
- Johansson, S., Wadsö, L., Sandin, K. (2010). Estimation of mould growth levels on rendered facades based on surface relative humidity and surface temperature measurements. *Building and Environment*, 2010, 45, pp. 1153-1160.
- Jukkola, E. (1997). Repair guide for building facades (in Finnish: julkisivujen korjausopas). Julkisivuyhdistys r.y., SPPaino. Hyvinkää, Finland. (ISBN 9519761101). 114 pp.
- Karagiozis, A.N., Desjarlais, A.O., Salonvaara, M. (2000). Integrated hygrothermal performance of building envelopes and systems in hot and humid climates, Proceedings of the Twelfth Symposium on Improving Building Systems in Hot and Humid Climates, San Antonio, TX, May 2000, ESL-HH-00/05-23, San Antonio, Texas, USA. pp. 547-554.
- Kari, O.P. (2009). Modelling the durability of concrete for nuclear waste disposal facilities, Licentiate thesis, Department of Civil and Environmental Engineering, Helsinki University of Technology, Espoo, Finland.
- Karimi, A. and Buenfeld, N. R. (2007). Service life prediction of concrete structures based on automated monitoring, Department of Civil and Environmental Engineering, Imperial College, London, UK.
- Kay, J. (2006). External moisture – An introduction to weather tightness design principles. New Zealand Government - Department of Building & Housing. Retrieved from: <http://www.dbh.govt.nz/UserFiles/File/Publications/WHRS/pdf/external-moisture-an-introduction.pdf> [Accessed 19.1.2013].
- Kumaran K. (1996). Heat, air and moisture transfer in insulated envelope parts. Final report, volume 3, Task 3: Material properties. Building Performance Laboratory, National Research Council, Canada.
- Kumaran, K. (2009). Fundamentals of transport and storage of moisture in building materials and components. In: Trechsel, H. R., Bomberg, M.T., Moisture control in buildings: The key factor in mould prevention, 2nd edition. ASTM International, USA. Ch. 1.
- Künzel, H.M., Holm, A.H., Krus, M. (2008). Hygrothermal properties and behaviour of concrete. WTA-Almanach 2008, Restoration and Building Physics. WTA Publications, Germany. pp. 161-181.



- Künzel, H.M., Karagiozis, A.N., Holm A.H. (2001). A hygrothermal design tool for architects and engineers (WUFI ORNL/IBP): Chapter 9 of the book (Moisture analysis and condensation control in building envelopes) by Trechsel H. R., American Society for Testing and Materials (ASTM) manual series: MNL40.
- Lahensivu, J. (2012). Durability properties and actual deterioration of Finnish concrete facades and balconies. Ph.D. thesis, Publication 1028. Tampere University of Technology, Department of Civil Engineering, Institute of Structural Engineering, Tampere, Finland.
- Lambert, P. (2002). Steel reinforced concrete – corrosion of the reinforcing steel. Retrieved from <http://www.azom.com/details.asp?articleID=1318> [Accessed 9.9.2012]
- Laugesen, P., Geiker, M., Pedersen, J.E., Thaulow, N., Thogersen F. (1996). HETEK. Method for test of the frost resistance of high performance concrete: state of the art. The Danish Road Directorate, Denmark. Report No. 55, 1996.
- Lay, S., Schiessl, P. (2003). Life cycle management of concrete infrastructures for improved sustainability—service life models. LIFECON deliverable D 3.2, VTT Building Technology, Espoo, Finland. Online at: <http://lifecon.vtt.fi/d32.pdf> [Accessed 5.12.2010].
- Lemieux, D.J., Totten, P.E. (2010). Building envelope design guide – wall systems. Online at: [http://www.wbdg.org/design/env\\_wall.php](http://www.wbdg.org/design/env_wall.php) [Accessed 24.2.2010].
- Li, Y. (2007). Mould on building materials: A calorimetric study of fungal activity as a function of environmental factors. Ph. D. thesis. Lund Institute of Technology, Division of Building Materials, Lund, Sweden. Report TVBM-1026.
- Light Network System “LINET” (2007). Network systems and components for industrial applications. Retrieved from <http://www.sitecno.fi/en/> [Accessed 19.1.2013]
- Markeset G., Myrdal R. (2009). Modelling of reinforcement corrosion in concrete – State of the art : COIN P4 Operational service life design: SP 4.1 F Service life modelling and prediction. (COIN Project Report (SINTEF Byggforsk); 7)
- Martin J.W., Bauer, D.R. (2002). Surface moisture and time of wetness measurements. Service life prediction methodology and metrologies, ACS Symposium Series 805, American Chemical Society, 2002, pp. 23-36.
- Mattila, J.S., Pentti, M.J. (2008). Residual service-life of concrete façade structures with reinforcement in carbonated concrete in Nordic climate. Taylor & Francis Group, London. pp. 75-79.

- Mensinga, P., Straube, J., Schumacher, C. (2010). Assessing the freeze-thaw resistance of clay brick for interior insulation retrofit projects. Thermal Performance of the Exterior Envelopes of Whole Buildings XI International Conference, Clearwater, Florida, USA. December 5-9, 2010. Retrieved from <http://www.buildingscience.com/documents/reports/rr-1013-freeze-thaw-resistance-clay-brick-interior-insulation-retrofits> [Accessed 30.9.2012]
- Mihashi, H., Zhou, Z.Y., Tata, S. (2004). Micro mechanics model to describe freezing induced strain behavior of concrete, Proceedings of the International Workshop on Microstructure and Durability to Predict Service life of Concrete Structures, Sapporo, Japan, February 9-16 2004.
- Miura, T., Lee, D.H. (1991). Deformation and deterioration of concrete subjected to cyclic cooling down to very low temperatures, Proceedings of the National Research Council, Canada, Second Canada/Japan Workshop on Low Temperature Effects on Concrete, 1991, pp. 23-37.
- Moreno, E., Solis, G., Lopez-Salazar L. (2006). Carbonation-induced corrosion in urban concrete structures. Materials Performance, Volume 45, Number. 5, USA. pp. 56-60.
- Moreno, I., Sagues, A. (1998). Carbonation-induced corrosion of blended cement concrete mix designs for highway structures. CORROSION/98, NACE International, Houston, Texas, USA. Paper 636.
- Mukhopadhyaya, P., Kumaran, K., Rousseau, M.Z., Tariku, F., van Reenen, D., Dalglish, W.A. (2003). Application of hygrothermal analyses to optimize exterior wall design. The Proceedings of the 2nd International Conference on Research in Building Physics. 14 September, 2003. Leuven, Belgium. pp. 417-426.
- Mukhopadhyaya, P., Kumaran, M.K., Nofal, M., Tariku, F., van Reenen, D. (2005). Assessment of building retrofit options using hygrothermal analysis tool. 7th Symposium on Building Physics in the Nordic Countries (Reykjavik, Iceland, June 13, 2005), pp. 1139-1146, June 01, 2005 (NRCC-47742)
- Müller, H.S., Bohner, E., Vogel, M. (2009). Repair of architectural concrete and related modelling of carbonation-induced corrosion. In: Concrete repair, rehabilitation and retrofitting II (ICCRRR), Cape Town, South Africa, November 24-26, 2008, Alexander M. et al. (Hrsg.) Taylor and Francis Group, London.
- Naik, T., Kumar, R. (2010). Global warming and cement-based materials. The Second International Conference on Sustainable Construction Materials and Technologies, Ancona,

- Italy, June 2010. ISBN 978-1-4507-1492-1, CBU-2010-01, Ancona, Italy, 85 pp.
- Naus, D.J. (2007). Primer on durability of nuclear power plant reinforced concrete structures – A review of pertinent factors. NUREG/CR-6927, U.S. Nuclear Regulatory Commission, Washington, D.C., February 2007.
- Neuvonen, P. (2009). Multistorey apartment building facade repair: facade characteristics and repairing method selection. (In Finnish: Kerrostalon julkisivukorjaus: Julkisivun ominaispiirteet ja korjaustavan valinta). The Building Information Foundation RTS, Helsinki, Finland. 48 pp.
- Nijland, T.G., Siemes, A.J.M. (2002). Alkali-silica reaction in the Netherlands: Experiences and current research, Heron, 2002, Netherlands School for Advanced Studies in Construction, Delft. pp. 81-86.
- Nilsson, L.O. (2003). Durability concept; pore structure and transport processes. Chapter for advanced concrete technology book, Vol 2 – Durability, Butterworth Heinemann, London. England. 26 pp.
- Norberg, P. (2002). Surface moisture and time of wetness measurements. Service life prediction methodology and metrologies, ACS Symposium Series 805, Jonathan W Martin and David R. Bauer, Eds., American Chemical Society, Washington, DC, pp. 23-36.
- Nygaard, P.V. (2009). Non-destructive electrochemical monitoring of reinforcement corrosion. Ph.D. Thesis. Department of Civil Engineering. Technical University of Denmark (2009).
- Official Statistics of Finland (OSF). (2013). Renovation building [e-publication]. ISSN=1799-2974 Helsinki: Statistics Finland Retrieved from [http://tilastokeskus.fi/til/kora/2010/01/kora\\_2010\\_01\\_2011-09-16\\_en.pdf](http://tilastokeskus.fi/til/kora/2010/01/kora_2010_01_2011-09-16_en.pdf) [Accessed 27.4.2013]
- Page, C.L. (1992). Nature and properties of concrete in relation to reinforcement corrosion. Conference on corrosion of steel in concrete, Aachen, Germany. 17-19 February 1992.
- Papadakis, V.G. (2005). Estimation of concrete service life: the theoretical background. Patras, Greece: Building technology & durability, Patras Science Park S.A. Retrieved from: <http://www.ppap.info/eucon.gr/images/stories/docs/tb/tb.pdf> [Accessed 9.8.2012]
- Papadakis, V.G., Fardis, M.N., Vayenas, C.G. (1992). Effect of composition, environmental factors and cement-lime mortar coating on concrete carbonation. Materials and Structures Volume 25, Number 5, pp. 293-304.

## References

- Parameswaran, L., Kumar, R., Sahu, G.K. (2008). Effect of carbonation on concrete bridge service life. *Journal of Bridge Engineering*, ASCE, Volume 13, Issue 1, pp. 75-82.
- Paul, T.C. (2009). Moisture migration in building envelopes and its impact on indoor air quality (IAQ). Master's thesis, Mechanical Engineering Department, Tuskegee University, Tuskegee, Alabama, U.S.A.
- Pel, L., (1995). Moisture transport in porous building materials. Ph.D. thesis, Eindhoven University of Technology, Eindhoven, Netherlands. 140 pp.
- Penttala, V. (1998). Freezing-induced strains and pressures in wet porous materials and especially in concrete mortars, *Advanced Cement Based Materials*, No.7, pp. 8-19.
- Pessi, A.-M., Helkiö, K., Suonketo, J., Pentti, M., Rantio-Lehtimäki, A. (1999). Microbial growth inside exterior walls of precast concrete buildings as a possible risk factor for indoor air quality, *Indoor air 99*. Proceedings of the 8th International Conference on Indoor Air Quality and Climate, vol. 1. Construction Research Communications Ltd., London, United Kingdom. Edinburgh, Scotland. pp. 899-904.
- Petersen, L. Lohaus, L. Polak, M.A. (2007). Influence of freezing-and-thawing damage on behavior of reinforced concrete elements. *ACI Materials Journal* volume 104; number 4, American Concrete Institute, USA, pp. 369-378.
- Pigeon M., Pleau, R. (1995). *Durability of concrete in cold climates*. New York, NY: E and FN Spon.
- Pirinen, P., Simola, H. Aalto, J. (2012). Climatological statistics of Finland 1981-2010 (in Finnish). Report 2012:1, Finnish Meteorological Institute, Helsinki, Finland
- Ramachandran, V.S., Beaudoin, J.J. (2001). *Handbook of analytical techniques in concrete science and technology: principles, techniques, and applications*. Park Ridge, N.J.: Noyes Publications.
- Saetta, A.V. (2005). Deterioration of RC structures due to chemical-physical phenomenon model based simulation. *Journal of Materials in Civil Engineering*, Volume 17, Issue 3, pp. 313-319.
- Saetta, A.V., Schrefler, B.A., Vitaliani R.V. (1993). The carbonation of concrete and the mechanism of moisture, heat and carbon dioxide flow through porous materials. *Cement and Concrete Research*, Volume 23, Issue 4, July 1993, pp. 761-772.
- Sakyi-Bekoe K.O. (2008). Assessment of the coefficient of thermal expansion of Alabama concrete. M.S. thesis, Auburn

- University, Auburn, Alabama. USA. Retrieved from [http://etd.auburn.edu/etd/bitstream/handle/10415/1435/Sak-yi-bekoe\\_Kwame\\_6.pdf](http://etd.auburn.edu/etd/bitstream/handle/10415/1435/Sak-yi-bekoe_Kwame_6.pdf) [Accessed 18.9.2012]
- Salonvaara, M., Sedlbauer, K., Holm, A., Pazera, M. (2010). Effect of selected weather year for hygrothermal analyses. American Society of Heating, Refrigerating and Air Conditioning engineers (ASHRAE), Atlanta. Buildings XI, thermal performance of the exterior envelopes of whole buildings XI 2010. Proceedings. CD-ROM: December 5-9, 2010, Clearwater Beach, Florida. 12 pp.
- Salta, M. Pereira, E. (2006). Factors influencing the corrosion in reinforced concrete. State of the art. Report 2-3: Concrete in Marine Environment, report 2-3. [online] Lisboa, Brazil: Laboratório Nacional de Engenharia Civil, LNEC. Available from: [http://www.medachs.ubordeaux1.fr/projet/materiaux/beton/doc\\_beton/rapport2-3-ir.pdf](http://www.medachs.ubordeaux1.fr/projet/materiaux/beton/doc_beton/rapport2-3-ir.pdf) [accessed 09.01.2010]
- Sarja, A. (2006). Predictive and optimised life cycle management – buildings and infrastructure. Taylor & Francis, London & New York. 668 pp.
- Schmidt, J. Kornadt, O. (2012). Convection through lightweight timber constructions with mineral wool. In: World Academy of Science, Engineering and Technology, Stockholm, Sweden 67th edition, 2012, pp. 731-738. Retrieved from: <http://www.waset.org/journals/waset/v67/v67-68.pdf> [Accessed 8.9.2012]
- Schulson E.M. (1998). Ice damage to concrete. Special report 98-6, April 1998. US Army Corps of Engineers, Cold Regions Research and Engineering Laboratory. Retrieved from [http://www.crrel.usace.army.mil/library/specialreports/SR98\\_06.pdf](http://www.crrel.usace.army.mil/library/specialreports/SR98_06.pdf) [Accessed 16.9.2012]
- Sedlbauer, K. (2002). Prediction of mould fungus formation on the surface of and inside building components, Ph. D. thesis, Fraunhofer Institute for Building Physics, Kassel, Germany.
- Sedlbauer, K., Krus, M., Zillig, W., Künzle, H.M. (2001). Mould growth prediction by computational simulation. IAQ 2001 Conference proceedings CD, Indoor Air Quality and Moisture in Buildings, 4-7 November, 2001, San Francisco, California, USA. Available online at: [http://www.ibp.fraunhofer.de/Images/mould\\_growth\\_prediction\\_tcm45-35007.pdf](http://www.ibp.fraunhofer.de/Images/mould_growth_prediction_tcm45-35007.pdf) [Accessed 9.8.2012]
- Setzer, M.J. (1999). Micro ice lens formation and frost damage, Draft Proceedings of the Minneapolis Workshop on Frost Damage in Concrete in USA, No. 14, pp. 1-15.

- Shin, H-C., Chung, Y. (2011). Determination of coefficient of thermal expansion effects on Louisiana's PCC pavement design. Final report. Department of Civil and Environmental Engineering, Louisiana State University, Baton Rouge, LA, USA. Retrieved from [http://www.ltrc.lsu.edu/pdf/2011/fr\\_451.pdf](http://www.ltrc.lsu.edu/pdf/2011/fr_451.pdf) [Accessed 30.9.2012]
- Smith, J.L., Virmani, Y.P. (2000). Materials and methods for corrosion control of reinforced and prestressed concrete structures in new construction. Publication No. FHWA-RD-00-81, Federal Highway Administration Research, Development and Technology, US. Department of Transportation, McLean, Virginia, June 2000.
- Song, G., Shayan, A. (2000). Service life prediction of reinforced concrete structures, Project report AP-T07, Department of Infrastructure, Energy and Resources, Tasmania, Research report published by Austroads Incorporated Level 9, Sydney Australia.
- Soroka, I. (1994). Concrete in Hot Environments. Modern Concrete Technology Series. E & FN Spon Press, London.
- Straube, J. (2002). Moisture in buildings. American Society of Heating, Refrigerating and Air Conditioning Engineering Journal (ASHRAE), Volume: 44, Issue: 1, January 2002, pp. 15 - 19.
- Straube, J., Schumacher, C. (2006). Assessing the durability impacts of energy efficient enclosure upgrades using hygrothermal modeling. Building Science Press Research Report – 0605. Retrieved from <http://www.buildingscience.com/document/s/reports/rr-0605-assessing-durability-energy-efficient-enclosure-upgrades-using-hygrothermal-modeling> [Accessed 9.8.2012]
- Takewaka, K., Sakai, k. (2005). Evaluation method of durability in concrete structures. JSCE-CICHE joint seminar in Mongolia, Japan. May 19, 2005. Retrieved from [http://www.jsce.or.jp/committee/concrete/newsletter/newsletter02/newsletter02f/8-Mongolia \(Takewaka\).pdf](http://www.jsce.or.jp/committee/concrete/newsletter/newsletter02/newsletter02f/8-Mongolia%20(Takewaka).pdf) [Accessed 30.9.2012]
- Tanesi, J., Meininger, R. (2006). Freeze-thaw resistance of concrete with marginal air content. Federal Highway Administration, Washington, DC, USA. Publication No. FHWA-HRT-06-117.
- The Finnish Meteorological Institute. (2013). Weather observations in Finland. Retrieved from. <http://en.ilmatieteenlaitos.fi/observations-in-finland> [Accessed 26.4.2013]
- Thelandersson, S, Isakson, T, Ekstrand-Tobin, A, Johansson, P. (2009). Modeling of onset of mould growth for wood exposed to varying climate conditions. Document IRG/WP 09-20414.

- International Research Group on Wood Protection, Stockholm, Sweden.
- Tuutti, K. (1982). Corrosion of steel in concrete. Swedish Foundation for Concrete Research (CBI), CBI research report no. 4.82. Stockholm, Sweden.
- Vesikari, E. (1999). Prediction of service life of concrete structures with regard to frost attack by computer simulation. Proceeding of Nordic Seminar on Frost Resistance of Building Materials, Aug. 31–Sept. 1 1999, Lund. Lund Institute of Technology, Division of Building Materials. 13 pp.
- Vesikari, E. (2009). Carbonation and chloride penetration in concrete – with special objective of service life modelling by the factor approach. Research report VTT-R-04771-09. Technical Research Centre of Finland (VTT).
- Viitanen, H., Ojanen, T. (2007). Improved model to predict mould growth in building materials. Proceedings of Thermal Performance of the Exterior Envelopes of Whole Buildings X [on CD]. Retrieved from [http://www.ornl.gov/sci/buildings/2012/Session%20PDFs/162\\_New.pdf](http://www.ornl.gov/sci/buildings/2012/Session%20PDFs/162_New.pdf) [Accessed 18.10.2012]
- Viitanen, H., Vinha, J., Salminen, K., Ojanen, T., Peuhkuri, R., Paajanen, L., Lähdesmäki, K. (2009). Moisture and Bio-deterioration Risk of Building Materials and Structures, Journal of Building Physics 2009, volume 33, number 3.
- Walton, J.C., Plansky, L.E., Smith, R.W. (1990). Models for estimation of service life of concrete barriers in low-level radioactive waste disposal. Washington, DC: Division of Engineering, Office of Nuclear Regulatory Research. NUREG/CR-5542.
- Weather Forecast. (2013). Helsinki Malmi (EFHF) Airport. Retrieved from <http://www.wunderground.com/q/zmw:00000.3.02975> [Accessed 21.4.2013]
- Wessman, L. (1997). Studies on the frost resistance on natural stone. Lund Institute of Technology. Division of Building Materials. Report TVBM-3077. Licentiate thesis. 199 pp.
- Yang, Z., Weiss, W., Olek, J. (2004). Interaction between micro-cracking, cracking, and reduced durability of concrete: developing methods for quantifying the influence of cumulative damage in life-cycle modeling. Joint transportation research program, Indiana Department of Transportation and Purdue University, West Lafayette, Indiana, USA. Publication FHWA/IN/JTRP-2004/10.
- Zander, A. (2009). The COMSY - code for the Detecting of Piping Degradation due to Flow-accelerated Corrosion. IAEA -

## References

Workshop on Flow Accelerated Corrosion (FAC) and Environmentally Assisted Cracking (EAC); April 21- 23, 2009; Moscow, Russia.

Zander, A., Nopper, H., Roessner, R. (2007). COMSY - A Software Tool for PLIM + PLEX with Integrated Risk-Informed Approaches. Proceedings of the 19th International Conference on Structural Mechanics in Reactor Technology (SMiRT 19). 12-17, August 2007, Toronto, Ontario, Canada

Zander, A. and Nopper, H. (2003). COMSY software assists lifetime management activities. Transactions of 17th International Conference on Structural Mechanics in Reactor Technology (SMiRT 17). 17-22, August 2003, Prague, Czech Republic.



# Appendices

## Appendix A. RHT-MAPS sensor network component.

Table A-1: The specifications of the network controller (LICo4)

Parameter	Value	Units
<b>Power supply</b>		
Supply voltage	24 (+/5%)	Vdc
Average supply current, max. with 200 nodes (LN1004)	0.5	Adc
<b>Linnet bus connection</b>		
Supply voltage	40	Vpp
Supply current, max. (200 nodes)	0.7	A (peak)
Power consumption, max. (200 nodes)	12	W
Bus frequency, sine wave	20	kHz
Number of nodes, maximum	200	pcs
Length of network cabling, maximum (CAT5E)	1000	m.
<b>Serial interface</b>		
Standard interface	RS232	
Standard interface speed	19200	bits/s
Standard interface settings (data, stop, parity)	8,1,N	
Selectable interface (option)	RS485	
Isolation	100	Vdc
<b>Ethernet interface</b>		
Network interface	10BASET	
Network connector	RJ45	

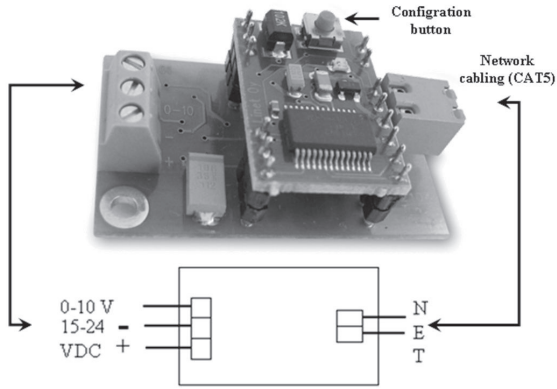


Figure A-2: The network hybrid data node (LN1003)

Table A-2: The specifications of the network hybrid data node (LN1003)

Parameter	Value	Units
<b>General parameters</b>		
Network voltage	22	V <sub>pp</sub> (max.)
DC test voltage	22	VDC (max)
Average power consumption	3,5	mW
IC current output capacity, sum of all output pins	3	mA (max.)
Output voltage	3.3	V
Frequency of XO pin	1	MHz
Operating temperature range, the hybrid node	-40... +85	°C
<b>Data groups</b>		
Serial full duplex data capacity	80 / 160 / 320	bits/sec.
<b>A/D converter</b>		
Resolution	12	bits
Input voltage range	0 – 1.25	V
Linearity	0.5	%
Non-calibrated accuracy	2	%
Temperature coefficient	85	ppm/K

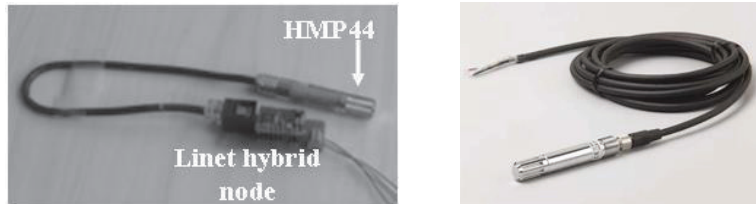


Figure A-3: The HMP44 humidity and temperature probe

Table A-3: The specifications of the HMP44 humidity and temperature probe

<b>Relative humidity</b>	
Measurement range	0...100% RH
Accuracy	
0...90% RH	±2% RH
90...100% RH	±3% RH
Typical long-term stability in air	1% RH/year
Response time (90%) at +20°C in still air	15s
Typical response time when the concrete and the probe are at the same temperature (stabilised hole)	30 min
Humidity sensor	HUMICAP® 180
<b>Temperature</b>	
Measurement range	-20...+60°C
Accuracy at +20°C	±0.4°C
Temperature sensor	Pt 1000 Class B
<b>General</b>	
Operating temperature range for electronics	-40...+60°C
Sensor diameter	12 mm
Cable length	2.7 m
Probe length	69 mm
Housing material	ABS plastic
Housing classification	IP65
Sensor protection	membrane filter 17039HM
Bore hole diameter	16 mm
Measurement depth	Min. 30 mm, max. 90 mm

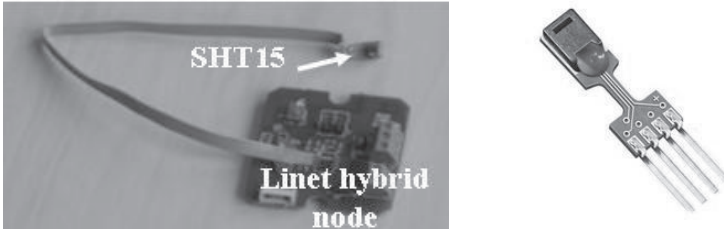


Figure A-4: The SHT15 humidity and temperature sensor

Table A-4: The specifications of the SHT15 humidity and temperature sensor.

<b>Relative humidity</b>	
Measurement range	0...100% RH
Accuracy	
0...10% RH	±4...2% RH
10...90% RH	±2% RH
90...100% RH	±2...4% RH
Response time	4 s
Repeatability	+/- 0.1% RH
<b>Temperature</b>	
Measurement range	-20...+123.8°C
Accuracy at +25°C	±0.3°C
Response time	30 s
<b>General</b>	
2-wire interface	
Voltage supply	between 2.4 and 5 V
Power consumption	30 µW
Sensor size	7.62 x 5.08 x 2.5 mm
Weight	100 mg

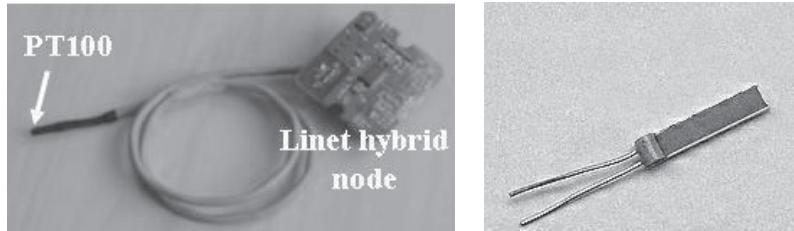


Figure A-5: PT100 temperature sensor

Table A-5: The specifications of the PT100 temperature sensor

Recommended measuring current for self-heating < 0.1K	DC 1...3 mA
Sensor resistance at 0°C	100 ± 0.1 Ω
Change in resistance 0...100°C	0.385 Ω /K
Application temperature	-50...+200°C
Connection	PTFE-strand 0.14 mm <sup>2</sup> (AWG 26)
Insulation test voltage U <sub>is</sub>	AC 2.5 kV
Protection class acc. to EN 60529	IP54
Bending radius	> 25 mm



## Appendix B. RHT-MAPS sensor network configuration

### Connecting to the network configuration software

Start the connection between the host computer and the network controller by starting a telnet program. To enter the configuration mode, type "config" and press Enter. The configuration is based on a menu-driven system: you start from the menu root, then enter each submenu by pressing the appropriate number key, and return to the previous menu by pressing Backspace.

You can check the status of the network by pressing the key '2' as shown in Figure B1. The status of the network shows the number of nodes in the network, the number of connected nodes, and the number of missing nodes.

```

Linnet ver. 7.0.5
Type a question mark and press ENTER for help
> OK?
> config
CONFIGURE
1  Configure net
2  Status
3  Configure input/output
NETWORK STATUS
6 nodes present, 6 connected, 0 missing, Running

```

Figure B-1: The start-up screen of the network system configuration

### Configuring data group

Each Linet node has one input and one output in use at a time. The inputs are:

- SWNO - switch input
- SDI - serial data input
- AIN - analog input

The outputs are:

- FOUT - (filtered) switch output
- SDO - serial data output
- PWM - pulse width modulation output

The group into which the node is configured determines which input and which output is active in the node. The node can belong to one group at a time.

Each node has a unique network identifier, "nid", which is an integer between 1 and 200 (inclusive). When a node is configured, the controller automatically creates a new identifier and writes it into the node's internal non-volatile memory. The identifier remains in the memory during power shutdowns, and can be re-written later, if needed. The groups are also created when the operator configures the network. Each group has a group identifier, "gid", which is an integer between 1 and 200 (inclusive). When a new group is created, the user indicates the nodes to be included in the group by pressing the push button on the nodes.

### Configuring data groups

The nodes used in the RHT monitoring network can be configured into data groups. The following nodes are used in the data group:

- I/O node
- 8-bit data
- 12-bit data (SHT15, relative humidity sensor)
- 16-bit data
- data exchange
- AD/state (HMP44, relative humidity sensor, and PT100, temperature sensor)

The I/O group is a single node consisting of one input and one output, intended to switch input and output. Data nodes send and receive 8-, 12-, or 16-bit words of data between the node and the controller. The AD/state group is a combined analog input and switch output node. In a data group, there can be only one node. In a data exchange group there must be exactly two nodes.

### Adding a node to a data group

Figure b2 shows an example of creating a new 12-bit data group and adding a node to it. In the configuration menu do the following:

- press key '1' (Configure net)
- press key '1' (Add a Linet node)
- press key '1' (Add to a new group)
- press key '3' (Add to a new data group)
- press key '3' (12 bit data group)



- the terminal prompts "Push buttons of nodes to be added to this group". Push the push button of a node and hold it down for a while. While the push button is pressed down, the controller automatically assigns the lowest unused identifier to the node, if the node was unidentified
- press Backspace to return to the command mode.

Adding a node to an AD/State group is shown in Figure b3. The procedure is the same as above, except for selecting the 12 AD/State group type (key '6').

```

Linnet ver. 7.0.5
Type a question mark and press ENTER for help
> OK!
> config
CONFIGURE
1 Configure net
2 Status
3 Configure input/output
CONFIGURE NET
1 Add a Linet node
2 Delete a Linet node
3 Set group master controls
4 Set frame size
5 Set clock
6 Save net configuration
7 Restore net configuration
8 Delete connections
9 Set delay group time
A Set control group setpoint
B Network debug
ADD A LINET NODE
1 Add to a new group
2 Add to an existing group
ADD TO NEW GROUP
Select a group to add into
1 Add to a new toggle group
2 Add to a new dimmer group
3 Add to a new data group
4 Add to a new extended group
ADD TO NEW DATA GROUP
Select a data group type
1 I/O node
2 8 bit data
3 12 bit data
4 16 bit data
5 data exchange
6 AD / state
7 Control
ADD A LINET NODE
Data 12 group 7
Push buttons of nodes to be added to this group
When all is done push back space
=
    
```

Figure B-2: Adding a new node to a 12-bit data group.

```

ADD TO NEW DATA GROUP
Select a data group type
1 I/O node
2 8 bit data
3 12 bit data
4 16 bit data
5 data exchange
6 AD / state
7 Control
ADD A LINET NODE
AD/State group 2
Push buttons of nodes to be added to this group
When all is done push back space
Node 2 added
    
```

Figure B-3: Adding a new node to an AD/State group

Removing a node from a data group

To remove a node from a data group do the following:

- press key '1' (Configure net)
- press key '2' (Delete a Linet node)
- press the push button of the node to be removed from the data group.
- press Backspace to return to the command mode.

```

CONFIGURE NET
1 Add a Linet node
2 Delete a Linet node
3 Set group master controls
4 Set frame size
5 Set clock
6 Save net configuration
7 Restore net configuration
8 Delete connections
9 Set delay group time
A Set control group setpoint
B Network debug

REMOVE A LINET NODE
Push buttons of nodes to be deleted
When all is done push back space
No group 2
Node 2 removed

```

Figure B-4: Removing a node from a data group

Saving and loading the network configuration

During the power start-up, the controller loads the configuration from its non-volatile memory. The configuration in this context means the settings controlled by the controller:

- list of groups and their types
- list of nodes belonging to each group (node identifiers and node configuration bits are controlled by each node)

After changing the configuration you must save it in the non-volatile memory until the 'save configuration' instruction has been given. To do that:

- press key '1' (Configure net)
- press key '6' (Save net configuration)

If you want to return to the previous configuration:

- press key '1' (Configure net)
- press key '7' (Restore net configuration) and select from two of the latest saved configurations

```

CONFIGURE NET
1 Add a Linet node
2 Delete a Linet node
3 Set group master controls
4 Set frame size
5 Set clock
6 Save net configuration
7 Restore net configuration
8 Delete connections
9 Set delay group time
A Set control group setpoint
B Network debug
Saving net ... done

```

Figure B-5: Saving the network configuration

### Setting the network controller IP address

The controller uses one User Datagram Protocol (UDP) port. The port number and the Internet Protocol (IP) address of the controller are configured during the controller setup. The IP address should belong to the IP subnet of the Ethernet segment that the controller is to be connected to. In the test versions, the IP address is 192.168.42.13 and the port is 1313.

To set the IP address of the network controller shown in Figure B6:

- press key '3' (Configure input/output)
- press key '3' (Set IP address). The terminal prompts (IP:xxx.xxx.xxx.xx) the network IP address and asks for a new IP address.

```

CONFIGURE
1 Configure net
2 Status
3 Configure input/output

INPUT / OUTPUT SETUP
1 Set serial I/O bit rate
2 Set serial I/O parity
3 Set IP address
4 Set UDP port
IP: 130.233.132.63; enter IP: >

```

Figure B-6: Setting the network controller IP address.



## Appendix C. RHT-MAPS monitoring software user's guide

The RHT-MAPS monitoring software is designed for use with Windows®2000/XP operating systems. The main window of the RHT-MAPS monitoring software is shown in Figure C1.

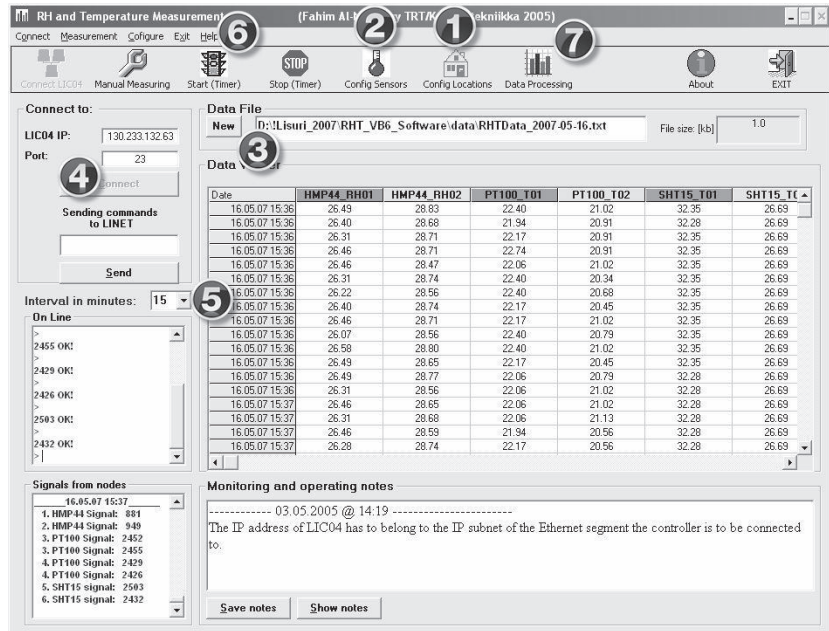


Figure C-1: General overview of RHT-MAPS monitoring software.

The program is configured and used as follows

### Step 1: Configuring the locations being monitored.

Configuration of the locations being monitored within the facade wall as shown in Figure C2. The configuration includes the layer within the wall structure that is being monitored, the first node number, and the last node number.

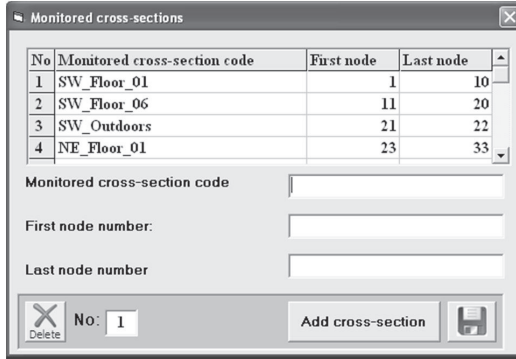


Figure C-2: Configuration of the locations being monitored.

### Step 2: Configuring the relative humidity and temperature sensors

As shown in Figure C3, the configuration includes the number of the node connected to the sensor, the sensor code, the sensor type, the sensor gain and offset, and the location in the facade that is being monitored.

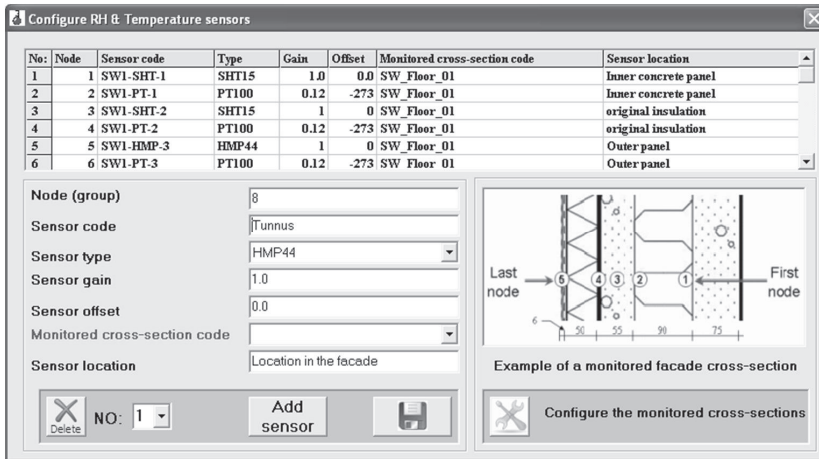


Figure C-3: Configuration of the relative humidity and temperature sensors.

### Step 3: Setting the output data file name.

The name is assumed on the basis of the site being monitored and the current date, but the file name could be edited by the software user.

#### Step 4: Connecting to the RHT-MAPS monitoring network.

The user sets the network's IP (Internet Protocol) address and the communication port. After connection, a list of connected nodes and their statuses will appear as shown in Figure C4.

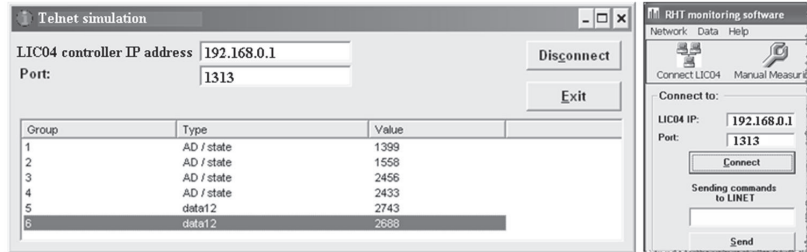


Figure C-4: Connecting to the RHT-MAPS monitoring network.

#### Step 5: Setting the interval measurements

A time interval for the relative humidity and temperature data measurements is set. The default interval value is set as 15 minutes.

#### Step 6: Starting the measurements.

The software will send signals to the RHT-MAPS sensor network at the predefined intervals and receives relative humidity and temperature data. The software processes the data and displays them on the screen and saves them to the predefined output ASCII file.

#### Step 7: Processing the relative humidity and temperature data.

The data-processing module was developed using Visual Basic for Applications under Microsoft Excel. The starting window for the module is shown in Figure C5.

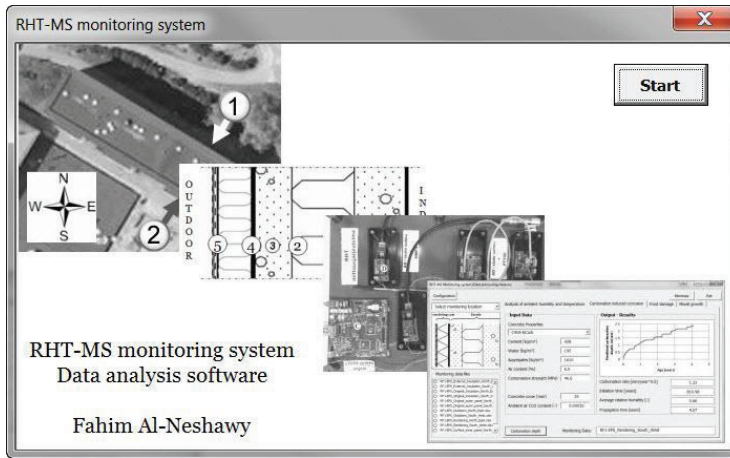


Figure C-5: Starting the RHT-MAPS data processing module.

For configuring the RHT-MAPS data processing module, the input configuration window is used as shown in Figure C6. In the configuration window, the user sets information about the data input and output folders and the types of concrete used in the facade construction. The configuration data are saved in “configurations.xlsx” and used by the data-processing module.

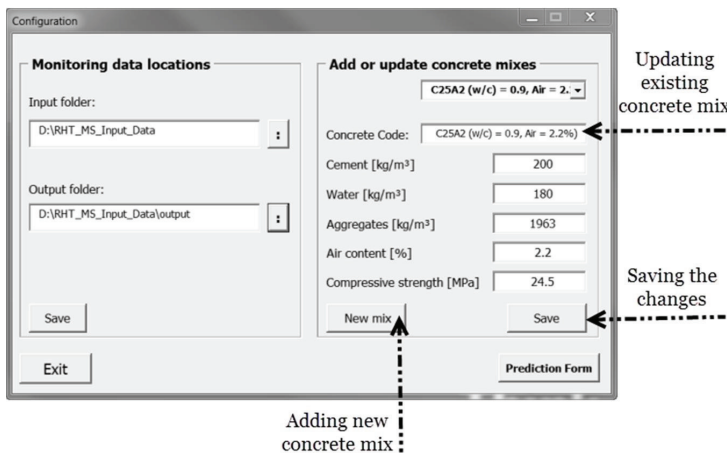


Figure C-6: Configuring the RHT-MAPS data analysis software.

The relative humidity and temperature data should be arranged in an Excel spreadsheet in the way that is shown in Figure C7 for performing the calculation using the data-processing module. In this thesis, the data spreadsheet is formatted by the user before starting the data analysis.



	A	B	C	D
1				
2				
3				
4				
5				
6				
7				
8				
9				
10	Date	T_[SW]	RH_[SW]	
11	2.6.2005 16:00	14.3	46	
12	2.6.2005 17:00	10.8	63	
13	2.6.2005 18:00	10.3	69	
14	2.6.2005 19:00	13.0	65	
15	2.6.2005 20:00	12.6	63	
16	2.6.2005 21:00	10.3	74	
17	2.6.2005 22:00	8.9	81	
18	2.6.2005 23:00	7.7	85	

Figure C-7: Spread sheet template for the input data.

The RHT-MAPS data processing module is divided into several tabs; each of them performs specific calculations. These tabs are used as follows:

- i) analysing the hygrothermal conditions and time-dependent moisture and thermal indices;
- ii) predicting the carbonation-induced corrosion of concrete building facades and calculating their remaining service life;
- iii) predicting the frost damage to concrete building facades and calculating their remaining service life;
- iv) predicting the potential risk of mould growth in concrete building facades.

The use of the RHT-MAPS data processing module is illustrated in Figures C8 to C18.

In the humidity and temperature tab, the user has to select the monitoring data file and then to press the calculation button in order to analyse the monitoring data and plot the resulting graph. The algebraic formulae used for these calculations are discussed in Chapter 2.

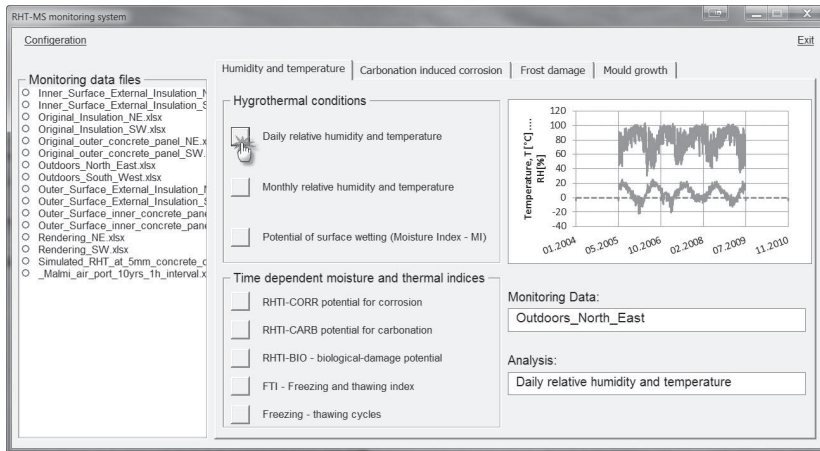


Figure C-8: Calculating the daily relative humidity and temperature.

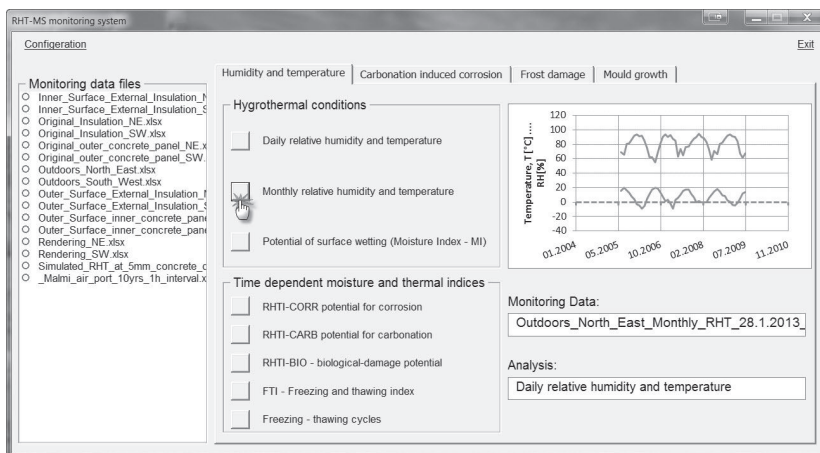


Figure C-9: Calculating the monthly relative humidity and temperature.

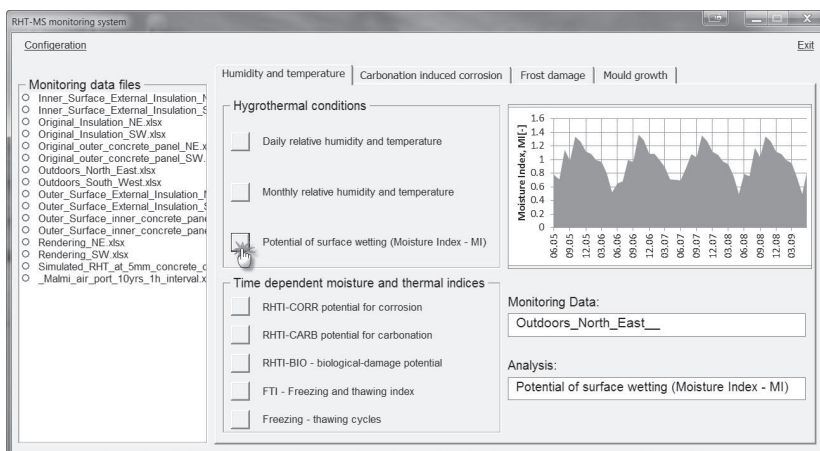


Figure C-10: Calculating the monthly moisture index.

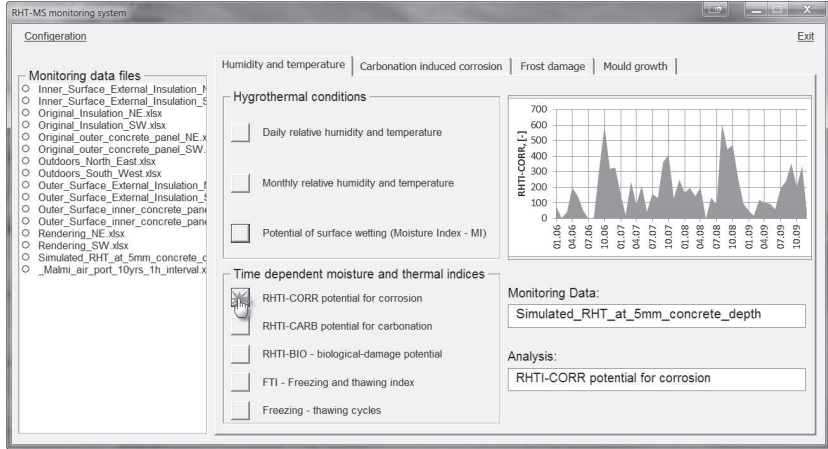


Figure C-11: Calculating the potential for corrosion damage RHTI-CORR.

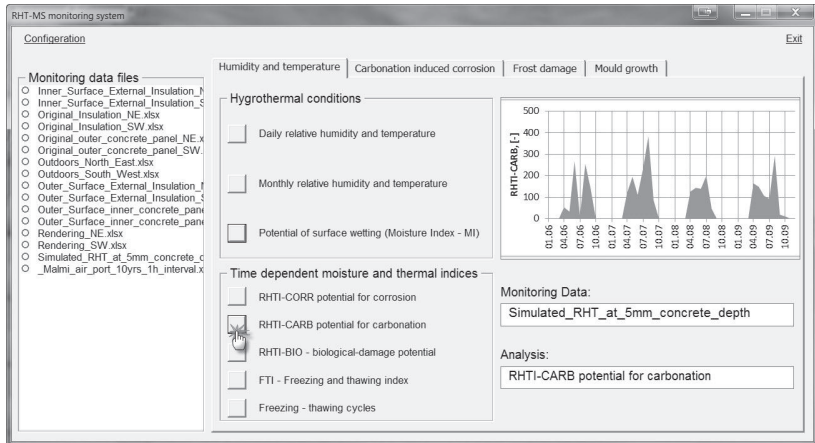


Figure C-12: Calculating the potential for carbonation damage RHTI-CARB.

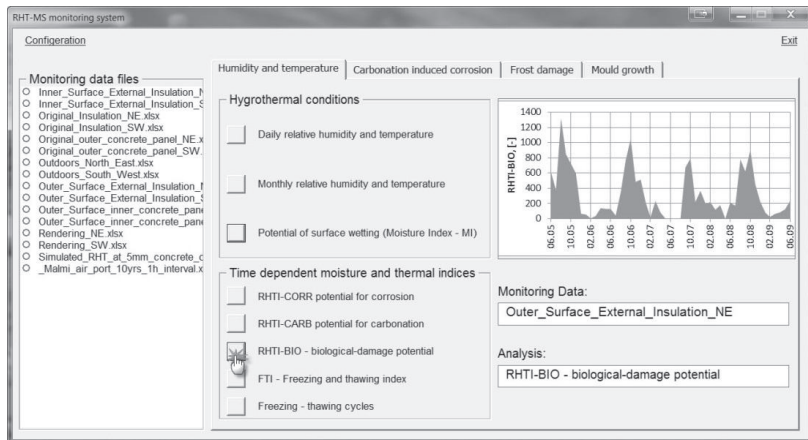


Figure C-13: Calculating the potential for biological damage RHTI-BIO.

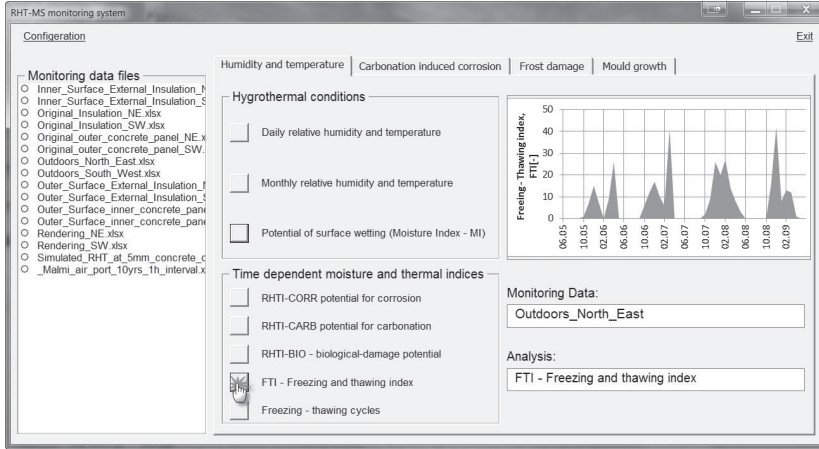


Figure C-14: Calculating the potential for freezing and thawing damage FTI index.

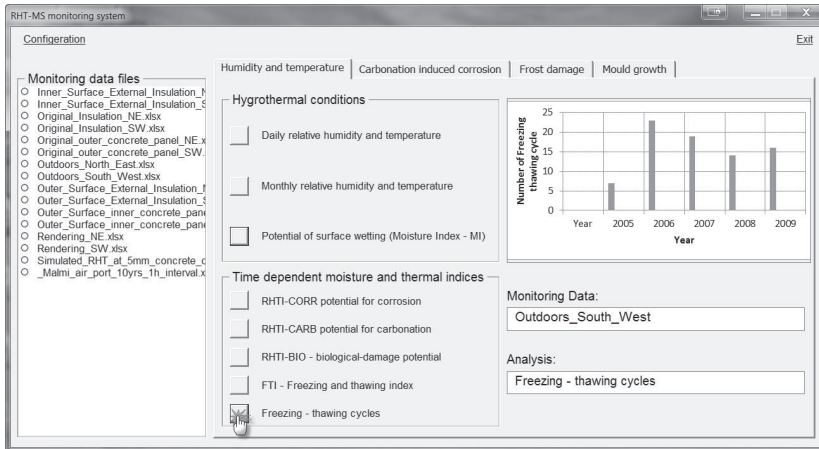


Figure C-15: Calculating the number of freezing and thawing cycles.

The freezing and thawing cycle occurs when the temperature crosses +2°C, drops down below at least -5°C, and then returns to above +2°C again.

In the carbonation-induced corrosion tab, the user has to select the monitoring data file, select the properties of the concrete for the building facade, input the depth of the concrete cover and the diameter of the reinforcing bar, and then press the calculation button. The output results are the carbonation depth graph, the carbonation rate, and the initiation and propagation time for corrosion of the reinforcement steel. The carbonation depth and service life calculation formulae used for these calculations are discussed in Chapter 6.

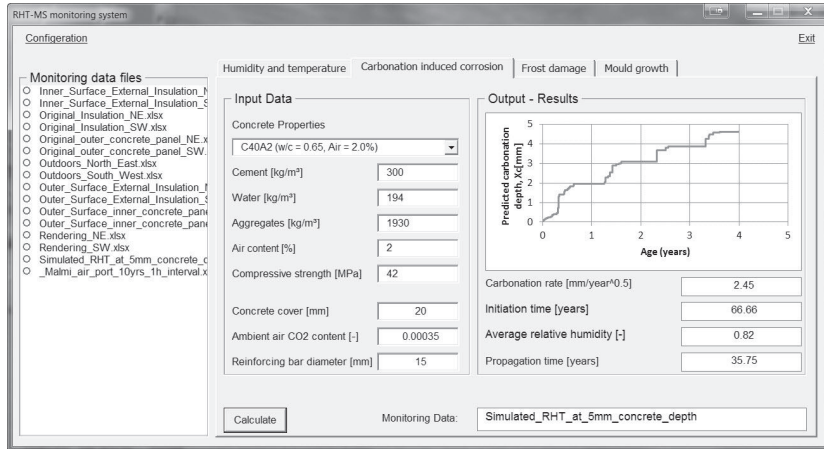


Figure C-16: Prediction of the corrosion of steel reinforcements as a result of carbonation.

In the frost damage tab, the user has to select the monitoring data file, select the properties of the concrete for the building facade, input the annual number of freezing and thawing cycles and the level of frost damage, and then press the calculation button. The user can also change the temperature threshold for the freezing and thawing cycle. The output results are the freezing-thawing cycle graph, the RDM (Relative Dynamic Modulus) graph, and the remaining service life of the concrete building facade once frost damage has been taken into consideration. The frost damage and service life calculation formulae used for these calculations are discussed in Chapter 6.

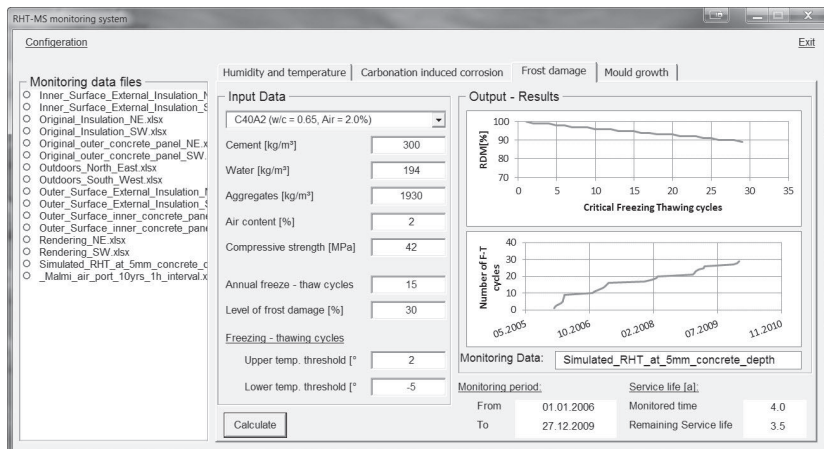


Figure C-17: Prediction of the frost damage to concrete building facades.

In the mould growth tab, the user has to select the monitoring data file for the concrete building facade layers that could be at risk of mould growth, and then to press the calculation button. The output results are the critical relative humidity graph for mould growth and the potential for mould growth during the monitoring period. The risk of mould growth formulae used for these calculations are discussed in Chapter 6.

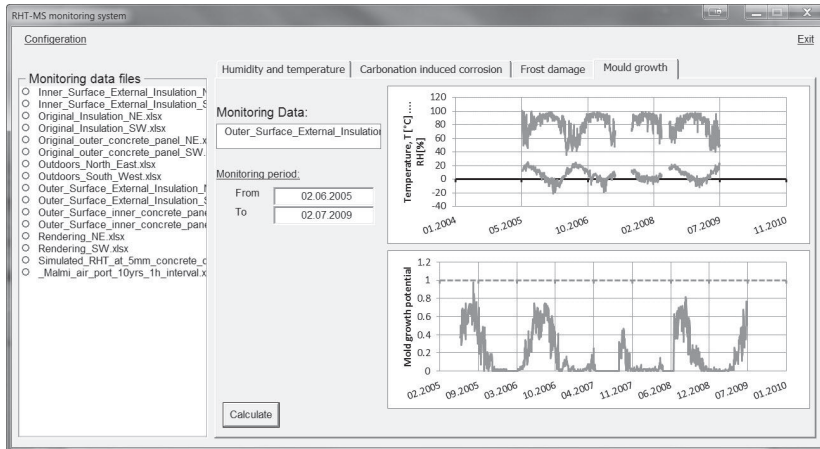


Figure C-18: Prediction of the risk of mould growth in concrete building facades.

## Appendix D. Laboratory testing of concrete

### Accelerated carbonation test: mix design

Table D-1: Basic mix proportions and properties of the test concrete in the accelerated carbonation test.

		C40A2- Y	C40A6- Y	C40A2- SR	C40A6- SR
Cement [kg/m <sup>3</sup> ]		321	321	321	321
Total effective water [kg/m <sup>3</sup> ]		185	192	192	191
Aggregate total [kg/m <sup>3</sup> ]		1903	1858	1887	1805
Aggregates	R 0 - 1 mm	77	75	56	53
	R 0 - 8 mm, fine	197	192	167	160
	R 0 - 8 mm, washed	887	866	865	828
	R 5 - 16	743	725	799	764
Air- entraining agent	Product name	Ilma- Parmix		Ilma- Parmix	
	Amount [% of cement]	0.007		0.012	
Basic properties	Slump value [mm]	12	4	42	115
	Temperature [°C]	22	25	24	24
	Density [kg/m <sup>3</sup> ]	2408	2319	2404	2308
	Fresh concrete air content [%]	2.6	5.0	1.7	5.4
Compressive strength	7d		24.5	31.3	24.2
	28d	44.7	38.0	40.0	35.7
Y = CEM II/A-M(S-LL) 42.5 N SR = CEM I 42.5 N-SR					

Table D-2: Grading of the combined aggregates of the test concrete in the accelerated carbonation test.

Aggregate size [mm]	Passing by mass (%)										
	0.063	0.125	0.25	0.5	1	2	4	8	16	32	64
R 0 - 1	11.9	45	88	98	100	100	100	100	100	100	100
R 0 - 8, fine	1.3	6	27	59	79	60	96	100	100	100	100
R 0 - 8, washed	1.3	4	13	26	41	59	75	94	100	100	100
R 5 - 16	0.4	1	1	1	1	2	2	15	96	100	100

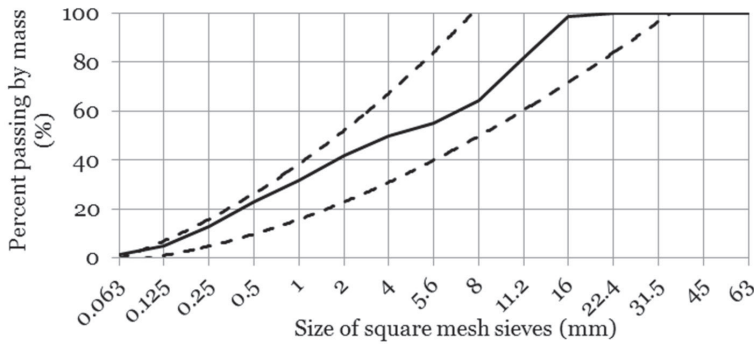


Figure D-1: Aggregate grading chart for the test concrete in the accelerated carbonation test.

**Natural carbonation test: mix design**

Table D-3: Basic mix proportions and properties of the test concrete in the natural carbonation test.

		C30A2- carb	C30A6- carb	C35A5- carb	C40A2- carb	C45A6- carb
Cement	[kg/m <sup>3</sup> ]	266	250	343	270	428
Total effective water	[kg/m <sup>3</sup> ]	206	144	167	204	195
Aggregate total						
	[kg/m <sup>3</sup> ]	1779	1907	1786	1874	1610
Aggregates	R 0 - 8	1405				1524
	R 4 - 8	374				86
	R 8 - 16					
Air-entraining agent	Product name		Ilma-Parmix	Ilma-Parmix		Ilma-Parmix
	Amount [% of cement]		0.050	0.027		0.055
	Slump value [mm]		25	55		
Basic properties	Temperature [°C]					
	Density [kg/m <sup>3</sup> ]		2300	2330		
	Fresh concrete air content [%]		6.0	5.0		
Compressive strength	28d	35.2	30.0	38.0	42.0	46.6



**Thermal expansion of concrete: mix design**

Table D-4: Grading of the combined aggregates of the test concrete in the thermal expansion test.

Aggregate size [mm]	Passing by mass (%)									
	0.125	0.25	0.5	1	2	4	8	16	32	64
filler 96	64	90	94	96	97	98	98	99	100	100
R 0.1 - 0.6	4	37	89	100	100	100	100	100	100	100
R 0.5 - 1.2	0	1	5	80	100	100	100	100	100	100
R 1.0 - 2.0	0	0	1	14	89	100	100	100	100	100
R 2.0 - 5.0	0	0	0	0	1	50	100	100	100	100
R 5.0 - 10.0	0	0	0	0	0	4	78	100	100	100
R 8.0 - 16.0	0	0	0	0	0	0	1	97	100	100

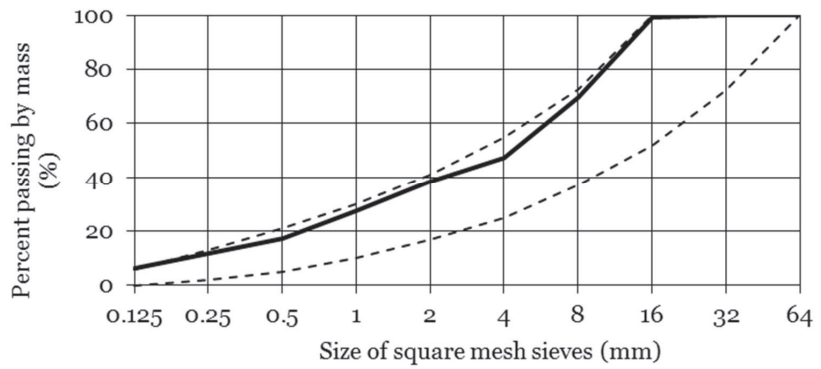


Figure D-2: Aggregate grading chart for the test concrete in the thermal expansion test.

Table D-5: Basic mix proportions and properties of the test concrete in the thermal expansion test.

Materials	C25A2- R-TE	C40A2- R-TE	C25A3- R-TE	C25A4- R-TE	C35A9- R-TE	C40A7- R-TE	C45A6- R-TE
Cement [kg/m <sup>3</sup> ]	201	281	250	250	475	475	475
Effective water [kg/m <sup>3</sup> ]	181	181	190	190	190	190	190
Aggregate [kg/m <sup>3</sup> ]	1970	1903	1867	1815	1502	1557	1610
Filler	197	190	75	73	60	62	64
R 0.1 - 0.6	158	209	187	182	150	156	161
R 0.5 - 1.2	197	190	131	127	105	109	113
R 1.0 - 2.0	236	171	187	182	150	156	161
R 2.0 - 5.0	256	228	336	327	270	280	290
R 5.0 - 10.0	414	400	317	309	255	265	274
R 8.0 - 16.0	512	514	635	617	511	529	547
Air-entraining agent			Ilma- Parmix	Ilma- Parmix	Ilma- Parmix	Ilma- Parmix	Ilma- Parmix
Amount [% of cement]	0	0	0.04	0.13	1.20	0.71	0.38
Slump value [mm]			13	125	70	30	60
Temperature [°C]	23	22	25	25	28	27	26
Density [kg/m <sup>3</sup> ]	2395	2420	2358	2300	2170	2214	2233
Fresh concrete air content [%]	1.7	1.6	2.8	4.3	9.5	6.8	5.9
Compressive strength, 28d [MPa]	30.0	45.8	26.5	28.7	34.0	40.0	44.4
Concrete density [kg/m <sup>3</sup> ]			1816	2251	2163	2224	2241

R = Rapid cement (CEM II/A-LL 42.5 R)

TE = Thermal Expansion

### Thermal expansion of concrete: Results

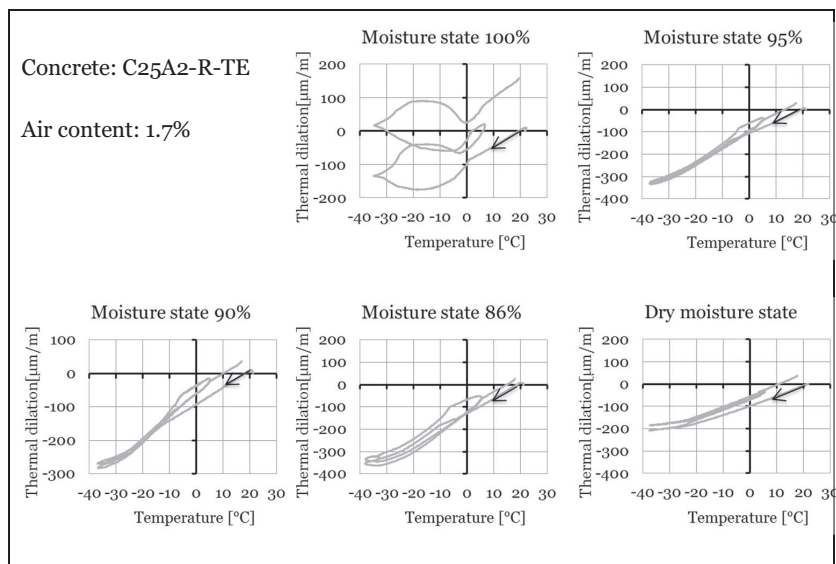


Figure D-3: Length changes resulting from the freezing and thawing of C25A2-R-TE concrete.

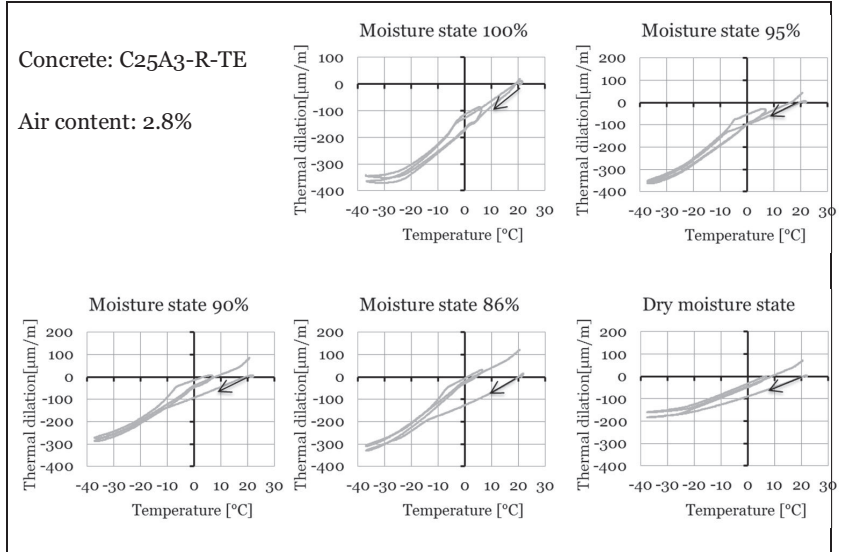


Figure D-4: Length changes resulting from the freezing and thawing of C25A3-R-TE concrete.

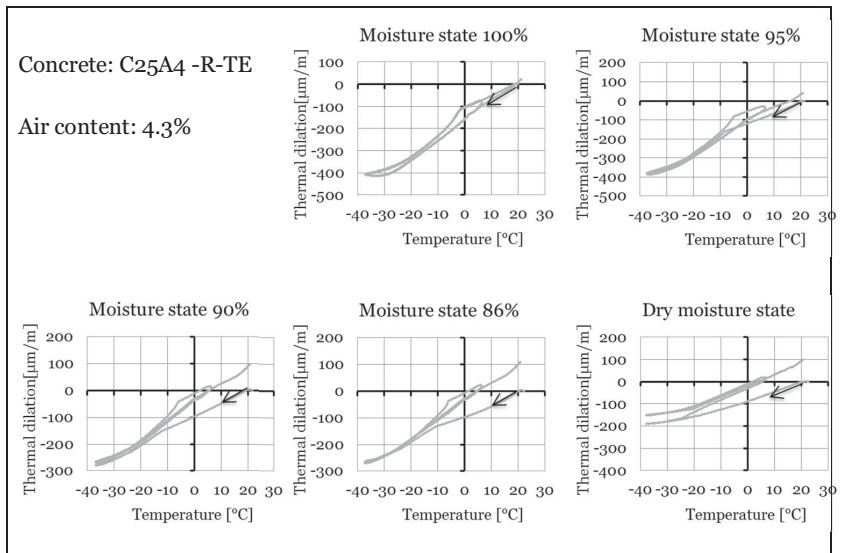


Figure D-5: Length changes resulting from the freezing and thawing of C25A4-R-TE concrete.

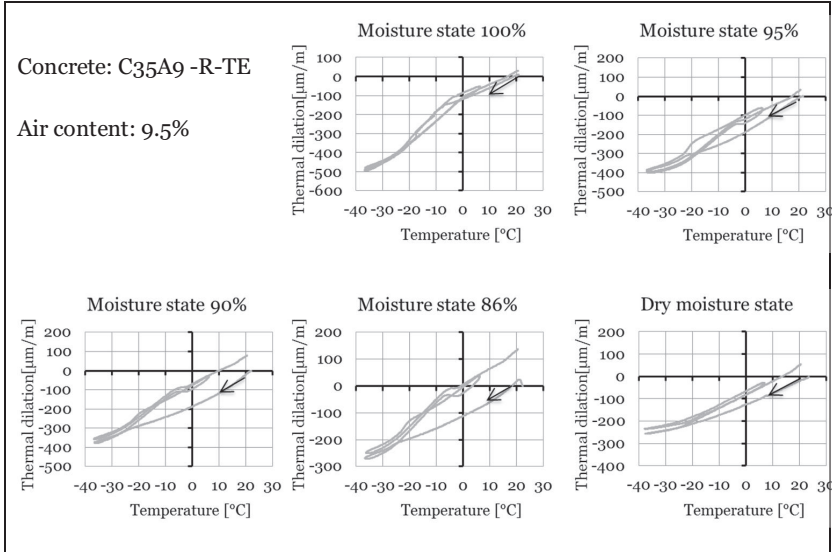


Figure D-6: Length changes resulting from the freezing and thawing of C35A9-R-TE concrete.

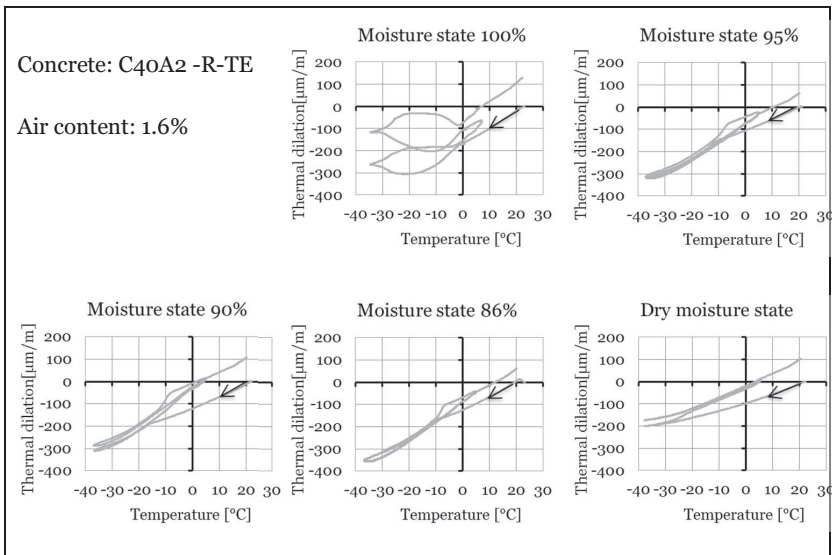


Figure D-7: Length changes resulting from the freezing and thawing of C40A2-R-TE concrete.

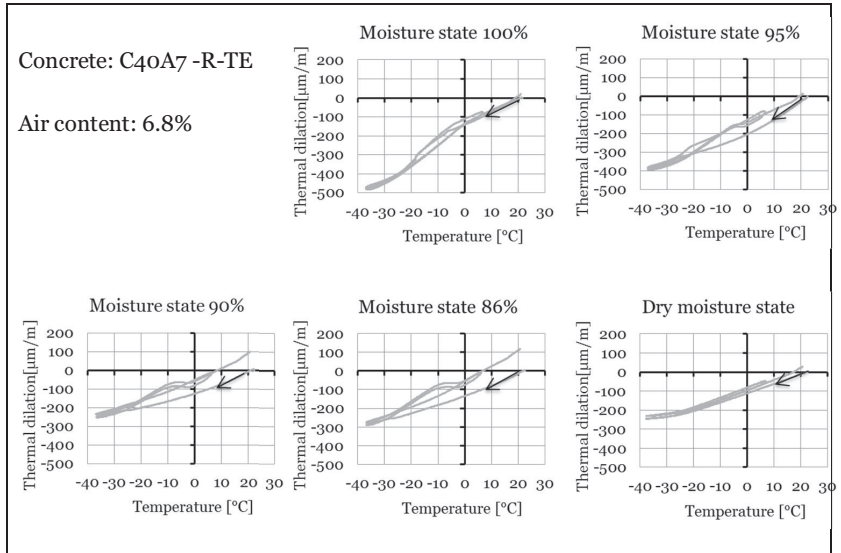


Figure D-8: Length changes resulting from the freezing and thawing of C40A7-R-TE concrete.

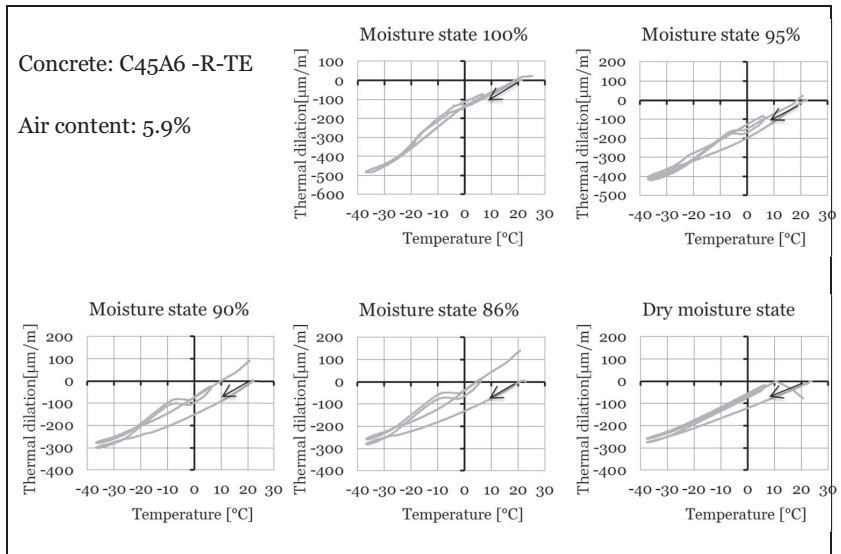


Figure D-9: Length changes resulting from the freezing and thawing of C45A6-R-TE concrete.

**Freezing and thawing resistance of concrete: mix design**

Table D-6: Basic mix proportions and properties of the test concrete in the freezing and thawing resistance test.

		<b>C40A2- Y</b>	<b>C40A6- Y</b>	<b>C40A2- SR</b>	<b>C40A6- SR</b>
Cement [kg/m <sup>3</sup> ]		321	321	321	321
Total effective water [kg/m <sup>3</sup> ]		185	192	192	191
Aggregate total [kg/m <sup>3</sup> ]		1903	1858	1887	1805
Aggregates	R 0 - 1 mm	77	75	56	53
	R 0 - 8 mm, fine	197	192	167	160
	R 0 - 8 mm, washed	887	866	865	828
	R 5 - 16	743	725	799	764
Air-entraining agent	Product name	Ilma-Parmix		Ilma-Parmix	
	Amount [% of cement]	0.007		0.012	
Basic properties	Slump value [mm]	12	4	42	115
	Temperature [°C]	22	25	24	24
	Density [kg/m <sup>3</sup> ]	2408	2319	2404	2308
	Fresh concrete air content [%]	2.6	5.0	1.7	5.4
Compressive strength	7d		24.5	31.3	24.2
	28d	44.7	38.0	40.0	35.7

Y = CEM II/A-M(S-LL) 42.5 N

SR = CEM I 42.5 N-SR

Figure D-7: Grading of the combined aggregates for the test concrete in the freezing and thawing resistance test.

Aggregate size [mm]	<b>Passing by mass (%)</b>										
	0.063	0.125	0.25	0.5	1	2	4	8	16	32	64
R 0 - 1	11.9	45	88	98	100	100	100	100	100	100	100
R 0 - 8, fine	1.3	6	27	59	79	60	96	100	100	100	100
R 0 - 8, washed	1.3	4	13	26	41	59	75	94	100	100	100
R 5 - 16	0.4	1	1	1	1	2	2	15	96	100	100

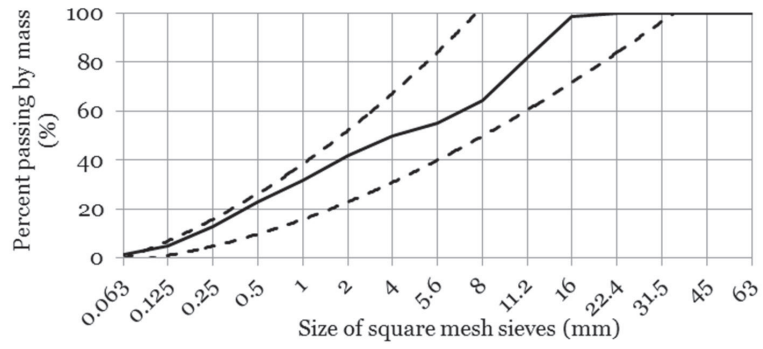


Figure D-3: Aggregate grading chart for the concrete mixes of the freezing and thawing test





## Appendix E. Data of Tanesi and Meininger, 2006

Table E-1: Mix proportions and properties of the test concretes.

Tanesi and Meininger (2006) - codes	350	115-3	118-1	115-1	116-2	227
Code	C30A4	C45A5	C40A5	C40A4	C35A2	C40A2
Cement, [kg/m <sup>3</sup> ]	356	355	355	355	356	356
Water, [kg/m <sup>3</sup> ]	160	142	178	163	142	160
Aggregates, [kg/m <sup>3</sup> ]	1820	1869	1775	1842	1923	1851
W/C ratio	0.45	0.40	0.50	0.46	0.40	0.45
Air agent (dm <sup>3</sup> /100 kg-cement)	0.14	0.07	0.04	0.03	0.00	0.01
Water reducing admixture (dm <sup>3</sup> /100 kg-cement)	0.27	0.26	0.26	0.26	0.26	0.21
Fresh concrete density (kg/m <sup>3</sup> )	2339	2374	2352	2361	2401	2393
Air content (%)	4.3	4.6	4.6	3.5	2.5	2.4
Compressive strength [MPa]	32.6	43.1	41.0	39.9	35.2	43.2

Table E-1: Calculated and measured RDM versus number of freezing and thawing cycles.

C40A2			C45A5			C35A2		
Number of cycles	Calculated RDM	Measured RDM	Number of cycles	Calculated RDM	Measured RDM	Number of cycles	Calculated RDM	Measured RDM
1	100	100	1	100	100	1	100	100
9	99	97	19	100	95	18	97	92
18	98	96	32	99	95	37	94	89
29	97	96	50	99	94	50	92	86
37	96	96	69	99	93	84	86	78
63	93	96	84	98	93	103	83	66
84	91	96	103	98	93	112	82	61
97	90	96	132	98	92			
112	88	95	141	97	92			
132	86	94	161	97	90			
146	84	94	174	97	90			
161	83	94	196	96	89			
190	80	93	220	96	89			
196	79	93	253	95	86			
217	77	92	288	95	86			
236	75	87	300	95	86			
253	73	88						
265	72	86						
288	69	88						
300	68	86						

C30A4			C40A5			C40A4		
Number of cycles	Calculated RDM	Measured RDM	Number of cycles	Calculated RDM	Measured RDM	Number of cycles	Calculated RDM	Measured RDM
1	100	100	1	100	100	1	100	100
11	98	95	9	100	96	19	99	95
25	95	94	29	99	96	32	98	94
34	94	94	42	99	96	50	97	93
43	92	94	55	99	97	69	96	93
61	89	91	63	98	96	84	95	96
75	86	89	88	98	97	103	94	90
92	83	85	97	97	96	132	92	90
107	80	82	121	97	96	141	91	90
121	77	75	160	96	96	161	90	90
136	75	72	192	95	96	174	89	89
146	73	65	217	94	96	196	88	85
158	70	68	236	94	96	220	87	88
172	68	60	265	93	96	253	85	87
190	64	62	300	92	95	288	82	85
208	61	55				300	82	84

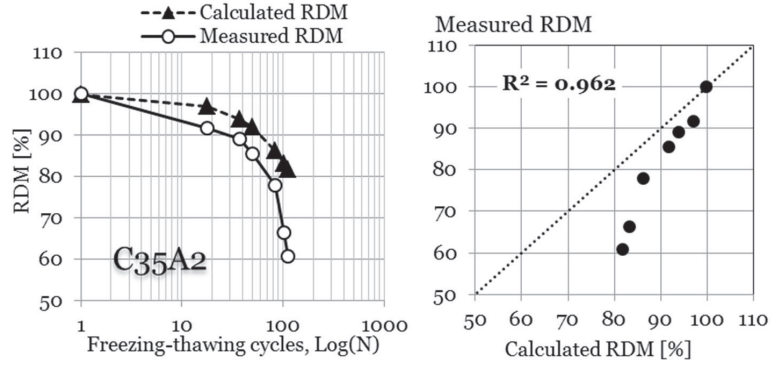


Figure E-1: Comparison between measured and calculated RDM for the C35A2 mix.

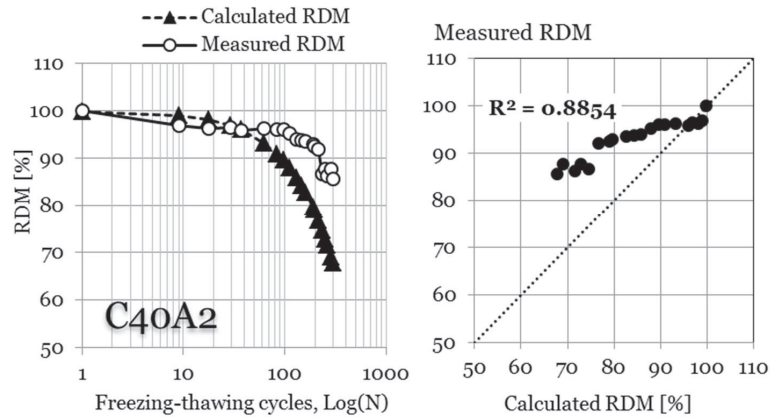


Figure E-2: Comparison between measured and calculated RDM for the C40A2 mix.

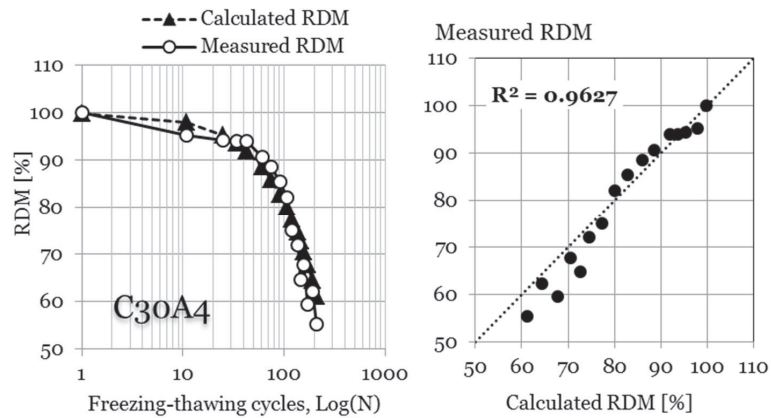


Figure E-3: Comparison between measured and calculated RDM for the C30A4 mix.

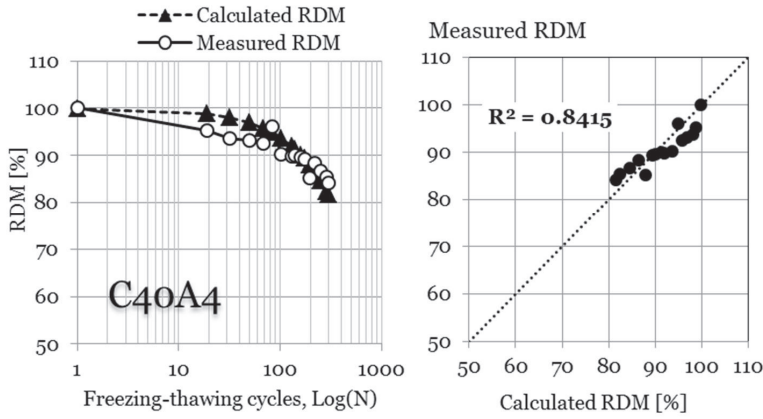


Figure E-4: Comparison between measured and calculated RDM for the C40A4 mix.

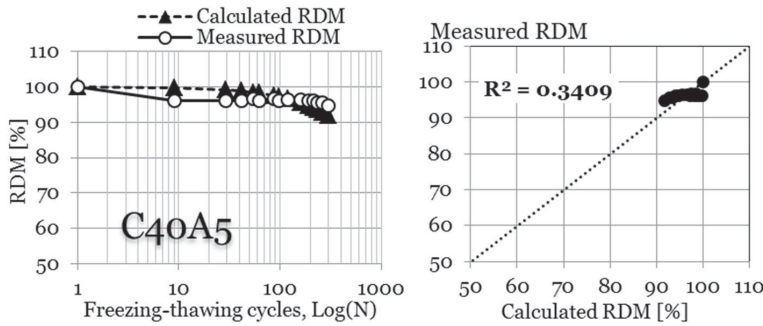


Figure E-5: Comparison between measured and calculated RDM for the C40A5 mix.

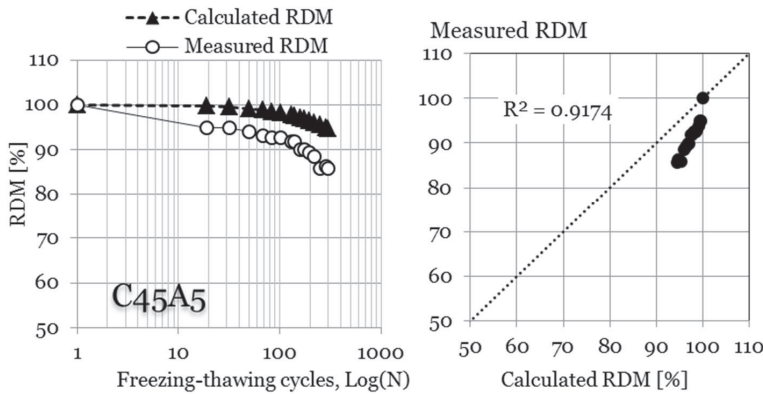


Figure E-6: Comparison between measured and calculated RDM for the C45A5 mix.





ISBN 978-952-60-5202-1  
ISBN 978-952-60-5203-8 (pdf)  
ISSN-L 1799-4934  
ISSN 1799-4934  
ISSN 1799-4942 (pdf)

**Aalto University**  
**School of Engineering**  
**Department of Civil and Structural Engineering**  
[www.aalto.fi](http://www.aalto.fi)

**BUSINESS +  
ECONOMY**

**ART +  
DESIGN +  
ARCHITECTURE**

**SCIENCE +  
TECHNOLOGY**

**CROSSOVER**

**DOCTORAL  
DISSERTATIONS**